TAMPEREEN TEKNILLINEN YLIOPISTO
TAMPERE UNIVERSITY OF TECHNOLOGY

JYRI ROPPOLA

PREPARATION AND CHARACTERIZATION OF ALL-CELLULOSE COMPOSITES

Master's thesis

Examiners:
Assistant Professor Mikko Kanerva
Professor Jurkka Kuusipalo
Approval of thesis topic & examiners:
31.05.2017

ABSTRACT

ROPPOLA, JYRI: Preparation and characterization of all-cellulose composites
Master's thesis, 91 pages, 2 apendix pages
Tampere University of Technology
May 2017
Material Science Program
Major: Paper Converting and Packaging
Examiners: Assistant Professor Mikko Kanerva, Professor Jurkka Kuusipalo
Keywords: Cellulose, paper, nanocellulose, all-cellulose, composite, laminate, nanofibrillated, sandwich

The aim of this study was to develop test method for adhesion testing for cellulosic materials in order to explain phenomena occurring at an interface of two unlike surfaces. Based on results of the developed test method and understanding of composites, novel all-cellulose composite sandwich structures were designed, fabricated and mechanically tested. Most of the experiments were carried out at Technical Research Centre of Finland, VTT with collaboration with Tampere University of Technology.

Peel testing (T-peel) was chosen to gauge adhesion in the developed method. Single two-fold strips were prepared from chosen sample materials that were joined in a hot-press with either using distilled water, nanofibrillated cellulose (NFC) particle suspension as a processing aid. Commercial liquid PVA glue suspension was used as a reference adhesive. The adhesion tests suggest important correlation with fiber based material porosity and adhesion gained with NFC particle suspension: Bond strength between two adherents are improved with higher porosity. This is attributed to the observation that NFC particles penetrate into porous medium and coalesce onto network of fibers forming an auxiliary strengthening web of film within the macrostructure. Also, significant adhesion was achieved with using only water as a processing aid with several specimen types.

Four types of innovative novel all-cellulose composites were prepared: Sandwich structures in either a narrow beam or wide panel configuration were fabricated using nanofibrillated cellulose films and cellulose fiber foam. Films were used as cell wall and face material while foam used as core material. Beam configuration represented the side profile of the structure while the panels represented the longitude structure of the sandwich composite. The specimen made out of delignified NFC film and delignified fiber foam were referred to as white ACC (WACC). The term brown ACC (BACC) was used for the specimens made using partially delignified NFC film and CTMP fiber foam. The BACC specimens preformed significantly better than the WACC specimens in flexural three-point bending testing. The ACCs were also compared to specimen series made using corrugated board (CB) designed for hazardous goods packaging.

Future work should be directed to prepare more elaborate ACC configuration and to testing of these types of composites. Also, the study of the effect of temperature on adhesion in laminate forming is highly recommended based on this work.

TIIVISTELMÄ

ROPPOLA, **JYRI**: Preparation and characterization of all-cellulose composites
Diplomityö, 91 sivua, 2 liitesivua
Tampereen teknillinen yliopisto
Materiaalitekniikan koulutusohjelma
Pääaine: Paperinjalostus -ja pakkaustekniikka
Toukokuu 2017
Tarkastajat: apulaisprofessori Mikko Kanerva, professori Jurkka Kuusipalo
Avainsanat: Selluloosa, paperi, nanoselluloosa, komposiitti, laminaatti, nanofibrilloitu, sandwich

Työn tarkoituksena oli kehittää koemenetelmä selluloosapohjaisien materiaalien välisen adheesion testaamiseen, jotta pystyttäisiin selittämään kahden eri pinnan rajalla tapahtuvia ilmiöitä. Kehitetyn menetelmän tuloksien ja komposiitti kirjallisuuden avulla suunniteltiin ja valmistettiin uudenlaisia selluloosa komposiitti (ACC) kerrosrakenteita (sandwich). Valmistusmenetelmien kehittämisen lisäksi komposiitteja testattiin mekaanisesti. Suurin osa tutkimustyöstä ja kokeellisesta osasta suoritettiin VTT:llä, Teknologian Tutkimuskeskuksessa yhteistyössä Tampereen Teknillisen Yliopiston kanssa.

Adheesion testaamiseen kehitetyssä menetelmässä valittiin 180 asteen kulmassa tehtävä T-peel testi. Valituista materiaaleista valmistettiin kaksin kerroin taitettuja liuskoja, joiden toisiaan vasten taitetut vastinpinnat liitettiin kuumapainamalla käsiprässissä. Liitettäviä vastinpintoja käsiteltiin joko tislatulla vedellä, nanofibrilloidulla selluloosa suspensiolla (NFC) tai vertailuaineena käytetyllä kaupallisella PVA-liima suspensiolla. Adheesiotestien perusteella havaittiin, että NFC-suspensiolla saavutetulla kuitumaisien pintojen välisillä sidosvoimilla ja materiaalin huokoisuudella oli huomattava yhteys: Mitä huokoisemmat liitetyt pinnat olivat, sitä korkeampi adheesio saavutettiin. Havaintojen mukaan perusteltiin, että NFC suspensio kykenee tunkeutumaan käsiteltyihin huokoisiin materiaaleihin ja kuivuessaan kerääntymään kuituverkoston ympärille muodostaen vahvistavan kalvomaisen verkon huokoisen rakenteen sisälle. Lisäksi useille pelkästään vedellä käsiteltyjen näytteiden pintojen välille saavutettiin merkittäviä sidoslujuuksia.

Tutkimuksessa valmistettiin neljää eri tyyppistä selluloosa komposiittia nanofibrilloidusta selluloosakalvosta ja sellukuituvaahdosta palkkeina ja paneeleina. Kalvoja käytettiin rakenteen kansina solukkojen seininä, kun taas vaahtoa käytettiin täyttävänä sisämateriaalina. Näytteet valmistettiin joko valkaistuista laaduista (= valkoiset laadut, WACC) tai osittain valkaistusta, ligniiniä sisältävästä nanoselluloosakalvosta ja CTMP-massasta valmistetusta vaahdosta (= ruskeat laadut, BACC). Ruskean laadun selluloosakomposiitit (BACC) suoriutuivat kolmipistetaivutuksessa merkittävästi valkoisia laatuja (WACC) paremmin. Lisäksi valmistettuja selluloosakomposiitteja vertailtiin aaltopahvista (CB) valmistettuihin näytteisiin.

Jatkotutkimuksia suositellaan tutkimaan ja kehittämään hienostuneempia ACC rakenteita, koemenetelmiä sekä lämpötilan vaikutusta laminointi adheesioon.

FOREWORD

The research in this work was done as a part of Design driven value chains in the world of cellulose 2.0 project (DWoC) which is funded by Tekes – the Finnish Funding Agency for Innovation. The work itself was expertly and professionally directed by Vesa Kunnari and Jaakko Pere from VTT. In addition to Vesa and Jaakko, I'd like to thank Atsushi Tanaka and the people working at VTT Espoo unit, as well as my professors (Mikko and Jurkka) and teachers at Tampere University of Technology for making this thesis possible.

Also, as professional note: In this work, I've tried to gather information from multiple sources and tried to piece them together. I wish that this effort will be used maybe as a template or a basis to facilitate future research. My research and experiments have covered only so little of the field of applicable all-cellulose composites. I hope that in the future, new development and research will really accelerate. But there is more I wish to say in terms of conclusion of studies.

Looking back, almost ever since I began my university studies in Hervanta, I've had close friends whom which I've spent countless relaxing evenings and cottage trips playing board games, chucking beers and enjoying sauna. Special mentions go to Antti, Ville, Esa, Viktor, Arttu and to both Juhos in our group for great, most memorable company. Thunderstone and other board games have definitely been the best pastime and have become my main, and somewhat expensive hobby – thanks Antti. Although we will continue our traditions, the professional and family lives will surely step in eventually and limit the time we can share. I will certainly miss the more simpler times, carefree nature and the relative freedom of university studying in this regard. Yet I wouldn't have this any other way, and it's time to move on.

Among the extensive time with my friends, I will miss the wonderful Hervanta district in Tampere. It has been a place where I truly became independent, found love, made lifelong friends, felt pain and experienced memorable student culture and traditions – A man can leave Hervanta, but Hervanta will never leave a man.

These past months writing this thesis have been hard and I've felt that I've neglected my friends and my lovely and supportive girlfriend Veera. With this negligence, I've tried to put more effort into finalizing this thesis in the anticipation that the graduation introduces wonderful aspect of every day life: there will be no more assignments filling my agenda in my private life. This crunch period has also been a lesson that professional work should stay within the professional life. Now, I can start finally paying back the time I've kept to myself and begin arranging time with the ones that matter to me the most – my family and friends. No matter where we are.

CONTENTS

LIST OF TABLES & FIGURES

Tables

Figures

TERMS AND DEFINITIONS

ACC	All-cellulose composite
BACC	Brown all-cellulose composite
BMIMAc	1-butyl-3-methylimidazolium acetate
CD	Cross direction
CESA	Cellulose synthase enzyme
CTMP	Chemi-thermomechanical pulp
DP	Degree of polymerization
DSC	Differential scanning calorimetry
FE-SEM	Field-emission scanning electron microscopy
IBS	Internal bond strength
LiCl/DMAc	Lithium chloride / *N,N'*-dimethylacetamide
MD	Machine direction
MFC	Microfibrillated cellulose
QCM-D	Quartz crystal microbalance with dissipation
SEM	Scanning electron microscope
TEM	Transmission electron microscope
TEMPO	2,2,6,6-tetramethylpiperine-1-oxyl
TFA	Trifluoroacetic acid
TGA	Thermogravimetric analyzer
WACC	White all-cellulose composite
EHL	Enzymatic hydrolysis lignin

1 INTRODUCTION

Today, an increasing demand on manufacturing environmentally friendly and carbon neutral products is set by our society. Paradigm shift towards sustainable design is enforced by industrial customers, governments and by consumers (Moon, et al., 2011; Soykeabkaew, et al., 2008; Halonen, 2012). Forest and cellulose industry is suitable to fulfill these emerging requirements through introduction of cellulose composites (Halonen, 2012). A good amount of research and development has been put into applying cellulose fibers and cellulose nanoparticles as reinforcement materials in existing polyolefin composites (Arévalo & Peijs, 2015; Liu, et al., 2014; Lu, et al., 2003). However, these composites are not fully biodegradable and additionally, a great deal of effort is required in the form of special treatments to overcome the poor interfacial interactions between hydrophilic cellulose particles and hydrophobic polyolefin matrix (Lu, et al., 2003; Arévalo & Peijs, 2015). An alternative way to meet the described demand is to provide composites prepared wholly from cellulose (Arévalo & Peijs, 2015). All-cellulose composite design also facilitates design of products that need to perform well in life cycle assessment since the complete structure would be biodegradable.

Another aspect of all-cellulose composite (ACC) design is to offer forest industries new ways to capitalize on wood pulp and fibers as ever cheaper cost of Eucalyptus fibers are expected to dominate paper and board materials (Nilsson et al., 2010). This will be a part motivator to define clear scope for this thesis and focus on wood based lignocellulose materials: The prepared ACCs could be utilized in packaging, furnishing and structural and semi-structural applications. A first fundamental step towards preparing prototype composites for these applications is to find means of achieving feasible adhesion between composite constituents. To this end, a simple laminate specimen test method will be developed to test for adhesion between materials with varying parameters in joining methods. With this approach, interactions between laminate constituents can be characterized and suitable methods and materials for ACC development and preparation can be suggested. Based on these findings, novel all-cellulose composite beam and panel structures will be designed, fabricated and mechanically tested. This is aimed to contribute to future designs and gauge the performance of current ACC materials.

Concept of all-cellulose composites is not new, but the prototypes that have emerged today are commonly prepared using cellulose solvents or other chemicals to fuse components together (Nilsson et al., 2010). Reactive binding agents can be unfavourable for the environment and ruin possibilities of recycling (Sehaqui et al., 2011). A more feasible route therefore is to try and achieve sufficient adhesion with using e.g.

water induced swelling of cellulose, lignin and hemicellulose as a method of binding. Hot pressing pressure and temperature during laminate preparation are important parameters in this process. Also, cellulose based adhesive in form of nanofibrillated cellulose – water suspensions are used as binding agents. To correctly master and and control the phenomenon related to interactions between cellulosic materials, profound understanding of lignocellulosic material chemistry and physics must be discussed.

Cellulose morphology and physical properties found in wood are not easy to study (Siro & Plackett, 2010; Klemm, et al., 2006). Also, exact knowledge and research on unlike cellulose-cellulose material interface interactions are rare, but are of great interest. New experimental findings and literature work in this subject matter are therefore required to guide development of sustainable and viable all-cellulose composites.

2 BACKGROUND

In this section, three material groups and their properties are discussed. Although research on cellulose could be done with different cellulose types from multiple sources, only wood originated cellulose is discussed in detail.

It is suggested that molecular and mesostructural aspects of cellulose are taken into account when trying to understand interactions between cellulosic materials (Aulin, et al., 2009). Therefore, literature research will be directed to give enough insight to predict and characterize these phenomena. Effects of moisture, temperature, swelling and solvent dissolution on cellulose and associated biopolymers are needed to be understood to achieve adhesion between constituents within a composite material.

Strength and tensile properties are also evaluated briefly to enable comparison between any results during adhesion testing to strength of individual materials. Also, current research on all-cellulose composites and various composite preparation methods are reviewed. Existing data will also give insight in characterizing feasible tensile properties or adhesion of the composite assemblies.

Lastly, cellulose-cellulose material adhesion characterization will be discussed.

2.1 Wood fiber

Use of wood fibers (WF) along with plant fibers have dominated the paper making industry for centuries (Moon, et al., 2011). WF structure, chemistry, physical properties, bonding and network forming capabilities have been researched over decades in pursuit of performance optimization on industrial scale. Reviewing wood fiber, its structure and composition is still of interest in designing of cellulose composites involving wood. This includes researching cellulose interactions with other polysaccharides and biopolymers found in wood.

Wood fibers have great mechanical strength attributed to their extra cellular cell wall structure. Cell wall of wood fibers consists mainly of cellulose, hemicelluloses and lignin, but other polysaccharides and extractives are also present in lesser quantities. (Halonen, 2012; Åkerholm, 2003) The cell wall itself is a matrix with strengthening and binding agents (Wertz, et al., 2010). Wood fibers differ in form, composition and size depending on tree species and seasonal growth (Halonen, 2012).

Wood fiber has a hierarchal structure with different layers, which is illustrated in Figure 2.1.

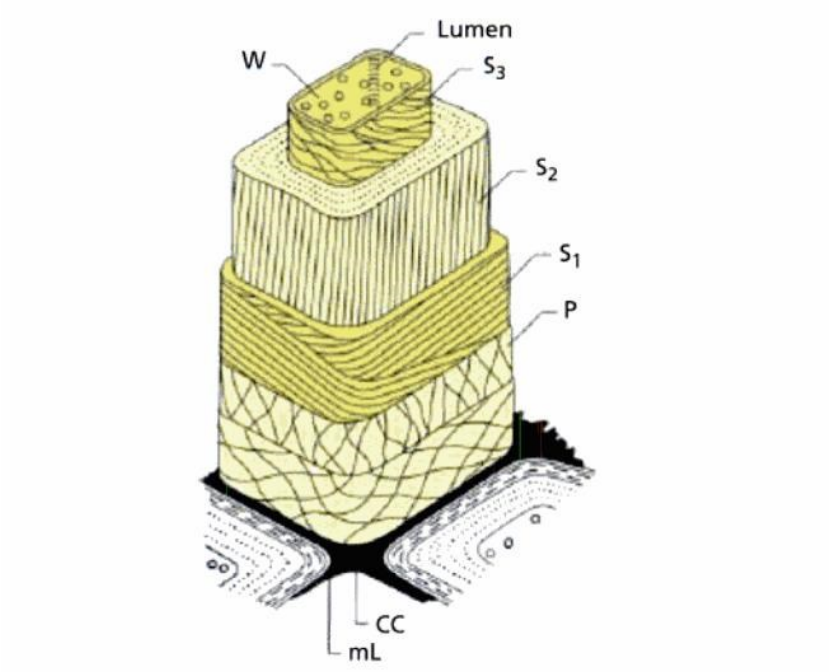

Figure 2.1. *Presentation of wood fiber and its hierarchal layer structure.* (Wertz, et al., 2010)

Three major cell wall components can be pointed out from the Figure 2.1: the highly lignified middle lamella (mL), primary cell wall (P) and the secondary cell wall (S). The secondary wall has three layers S1, S2 and S3 out of which the S2 is the most significant. S2 is relatively thick (1-5 μm) and constitutes roughly 80% of weight of cellulose within the fiber making it strong contributor to the mechanical properties of the fiber (Wertz, et al., 2010; Åkerholm, 2003). In the secondary wall, cellulose microfibrils differ by their alignment with respect to the fiber axis in helical manner. The angle between the axis and aligned microfibrils is usually referred to as the fibril angle (Leney, 1980). This can also be observed in the schematic in Figure 2.1. In the S2 layer, microfibrils are almost parallel to the fiber axis with fibril angle ranging from 5-30°. (Halonen, 2012; Wertz, et al., 2010) Strength of individual fibers is strongly affected by this angle. For flax fibers with fibril angle of ~10°, elastic modulus of 27-100 GPa can be obtained, compared to fibril angle ~21° and elastic modulus of 5-13 GPa of a cotton fiber. (Wertz et al., 2010) A tensile test for a softwood fiber can yield axial elastic modulus from 14 to 27 GPa (Mott et al., 2002). Reportedly, axial elastic modulus of 7,5±3 GPa was obtained for hardwood samples measuring 10-15 mm, 4-6 mm and 0,5-0,6 mm in length, width and thickness respectively (Liu et al., 2014).

As discussed before in wood fibers cellulose is accompanied by other polysaccharides and biopolymers forming a composite structure of their own. Multiple polysaccharides, pectins and proteins exist within the plant cell wall, and with cellulose ultrastructural aspect in mind, reviewing cellulose-hemicellulose and cellulose-lignin inter-

actions are decisive. Hemicellulose and lignin are expected to play a role in adhesion mechanisms between materials in composites including wood as a component.

2.1.1 Cellulose

Cellulose is the most abundant biopolymer in the world (Haygreen & Bowyer, 1982; Aulin, et al. 2009; Torres, et al. 2013) and it is found in plant-like organisms ranging from wood, to grass, to cotton (Siro & Plackett, 2010). Cellulose is also produced by algae, tunicates, fungi and bacteria (Halonen, 2012; Klemm, et al. 2006; Siro & Plackett, 2010). As mentioned previously, in plants, cellulose is accompanied by other polysaccharides but bacterial cellulose is free of these components.

Cellulose polymer consists of repeating D-anhydroglucapyranose (D-AG) units that are linked to one another by β-(1→4)-glyckosidic bonds (Granström, 2009; Sperling, 2006; Heino & Vuento, 2007). Two D-AG units form a cellobiose, the repeating unit of the polymer with DP ranging from 5000 to 10 000 (ThermoWood, 2003). The β-linkage results in alternating D-AG unit orientation: each unit is rotated 180° with respect to each other as illustrated in Figure 2.2 (Granström, 2009). This allows for intramolecular hydrogen bonding between D-AG units which makes the molecule stiff and provides cellulose molecule it's linear nature (Granström, 2009; Moon, et al. 2011). This also enables parallelly stacked separate cellulose chains to form hydrogen bonds between hydroxyl and oxygen groups of neighbouring chains (Granström, 2009), resulting in aggregation of chains into elemental fibrils which in turn coalesce into microfibrils (5–50 nm in diameter) (Moon, et al. 2011; Torres, et al. 2013).

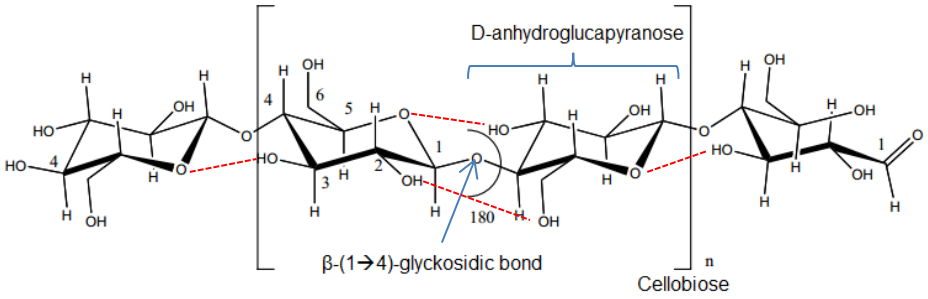

Figure 2.2. *Cellulose molecular structure: repeating cellobiose unit (n), reducing end-group on the right and non-reducing end-group on the left. Red dashed lines represent intramolecular hydrogen bonding between C3 hydroxyl group and cyclic O. Hydrogen bonds can also be formed between C2 and C6 hydroxyl groups. (Granström, 2009)*

Described fibrillar arrangement in tall plants is based on knowledge on cellulose biosynthesis by arranged cellulose synthase enzymes, CESAs (Torres, et al. 2013). This might

not be the case for other sources of cellulose and thus it must be aknowledged that cellulose supramolecular structure is still a subject of research (Halonen, 2012; Granström, 2009). Also, diverse terms are used for aggregations of cellulose chains in literature (Halonen, 2012).

Currently, it is understood that microfibrils are the foundation of the load bearing structure of tall plants (Moon, et al. 2011). However, it is suggested by Torres et al. that microfibrils form macrofibrils in order to form the cell wall of a plant fiber. An illustration of relations between cellulose molecule and cellulose supramolecular level is shown in Figure 2.3.

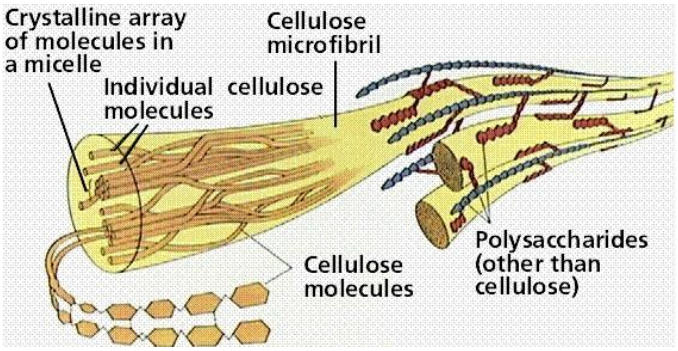

Figure 2.3. *Cellulose chains forming elemental fibrils (crystalline array). Microfibrils are associated by other polysaccharides such as lignin and hemicellulose. (Farabee, 2010)*

Within cellulose microfibrils the chain formation is not uniform (Granström, 2009) as observed in illustration in Figure 2.3. Experimental evidence suggests microfibril structure consists of two regions. There are highly ordered crystalline regions, where the independent molecules are closely and parallelly packed. Other half is considered to consist of less ordered amorphous regions, where cellulose chains are not aligned and are loosely packed. (Granström, 2009; Moon, et al. 2011; Torres, et al. 2013) These amorphous cellulose chain aggregates and crystalline elementary fibrils in the microfibril are then cohesively held together by network of hydrogen bonds (Torres, et al. 2013). The aggregate size is limited by closely associated cellulose bound branched hemicellulose chains (Nilsson et al., 2010), that will be discussed later in this section. The crystalline structure of cellulose can further be divided into sub groups based on source of origin and chemical treatment of cellulose.

Cellulose can exist in different polymorphic crystalline forms which are called cellulose I, II, III and IV. These types forms differ in the dimensions of their unit cells (Granström, 2009; Sperling, 2006), the repeating volume within the crystal structure. These different crystal structures affect both swelling and dissolution of cellulose, but also strength properties of cellulose (Aulin, et al., 2009; Moon, et al. 2011). For relevance purposes, polymorphs I, II and their differences will be discussed in detail.

Type I cellulose is often called natural cellulose because it's produced by a myriad of organisms such as trees, tunicates, algae and bacteria (Moon, et al. 2011). Cellulose I is further divided into into allomorphs of I_α and I_β, which exist in varying propor-

tions based on cellulose producing organism (Torres, et al. 2013; Pérez & Mackie, 2001). I_β is mostly present in tall plants while I_α is dominant in simpler organisms like algae and bacteria. Key difference between cellulose I allomorphs is their relative displacement of parallelly stacked cellulose chain sheets in the crystalline structure, which is illustrated in Figure 2.4 (Moon et al. 2011).

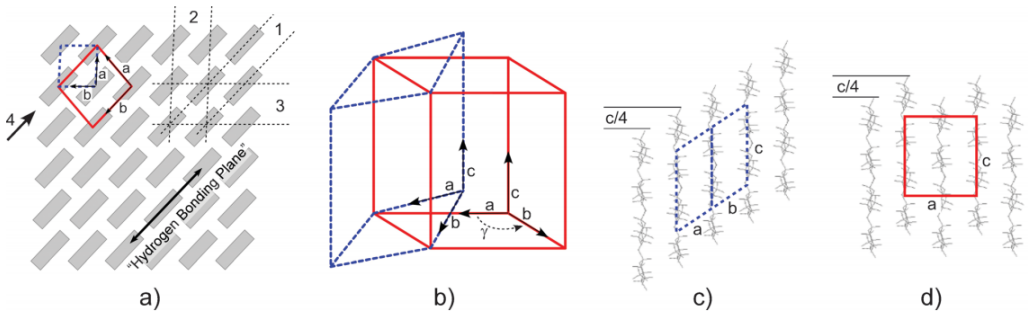

Figure 2.4. *(a) Projection orientation along cellulose chains shows similar repeating crystalline structure, (b) respective unit cell dimension for I_β (red solid line) and I_α (blue dashed line) and (c-d) displacement of sheets of bonding cellulose sheets: alternating relative displacement pattern of I_β and constant relative displacement for I_α. (Moon et al. 2011)*

Out of all cellulose polymorphs, type II is the most important and most extensively researched since it is thermodynamically most stable form of crystalline cellulose (Moon et al. 2011; Torres et al. 2013). Cellulose II is produced by some bacteria and algae at low temperatures but currently it is produced industrially by two types of processes. One is regeneration, in which cellulose is first solubilized by a solvent (e.g. by NMMO-water mixture) and then precipitated in water (Moon et al. 2011; Flink et al. 2001). The other process is called mercerization, in which cellulose is treated with aqueous sodium hydroxide (Torres et al. 2013).

Differences between tensile properties of the two polymorphs are of interest since solvent treatment during composite manufacture will transform some of native cellulose to type II. Experimental axial elastic modulus values of 120-138 GPa for type I_β and 9-90 GPa for type II. (Moon et al., 2011)

Both the type and degree of cellulose crystallinity can be determined by diverse techniques such as wide angle X-ray scattering (WAXS), X-ray diffraction and solid state NMR and FTIR (Granström, 2009). The degree of crystallinity also varies between cellulose polymorphs. Generally native cellulose shows higher amount of crystalline order than type II cellulose (Moon et al., 2011; Aulin, et al., 2009). Furthermore, it is suggested by Aulin et al. (2009) that the type of crystalline ordering and degree of crystallinity affects cellulose interaction with other materials. To illustrate differences between cellulose I_β and II, unit cell dimensions of these polymorphs are featured in Figure 2.4.

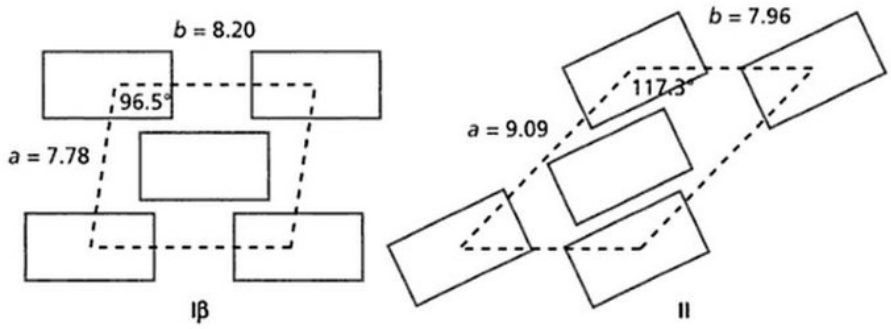

Figure 2.5. *Schematic of unit cell dimensions of cellulose type I_β and type II as a projection along the chain direction (Wertz et al. 2010).*

Because of its ability to form hydrogen bonds between adjacent cellulose chains and its tendency to form dense crystalline regions, cellulose polymer is stable and insoluble in most solvents and water (Granström, 2009; Moon, et al. 2011; Halonen, 2012). Dissolving of cellulose is therefore dependent on breaking down the hydrogen bond network (Torres et al. 2013). Dissolving of cellulose is discussed in detail later in this section.

Although cellulose is insoluble to water, it is highly hygroscopic in nature (Wertz et al. 2010). Acknowledging this is essential as cellulose-water interactions play a key role in cellulose processing from cellulose isolation to paper making. These interactions are also heavily dependent on the supramolecular structure of cellulose (Wertz, et al., 2010). Water can penetrate into amorphous regions of cellulose causing swelling and enlarging the structure (Aulin, et al., 2009). Water molecules interact with accessible hydrogen groups and are adsorbed into amorphous regions and to the surfaces of cellulose crystals. Enlarged pores further cause capillary water intake and more swelling of cellulose. Water adsorbed through hydrogen bonding is called bound water and water sorbed by capillary intake and pore swelling is called free water. (Wertz, et al., 2010) Sorbed water works as a plasticizing agent in cellulose amorphous structure, lowering the glass transition temperature, T_g of cellulose. Glass transition temperature is discussed later in section 2.1.4.

2.1.2 Hemicellulose

Hemicellulose is a large group of polysaccharides (DP 150 - 200) that form hydrogen bonds with cellulose microfibrils in the wood cell walls (Figure 2.2) (Srndovic, 2011; ThermoWood, 2003). Predominant hemicellulose depends on the tree species. (Wertz, et al., 2010) For instance, galactoglucomannan, also a group of different polysaccharides, is the prevalent hemicellulose in softwoods secondary cell wall (Åkerholm, 2003; Srndovic, 2011). Galactoglucomannan consist primarily of (1→4) linked ß-D-glucopyranose and ß-D-mannopyranose units that have α-D-galactose substituents

(Åkerholm, 2003). In hardwoods, major group of hemicelluloses are xylan which consist of (1→4) linked ß-D-xylopyranose units and are periodically substituted by 4-O-methyl-α-D-glucuronic acid groups.

Like cellulose, hemicellulose is insoluble to water; however, substantial hydrolysis and consequential dissolving of hemicellulose will occur in elevated temperatures (ThermoWood, 2003). In wood cells, hemicelluloses are closely associated with cellulose by extensive hydrogen bonding but also by strong covalent ether bonds (Winkworth-Smith, 2014; Zhang, et al., 2011; Harmsen, et al., 2010). Within the ultrastructure of cellulose in wood, hemicelluloses work as a spacer, limiting the aggregation of cellulose fibrils into larger bundles but also limits intermolecular hydrogen bonding between cellulose aggregates (Siro & Plackett, 2010; Åkerholm, 2003; Halonen, 2012). This is supported by research done observing bacteria synthesized cellulose in hemicellulose gel, where findings have shown that glucomannan is arranged parallel along cellulose fibrils and covering them. Xylan was found, on the other hand, to arrange itself discontinuously along the same fibrils. (Åkerholm, 2003) Newer studies point out that in hardwood, xylan is also oriented parallel to the cellulose microfibrils (Olsson, et al., 2011). Structures of xylan and glucomannan are presented in Figure 2.6.

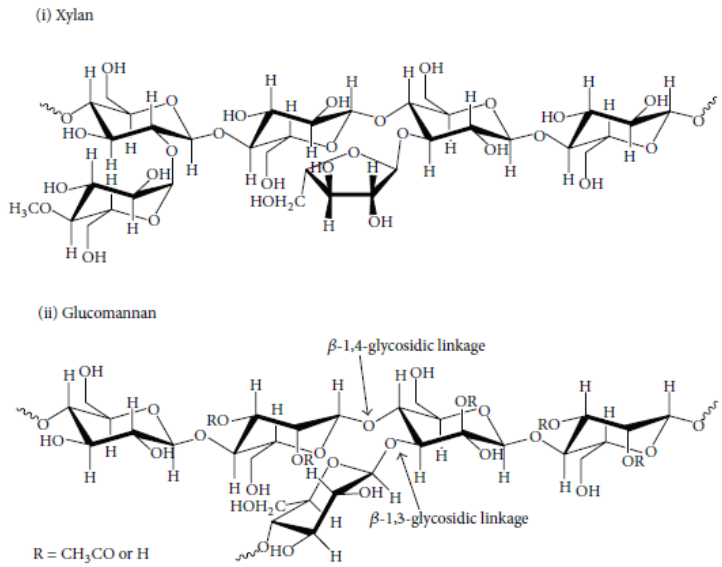

Figure 2.6. *Molecular structure of hemicellulose xylan (i) and glucomannan (ii) (Lee et al., 2014). There are noticeable structural similarities between cellulose and main chain of hemicellulose, which may explain why hemicellulose is so closely associated with cellulose and aligned along the chains in the microfibril.*

In addition to aligning close to cellulose surfaces, hemicelluloses also form bridges and loops to neighbouring micro and macrofibrils (Terashima et al., 2009; Altaner & Jarvis, 2008). In wood cell wall, the space between macrofibrils and the formed hemicellulose network is densely lignified (Altaner & Jarvis, 2008).

With all the insight discussed above, it is expected that hemicellulose will provide as a good binding agent between cellulose materials. However, due to its good bonding with cellulose and its branched nature, hemicellulose can reduce the effective bonding area for cellulose-cellulose hydrogen bonds, lowering desired hydrogen bonding between materials in composite structure (Srndovic, 2011).

2.1.3 Lignin

Lignin is a group of numerous branched aromatic polymers, that consist of hydroxypheny propane units (Srndovic, 2011). As a polymer, lignin shows a very low degree of polymerization ranging from 10 of 50 DP (ThermoWood, 2003). In wood, lignin is most abundant between individual fibers in the middle lamella where it helps to bindind neighbouring fibers together. Lignin is also present in cell wall layers forming three-dimensional structure that serves as an amorphous matrix for cellulose and hemicellulose. (Srndovic, 2011; Jin et al., 2015) As noted earlier, hemicellulose interacts with cellulose via hydrogen bonds, lignin in turn attaches to hemicellulose via strong covalent ether bonds (Zhang, et al., 2011; Altaner & Jarvis, 2008), but it can also bond this way with cellulose if accessible (Harmsen, et al. 2010). Bonding with hemicellulose is supported by recent studies indicating that in cell wall lignin has significant orientation along the fiber axis (Olsson, et al., 2011). In addition to working as a binding and a strengthening agent, lignin provides cellulose protection from microbial attacks and decay. Also, lignin is hydrophobic in nature, so it will deter swelling of both cellulose and hemicellulose in humid conditions, which is essential for water transportation in plants. (Srndovic, 2011; Maximova, et al., 2001)

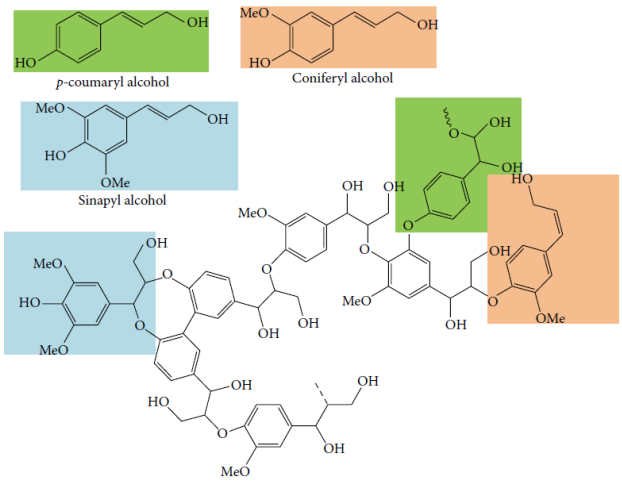

Figure 2.7. *Lignin molecule structure with monolignols highlighted in different colours (Lee et al., 2014)*

Lignin's hydrophobic properties can be illustrated with structural schematic in Figure 2.7. Although lignin has many functional groups that can interact with water, they are mostly used to form covalent bonds with other monolignols, hemicellulose or cellulose (Zhou et al., 2011). Therefore, the remaining hydrophobic aromatic core structure defines the hydrophobic nature of lignin.

2.1.4 Deformation mechanisms of lignocellulosic interfaces

Recently, interactions between cellulose, hemicellulose and lignin have been studied through molecular dynamics simulations. These simulations have often featured neighbouring cellulose surfaces of a software compiled model that are subjected to shear or tensile stress (Altaner & Jarvis, 2008; Jin et al., 2015; Zhang et al., 2015; Adler & Buehler, 2013). Despite depicting different models, a common failure mechanism is prevalent between them: the breaking of hydrogen bonds between hemicellulose and cellulose.

Altaner & Jarvis (2008) suggest that hemicellulose chains have four possible geometries in which they bind to cellulose: 1) completely binding alongside a single fibril, 2) forming a single bridge between fibrils, 3) forming a loop that binds one fibril once and the other twice, or 4) having a free chain end. These estimates are based on findings by Hafren et al. (1999) on immature xylem cells before lignification of interfibrillar gaps.

Molecular dynamics simulation study conducted by Zhang et al. (2015) focused on exploring cellulose-hemicellulose composite interactions, excluding lignin from the tested models. The models consisted of opposing cellulose layers bound together by hemicellulose chains with different conformations based on the classifications of Altaner & Jarvis (2008). Top half of the model was set to move at a constant velocity of 0,5 Å/ps while the lower half was fixed in place (Figure 2.8.). With the obtained shear force-displacement response curves of each model, the team ranked bridge hemicellulose conformation as the strongest link between neighbouring cellulose fibrils with loop binding as second. The team attributed the strength of the hemicellulose-cellulose composite interface system to the covalent bonds of the hemicellulose chains (bending and stretching motion) as well as to the hydrogen bonding between cellulose and hemicellulose. Permanent damage to the interphase was reported after shear stress increased to a point where cellulose-hemicellulose hydrogen bonds break, after which a depression was observed in the shear force.

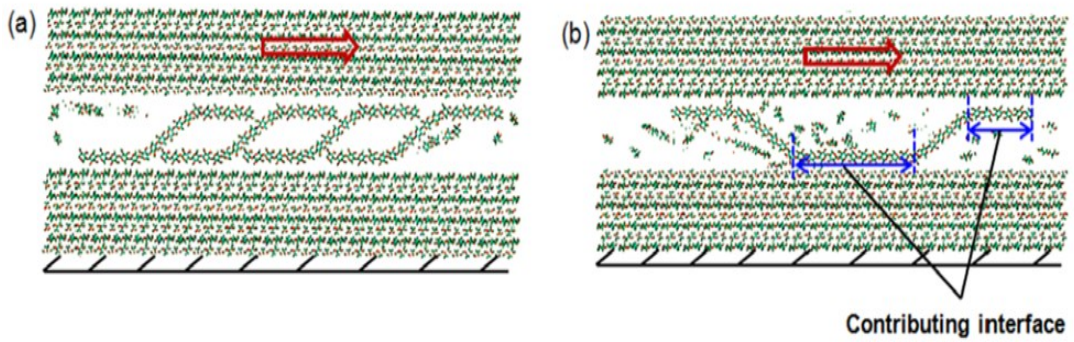

Figure 2.8. *Configuration of the molecular dynamics simulations depicting cellulose-hemicellulose structure binding modes: (a) bridge binding (b) loop binding with contributing interface. (Zhang et al., 2015)*

In the molecular model proposed by Jin et al. (2015) it is assumed there are no bridges or any connecting loops of hemicellulose between two bodies of cellulose. Instead, hemicellulose (Xylan) is closely associated as a sheet over cellulose fibril by hydrogen bonds. Between the layers of hemicellulose, covalently bound lignin of various units was built dynamically following the steps of lignin biosynthesis. The finished model was equilibrated and then the both outer cellulose layers were subjected to shear force. The stress-strain response of the model was then plotted as shown in Figure 2.9. Three regimes are identified form the curve: one elastic regime and two regions of plastic regimes.

After the elastic region, the matrix of lignin and hemicellulose begins to show signs of plastic deformation while the matrix was still attached to the cellulose fibril. More detailed observations of the molecules revealed irreversible reorganization of parts of the matrix: molecules would squeeze between surrounding ones. The second type of plastic deformation occurs when hemicellulose molecules of the matrix begin to slide along the surface of cellulose layer. However, this sliding effect is not continuous, rather occurring in cycles of sudden drops of stress after stress increases to a critical value. Sliding occurs in steps of discrete slips when the hydrogen bonds between cellulose and hemicellulose break. After each slip event, hydrogen bonds are reformed. (Jin et al., 2015) This phenomenon is referred to as “slip-stick” motion, which can also be observed in molecular simulation model created by Adler & Buehler (2013) with bridging hemicellulose chains between cellulose fibrils excluding the lignin matrix. In their model, increasing shear stress resulted in permanent deformation without any damage to the material. Instead, a softening behaviour was observed with increasing deformation (Adler & Buehler, 2013).

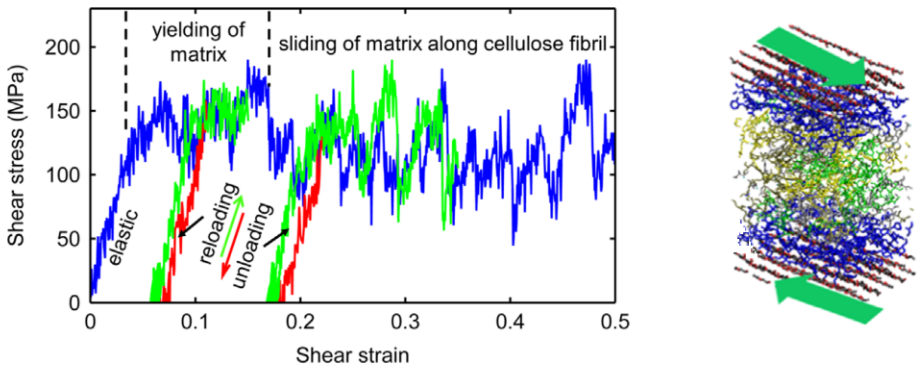

Figure 2.9. *Stress-strain responses of a shear action on model structure shown on the right. The outmost layers represent cellulose, blue layer corresponds to hemicellulose and center area is filled with lignin. Three regimes can be observed from the curve: elastic and two plastic regimes. Red (unloading) and green (reloading) curves are evidence of irreversible deformation during yielding of matrix and the slip-stick motion. (Jin et al., 2015)*

Another interesting molecular simulation was recently carried out to study deformation of cellulose nanofibrils in water (Paavilainen et al., 2012). The nanofibrils were modeled to include both amorphous and crystalline cellulose regions. The team simulated fibrils with varying number bound connecting chains that were covalently bound to the crystalline segments. Then an increasing force was applied to the crystalline segments of the created model and the strain response of the model was plotted. When sufficient stress was introduced, the connecting cellulose chains began to slide along neighbouring chains, slowly detaching from the rest of the crystallite (Figure 2.10.). The strain of the amorphous cellulose chains in the form of this sliding accounted for the majority of the total strain of the model. Like in the simulations conducted by Jin et al. (2015), the sliding was reported to occur one residue at a time resembling that of the slip-stick motion.

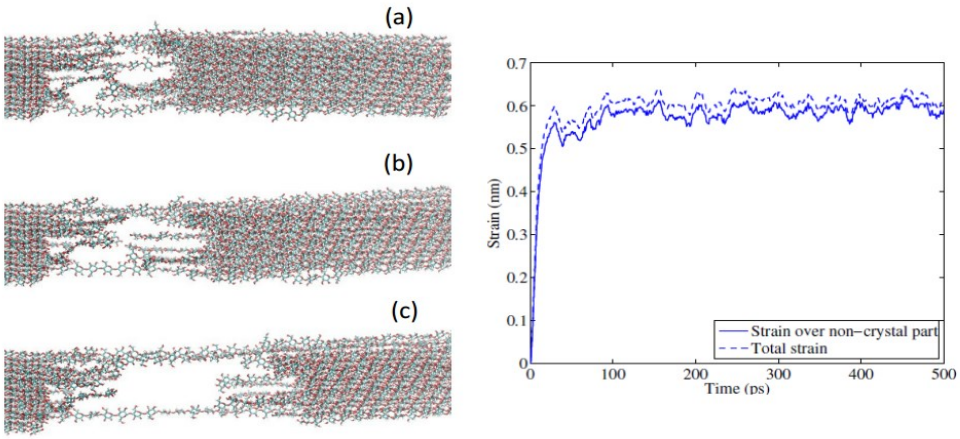

Figure 2.10. *Left: (a-c) Snapshots of the fibril molecular model with three connecting chains of the amorphous regime being pulled out of the crystallites during straining. Right: the strain response curves of both the whole model and the non-crystalline regimes when subjected to 5000 kJ/mol*nm stress. (Paavilainen et al., 2012)*

It is worth noting that no covalent bonds have failed during these modeling experiments: Mechanical failure tends to occur in the cellulose-hemicellulose interface connected with weaker hydrogen bonds. Single covalent bonds are particularly strong with typical bonding energy of 150-500 kJ/mol, whereas bonding energy of a hydrogen bond ranges from 8 to 32 kJ/mol (Niskanen, 2008). Interestingly, some molecular modeling work has been conducted by Besombes & Mazeau (2005) on lignin-cellulose surface interactions and further formation of 3D-structure of surrounding lignin layers in the presence of water. It is also widely reported that lignin will bind covalently to cellulose (Harmsen, et al. 2010; Jin et al., 2006; Suzuki et al., 1998). Research on this subject so far has not included mechanical straining of this type of interface.

2.1.5 Thermal properties of wood fiber constituents

Like with many polymers, physical properties of cellulose, hemicellulose and lignin are sensitive to temperature changes. Relevant thermal properties for composite manufacturing are glass transition temperature and thermic degradation of these materials. It is important to note that evaluation and exploitation of these properties is difficult because they are affected by water within the materials.

Glass transition temperature

Glass transition temperature (T_g) is a property of amorphous and semicrystalline polymers. Below this temperature polymer chains in the amorphous region are rigid and and macroscale material behaves like a glass. Above T_g, polymer chain mobility is enabled in the amorphous regions and as a consequence, material softens and becomes more fluid or rubber like. (Sperling, 2006; Niskanen, 2008; Szczes´niak, et al., 2007) For this softening behaviour, glass transition temperature is sometimes refered to as softening temperature. Amorphous bodies flow and are deformed by shear stress applied to the structure (Niskanen, 2008).

It is suggested by Niskanen that in wood fibers amorphous components hemicellulose and lignin are sole contributors of changes induced by heating in wood rheology. This is because in the fiber wall cellulose fibrils are embedded in a matrix of hemicellulose and lignin (Niskanen, 2008). A phase diagram featuring glass-rubber regions for hemicellulose and lignin is shown in Figure 2.11 (left). These findings are in line with earlier suggestions by Salmén (1982) when studying softening behaviour of various chemically treated dry paper grades. Glass transition temperatures for dry hemicellulose, lignin and cellulose, 170 °C, 205 °C and 230 °C respectively were obtained

(Salmen, 1982). In more recent work by Zhou et al. (2011), glass transition was determined to occur for enzymatic hydrolysis lignin at 189,4 °C.

At temperatures higher than T_g, that is usually lowered by introduction of water molecules as discussed previously, the chains in the amorphous region exhibit an increase in cellulose chain and fibrill mobility (Roig, et al., 2011; Nilsson, et al., 2010). Water molecules replace some of the hydrogen bonds in the amorphous region lowering interactions between individual chains and chain aggregates (Spence, et al., 2010). For high water content cellulose materials, the opposite is possible as a result of drying heat treatment. Nilsson, et al. (2010) suggest that for high cellulose content samples, heat induced hornification increases inter particle hydrogen bonding but also decreases swelling ability of the structure.

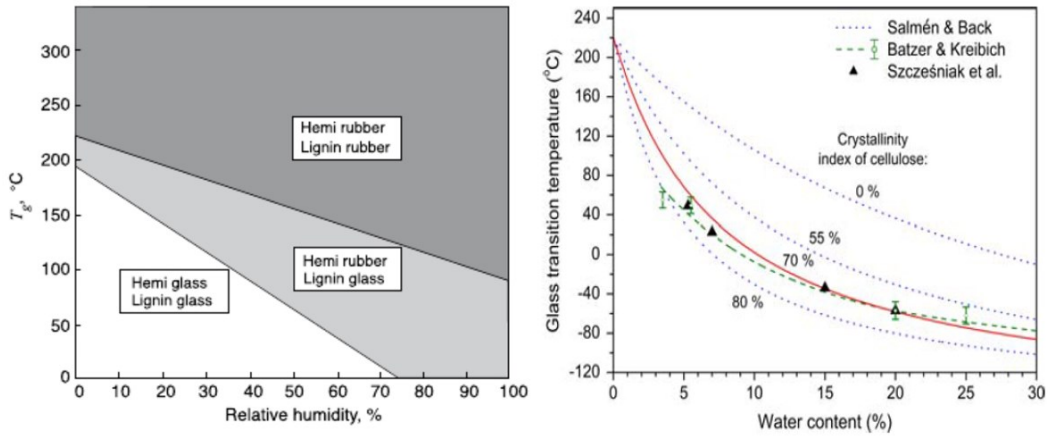

Figure 2.11. *Left: Simple phase diagram for hemicellulose and lignin (Niskanen, 2008). Right: Glass transition temperature of cellulose powder as a function of cellulose water content. In addition, glass transition dependence on cellulose crystallinity is shown. (Szczes´niak, et al., 2007) Results for cellulose are in agreement with study done by Salmén (1982).*

Also, glass transition temperature can be depressed by high cellulose crystallinity as seen in Figure 2.11. However, crystallinity affects adversely the extent of rubbery behaviour of semicrystalline structure since high crystallinity leaves less volume of amorphous chains able to move (Salmen, 1982).

Controlling glass transition temperature can be considered an important parameter when trying to achieve adhesion between cellulosic fibers and surfaces during fabrication of binderless boards and composites. (Zhou et al. 2011)

Degradation temperature

Another relevant thermal property of a wood constituent for this thesis is temperature induced degradation by pyrolysis. Pyrolysis characteristics of cellulose, hemicellulose and lignin were evaluated by Yang et al. (2007) by thermogravimetric analyzer shown in Figure 2.12. In this experiment for separate dry samples, pyrolysis of hemicellulose occurred mainly at 220-315 °C while same behavior for cellulose was observed at a range of 315-400 °C. Weight loss for lignin on the other hand occurred at wide temperature range from ambient to 900 °C, but at a very slow rate.

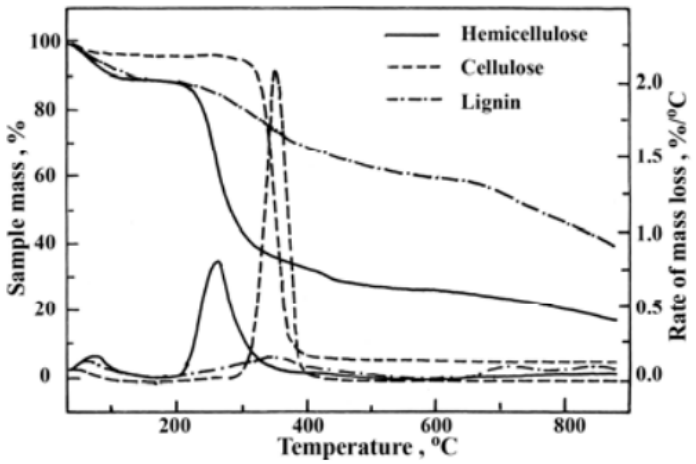

Figure 2.12. *TGA/DSC Pyrolysis curves for separate wood constituent samples heated to 900 °C at a rate of 10 °C/min. Curve series above are for sample mass, lower curves represent mass loss rate. (Yang et al., 2007) Early degradation of hemicellulose and lignin is observed even under 100 °C.*

Using size exclusion chromatography (SEC), Nilsson et al. (2010) showed that hot-pressing of bleached wet wood fiber pulp mats results in oxidative and hydrolytic degradation by cleavage of cellulose chains. This is observed as decrease in molar mass of these composite samples of high cellulose content, which is presented in Figure 2.13. The team speculated that the decreased cellulose molar mass indicates reduced fiber and subsequently fibril strength and stiffness. This was expected to improve inter fibril interactions inside cell wall structure. (Nilsson et al., 2010)

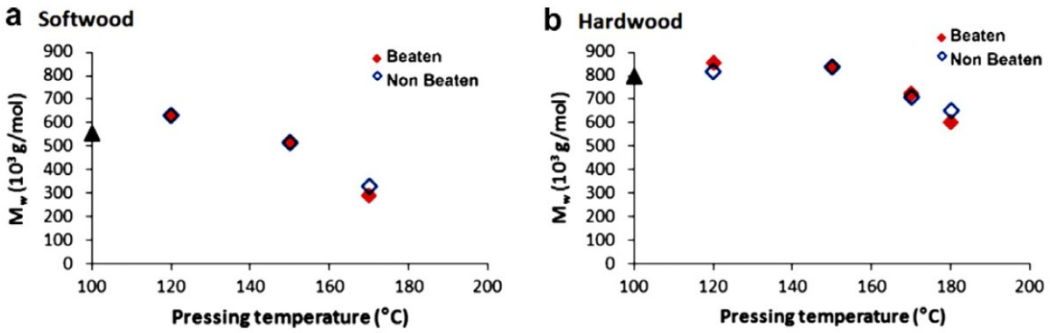

Figure 2.13. *SEC: weight average molar mass (M_w) of plates made of (a) softwood pulp (95.8% cellulose) and for (b) hardwood pulp (97.7% cellulose) versus press temperature (20 minutes). Black filled markers represent reference pulp. (Nilsson et al., 2010) Significant decrease in molar mass is observed at temperatures exceeding 150 °C.*

However, in wood, heating the composite structure results in formation of acetic acids by hydrolysis of acetylated hemicellulose at elevated temperatures (ThermoWood, 2003 ;Altaner & Jarvis, 2008). This is supported by pyrolysis data in Figure 2.12 since hemicellulose is the first wood constituent to experience great thermal degradation. The acids formed from hemicellulose catalyse hydrolysis of cellulose in its amorphous regions, breaking cellulose chains into shorter components. (ThermoWood, 2003). This can explain fingings of Liu et al. (2014) for wood flake specimens (50–70 mm in length, 7 – 10 mm in width and 0,5 – 0,6 mm in thickness) subjected to heat treatment of 80 °C for 24 h under ambient pressure. Results for heat treated and untreated samples are compiled in Table 2.1.

Table 2.1. *Tensile test results for wood flake (WF) samples in axial and transverse directions. Heat treatment is indicated with (H) (Liu et al., 2014).*

Sample	Elastic modulus E (GPa)	Ultimate tensile strength σ_f (MPa)	Strain to failure ε_f (%)
WF Axial	**6,4** ± 0,8	**49** ± 13	**1,3** ± 0,9
WF Axial (H)	**6,5** ± 1,8	**45** ± 7,0	**1,0** ± 0,2
WF Transv.	**0,3** ± 0,1	**2** ± 0,8	**1,3** ± 0,3
WF Transv. (H)	**0,6** ± 0,3	**1,3** ± 0,2	**0,7** ± 0,2

The results show only slight increase in elastic modulus between heat-treated and untreated samples in axial direction but great increase is seen for transverse samples. Ultimate tensile strength and values of elongation to failure suffer in both in axial and transverse direction. The team attributed these developments to reduced water content in the samples during heat treatment, while other factors were dismissed. (Liu et al., 2014) However, lignin deteriorates over a wide temperature range, and, as the treatment was performed for an extended period of time, lignin-bound structures was likely to be affected.

2.2 Cellulose nanoparticles

Cellulose nanoparticles, also referred to as nanocellulose, are a group of different discrete units of cellulose measured in nanoscale. Research in this field is already well-established with earliest publications and patents dating back to early 1980's (Siro & Plackett, 2010). However, research on cellulose and its nanoparticles has been extensive during past decades (Chirayil et al., 2014). These particles are of great interest since they have high aspect ratio and tensile properties but low density. (Moon et al., 2011; Liu et al., 2014) They make excellent constituents in many polymer matrixes and also perform well as films and fibers. As nanocellulose is discussed further, emphasis will be on cellulose obtained from wood fibers.

Cellulose nanoparticles can be extracted from organisms such as algae and bacteria (bacterial cellulose) in small quantities or they can be produced typically from pulp by either chemical or mechanical treatment (Siro & Plackett, 2010). Many nanocellulose preparation methods have been developed or improved, and subsequently, there are different grades of man-made cellulose nanoparticles varying e.g. in morphology, size and aspect ratio. (Moon et al., 2011; Sehaqui et al., 2011) Nanocellulose particle types refined and acquired from wood are listed in Table 2.2.

Table 2.2. *Compilation of man-made cellulose nanoparticle dimensions, their crystallinities and preparation methods reported in literature. Properties with wide value range depend source of cellulose in addition to manufacturing method. Cellulose microfibril found in wood is presented for reference purposes.*

Particle type	Length (µm)	Diameter (nm)	Crystallinity (%)	Preparation method	*Reference*
Microfibrillated cellulose (**MFC**)	0,1 - 10 <	10 - 100	51 - 69	Mechanical treatment (pulp)	*1, 2, 3*
Microcrystalline cellulose (**MCC**)	1 - 50	15(*nm)* - 50*(µm)*	80 - 85	Acid hydrolysis (pulp)	*1, 2, 3*
Nanofibrillated cellulose (**NFC**)	0,2 - 2	4 - 30	-	Mechanical treatment (pulp)	*1, 3*
Cellulose nanocrystals (**CNC**)	0,05 - 0,5	3 - 50	54 - 88	Acid hydrolysis (pulp, MFC, MCC, NFC)	*1, 3*
Cellulose microfibril (**CM**)	10	2 - 10 <	43 - 65	Biosynthesis	*2, 3*

References: 1 - (Moon et al., 2011) 2 - (Siro & Plackett, 2010) 3 - (Sehaqui et al., 2011)

It is essential to acknowledge that particle names and their abbreviations vary depending on source in literature. Cellulose nanocrystals are sometimes referred to as nanocrystal-

line cellulose, cellulose whiskers, cellulose nanowhiskers and cellulose microcrystal. In addition, terms for NFC and MFC are occasionally confused and incorrectly used to describe one another. (Moon et al., 2011)

Scale and morphology differences between cellulose nanoparticle types compiled in Table 2.2 are illustrated with electron microscope micrographs in Figure 2.14.

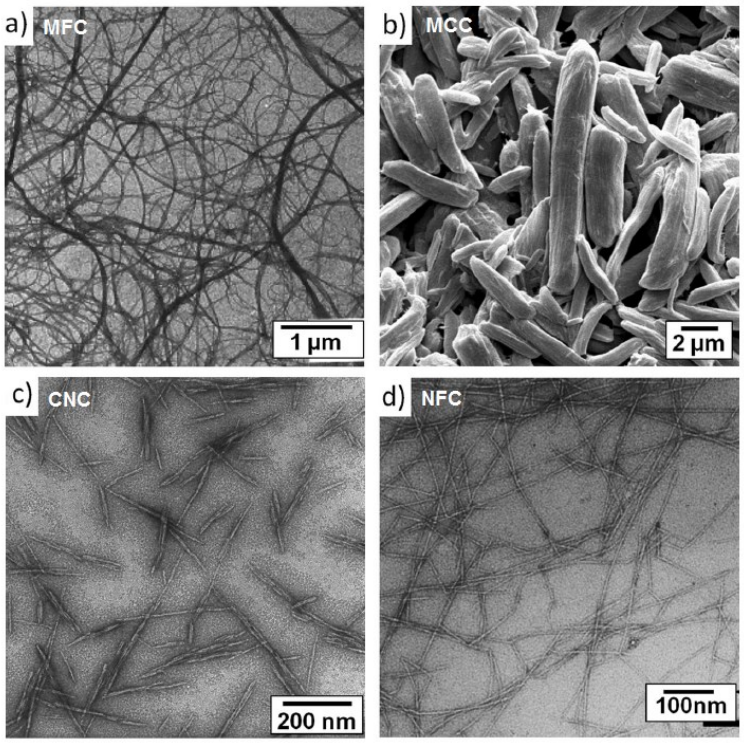

Figure 2.14. *(a) TEM image of MFC, (b) SEM image of deagglomerated MCC, (c) TEM image of CNC and (d) TEM image of TEMPO (2,2,6,6-tetramethylpiperine-1-oxyl) treated NFC (Moon et al., 2011)*

Today, both manufacturing of MFC and NFC is usually done by mechanical treatment in which diluted pulp fibers are first refined by directing them several times through a gap of grinding stone disks (rotor and stator) with surface grooves and bars (Siro & Plackett, 2010). In this step, external fiber cell walls are peeled off and then cellulose rich fibers are fibrillated both externally and internally. Dilute and filtrated cellulose slurry then goes through homogenization step. A high-pressure pump coupled with a spring-loaded valve assembly or a microfluidizer can be used in this process. (Moon et al., 2011; Siro & Plackett, 2010; Chirayil et al., 2014)

The outcome of mechanical treatment and its tremendous energy consumption can be affected with pre-treatment of fibers. Fiber treatment with alkaline solutions solubilises lignin, pectin and hemicellulose thus facilitating separation of cellulose (Chirayil et al., 2014). Alkali treatment can also induce cellulose degradation and even change its crystalline type from I to II (Bhatnagar & Sain, 2005). Cellulose can also be surface treated with 2,2,6,6-tetramethylpiperine-1-oxyl (TEMPO) radicals, which introduces carboxylate and aldehyde functional groups to cellulose surface structure.

These polar negatively charged functional groups experience strong electrostatic repulsion which facilitates defibrillation of the cellulose structure. This method may also cause changes to cellulose crystal structure based on required alkaline conditions. (Chirayil et al., 2014) Third method of pre-treatment is to use cellulose degrading enzymes, cellobiohydrolases and endoglucanases that can modify cellulose. Using enzymes has proven to preserve most of native celluloses properties (Siro & Plackett, 2010).

In essence, a more straight forward approach to acquire cellulose nanoparticles is to use acid hydrolysis in which applied acid, typically sulphuric acid, removes the amorphous regions of microfibrils. After the treatment, mixture of cellulose (Table 2.1) and acid is washed to remove remaining acid. (Moon et al., 2011)

Experimentally obtained strength properties for individual cellulose nanofibers are scarce but by using Raman spectroscopy, axial elastic moduli of 21-29 GPa and 57-105 GPa have been obtained for microcrystalline cellulose and nanocrystalline cellulose particles respectively. (Rusli & Eichhorn, 2008; Mark, 1968) However, strength properties for films prepared from nanocellulose particles are more relevant for the purposes of this research.

2.2.1 NFC films

Cellulose nanoparticles are used to produce films from low solid content suspensions (0,05 – 5 wt-%) usually by casting on a suitable surface followed by evaporation of medium (typically water). When water is removed from the cellulose-water gel, cellulose nanofibers form dense structure with network of hydrogen bonds. To improve film density and evaporation, mechanical pressing, vacuum filtration and freeze-drying methods may be used. (Lavoine et al., 2012) Acquired films generally have great strength properties, which are affected by used raw material, particle production process (i.e. particle pre-treatment discussed earlier), film preparation method and drying conditions (Kumar et al., 2014). Once films are dried, they cannot be redispersed due to extensive hydrogen bonding (Lavoine et al., 2012).

A film sample of NFC prepared from eucalyptus pulp by TEMPO oxidation and microfluidisation yielded elastic modulus of 15,8 ± 3 GPa and tensile strength of 179 ± 55 MPa (Liu et al., 2014). Similar elastic modulus of 14,2 GPa and a greater tensile strength of 256 MPa were obtained using carboxymethylation pretreatment for NFC film (Aulin et al., 2012). In a study done by Kumar et al. (2014), TEMPO treated soft- and hardwood pulp was used to produce NFC films with elastic moduli of 10,7 ± 0,6 GPa and 10,7 ± 0,3 GPa, and tensile strength of 151 MPa and 136 MPa respectively. Compared to NFC films, films prepared from MFC can have tensile strength range from 30 to 155 MPa increasing with the number of times the slurry is fibrillated. This also applies to films of NFC. (Moon et al., 2011; Kumar, et al., 2014)

NFC films are commonly refined from bleached kraft pulp (Lavoine et al., 2012). Therefore, these films are mainly comprised of cellulose and hemicellulose. Thermal properties of NFC films are subsequently dependent on hemicellulose. However, chemical pretreatments during nano particle preparation can also affect these properties by changing cellulose surface chemistry (Lavoine et al., 2012). NFC films have large specific surface area and nanoscale pores causing them to have high affinity with water (Lavoine et al., 2012). Nanocellulose films also have significant amount of moisture in their structure after drying. Moisture contents of 9,36 - 9,80 have been obtained for NFC films prepared by casting and evaporation at temperature of 23 °C and relative humidity of 50 % over five days (Kumar et al., 2014). Adsorbed and contained water serves as a plasticizer, lowering tensile strength and modulus of a film but increasing strain to failure (Liu et al., 2014).

2.3 All-Cellulose composites

The pursuit of enhancing matrix-reinforcement material interface has led to recent development and discovery of self-reinforcing polymer composites such as the all-propylene composites (Peijs, 2003; Soykeabkaew, 2007). These composites are typically prepared by impregnating reinforcing material (e.g. fibers) with a matrix material with a slightly lower melting temperature (Soykeabkaew, 2007). For fiber reinforced structures, selective melting of fiber surfaces may be used in which only fiber surfaces melt during heating thus 'welding' fibers together (Soykeabkaew, 2007). These single polymer composites are easily recyclable due to their uniform composition, making them environmentally friendly (Soykeabkaew, 2007) without being bio-based. A natural step forward is to apply similar aproach to cellulosic materials in the form of biodegradeable all-cellulose composites.

Interestingly, as stated in the introduction to this subject, all-cellulose composite fabrication isn't a new concept. Hazardous zinc-chloride solution has been used since the 1800s to partially dissolve paper fibers into 'vulcanized fibers' and produce dense all-cellulose composite with tensile strength of ~100 MPa and modulus of ~7 GPa (Nilsson et al., 2010). In more recent works, partial dissolution of cellulose in a filter paper is achieved using combination of *N,N'*-dimethylacetamide and lithium chloride solutions (LiCl/DMAc). Subsequently compressed filter paper sheet was obtained with tensile strength of 211 MPa and elastic modulus of 8,2 GPa (Nishino & Arimoto, 2007). The tensile properties were greatly increased when compared to unmodified filter paper.

Soykeabkaew (2007) prepared a more interesting ACC from sheets of bacterial nanocellulose (produced by *Acetobacter xylinum* bacterial strain) that were first compressed under pressure of 0,25 MPa at a temperature of 115 °C for 5 minutes. These assemblies were then pretreated, and then immersed in LiCl/DMAc (8% lithium chlo-

ride) solvent with varying immersion times to provide different degrees of dissolution of cellulose. This joining method is referred to as partial dissolution which will be discussed in section 2.4. BC nanocomposite (ACC) immersed for 10 minutes yielded tensile strength of 411 MPa and elastic modulus of 18 GPa compared to an untreated neat BC film with tensile strength of 400 MPa and elastic modulus of 20 GPa. Further dissolution resulted in higher elongation at break but also in deteriorated tensile strength and modulus. Some of the prepared all-cellulose composites are featured in Figure 2.15.

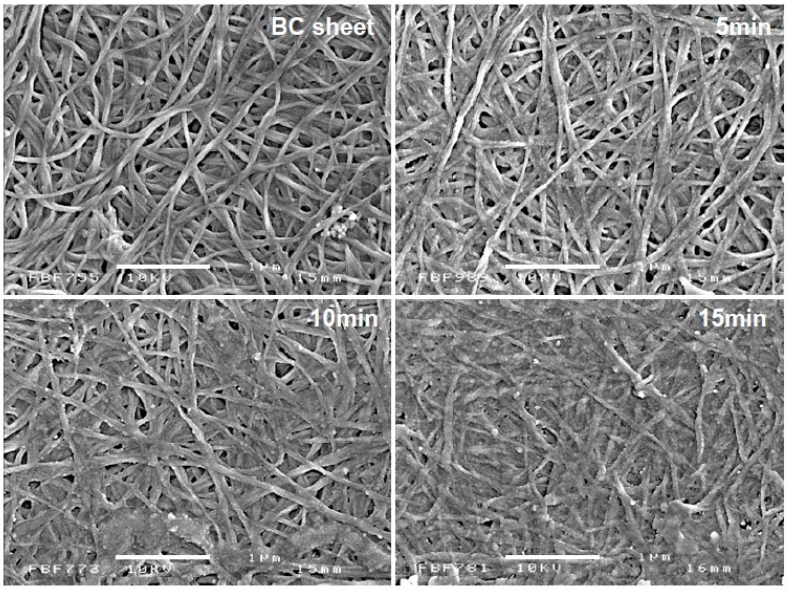

Figure 2.15. *SEM micrographs of all-cellulose composites produced from bacterial cellulose with varying immersion times. Image in the top left corner is of unmodified BC film. Scale bar represents 1 µm (Soykeabkaew, 2007).*

Ionic liquid dissolution method was also used to prepare fiber-reinforced all-cellulose laminate composites from cellulosic textiles by Huber et al. (2012). Four layers of chosen textile (rayon and linen) were hand-impregnated with 1-butyl-3-methylimidazolium acetate (BMIMAc) ionic liquid equal to average weight of each layer. These plies were then stacked, placed between aluminum plates and then pressed in a hot press at 110 °C for 60 minutes in 1,5 MPa pressure and 20 minutes in 2,5 MPa pressure. The samples were then washed in a bath of distilled water for 24 hours to remove the ionic liquid after which the sample was kept in distilled boiling water for 48 hours. After washing, the samples were dried under constant pressure of 0,5 MPa. Tensile testing along with SEM micrographs indicated substantial fiber-matrix adhesion: The produced ACC rayon laminate had tensile strength of 70,16 MPa while untreated rayon textile was tested to have tensile strength of 36,67 MPa.

Similar dissolution method was used recently by Duchemin et al. (2016) for MFC films made from enzymatically pretreated pulp and for filter papers. After pretreatment with NaOH, the films and filter papers were immersed with 7 wt-% NaOH and 12 wt-% urea solution for a duration. Dissolution was done in a freezer for 20 and

40 minutes after which samples were dried under 10 kPa pressure and 25 °C temperature for 12 hours in a vacuum oven. Changes in morphology of the MFC induced by dissolution can be seen in Figure 2.16 SEM micrographs.

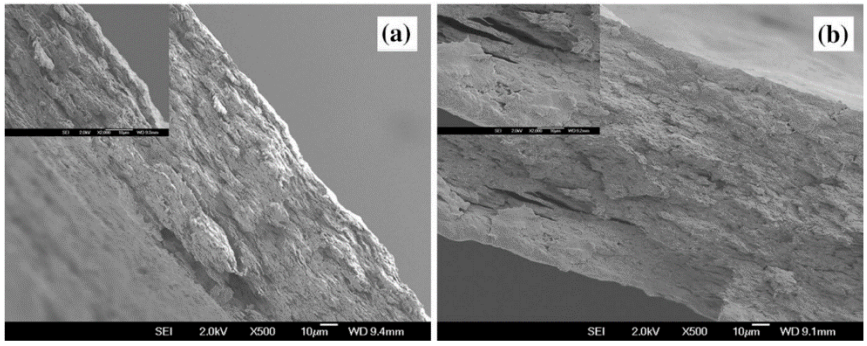

Figure 2.16. *SEM micrographs of fracture surfaces of (a) MFC film and (b) All-cellulose composite made from MFC with 40 min dissolution time. (Duchemin et al.,2016)*

Surprisingly, in tensile testing, the mechanical properties of the composites made from MFC were seemingly adversely affected by the dissolution time. Filter paper composite samples on the other hand benefited from extended immersion time in terms of tensile properties. These developments are better observed from Figure 2.17.

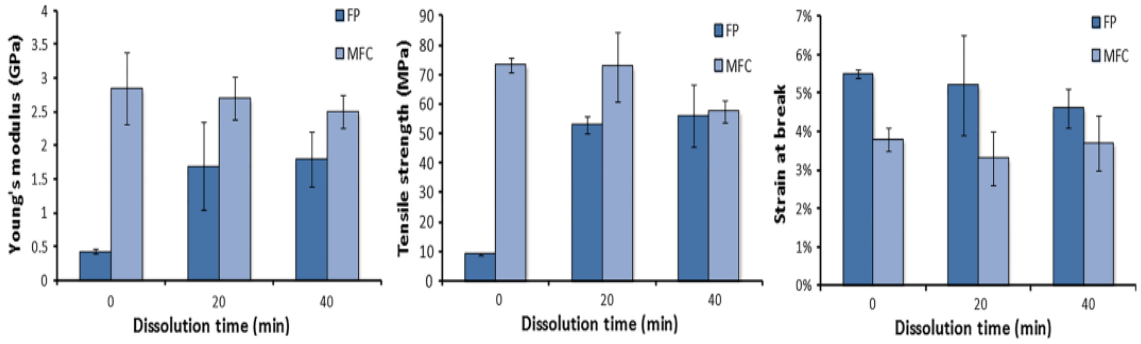

Figure 2.17. *Results of tensile testing for all-cellulose composite samples prepared from filter paper (FP) and Microfibrillated cellulose (MFC). (Duchemin et al., 2016)*

The team attributed the decrease in Young's modulus to loss of crystallinity compensated by consolidation. (Duchemin et al., 2016)

Despite the apparent advantages of dissolution methods, there are significant issues associated with solvents that also concern commercialization and process up scaling. Operational, economical and safety challenges cannot be dismissed since there is still no consensus about the most appropriate cellulose solvent. (Soykeabkaew, 2007; Gardner et al., 2008) Also, use of solvents will likely reduce adoption of all-cellulose composites as eco-friendly materials (Halonen, 2012). In addition, solvent based methods include several steps such as chemical pretreatments, washing and recovery of used

chemicals which further complicate these methods (Soykeabkaew, 2007; Aulin et al., 2012).

Preferable alternative ACC preparation method is to use a non-solvent approach. This usually achieved by using water as the sole processing aid, but also by exploiting good bonding capabilities between cellulose bodies.

Simple paper laminate structures were prepared from sheets of paper that were bound together by impregnating them with chemical free nanofibrillated cellulose suspension before assembly (Shivyari et al., 2016). In this study conducted by Shivyari et al. (2016), two different NFC-suspension-immersed paper sample types were prepared for 180° peel test and for tensile test: Two strips pressed together and dried under a weight, and a 25-layer laminate made by folding two long strips of paper that were cold pressed and then hot pressed with varying press temperature and time. Maximum tensile strength of 52 MPa and elastic modulus of 8,9 GPa were obtained for the folded laminate samples pressed at 180 °C for 3 minutes. Sample preparation and results for the peel test are represented in Figure 2.18.

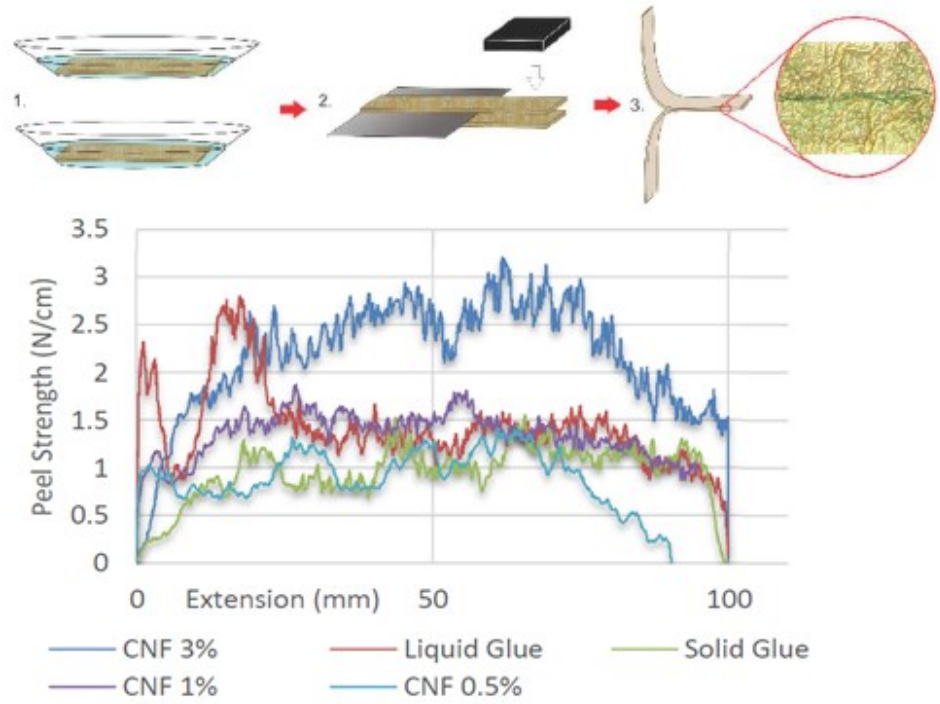

Figure 2.18. *(Above): Illustration of samples of paper strip laminates that were joined together using NFC-water suspensions and (Below): Peel test data for samples with different concentrations of NFC used: 0.5% NFC (light blue), 1% NFC (purple), and 3 % NFC (dark blue). Solid paper adhesive (green) and liquid paper adhesive (red) were used as a reference. (Shivyari et al., 2016)*

The results in Figure 2.18 suggest that cellulose nanoparticles can work as a competitive binding method for all-cellulose composites. Cellulose binder provides great strength to the interface throughout the test. Initial peel strength (t = 0), however, doesn't compare with commercial liquid glue.

NFC cellulose was also used in combination with bleached sulphite softwood pulp fibers by Sehaqui et al. (2011). In this study, a hot press was used to dry NFC-wood fiber slurry between two filter papers at a temperature of 93 °C under pressure of 70 mbar for 12 minutes. Structure of these materials consisted of collapsed wood fiber network with NFC particles adsorbed to the fiber surfaces. The nanofibrillated particles also contributed to filling micro-scale pores in the structure, improving load transfer between fibers. This is illustrated in FE-SEM micrographs in Figure 2.19. The tensile tests of samples provided modulus and tensile strength of 10±2 GPa and 165±16 MPa for reinforced paper containing 10% NFC. For reference, neat wood fiber sample (0% NFC) yielded a modulus of 8,1 ± 1,2 GPa and a tensile strength of 97,5±15 MPa. (Sehaqui et al., 2011)

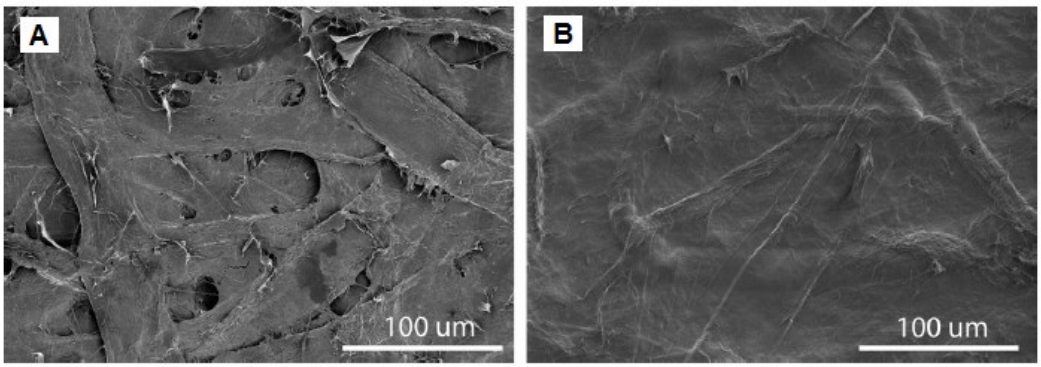

Figure 2.19. *FE-SEM micrographs of (a) 0 % NFC reference sheet and (b) 10 % NFC containing wood fiber-NFC composite (Sehaqui et al., 2011).*

Another solvent-free ACC prototype was manufactured by Nilsson et al. (2010). In their study, high cellulose content wood pulp was beaten and used to prepare paper sheets with random fiber orientation. The sheets were first cold pressed and then compression molded in a press with adjustable temperature. The samples were then subjected to pressure of 45 MPa for 20 minutes. Steps of this process are better illustrated in Figure 2.20. Ultimate tensile strength of 76 MPa was achieved at maximum temperature of 180 °C. Maximum elastic modulus of 12,8 GPa was obtained at 150 °C. In addition, the press temperature reportedly had adverse effect on strain to failure decreasing from 10,5 % to 1,7 % in range of ambient 20 °C to 180 °C. The team suggests increasing temperature introduces higher amount of fibril aggregation which is made possible by the reduced individual fiber strength, i.e. lowered cellulose weight average molar mass, which was pointed in Figure 2.13. Increased aggregation leads to improved cellulose-cellulose hydrogen bonding and ultimately to improved strength. CP/MAS ^{13}C NMR spectra of compression molded pulp at 170 °C showed no change in crystallinity but less accessible area for water molecules meaning crystalline ordering was not affected by heat treatment.

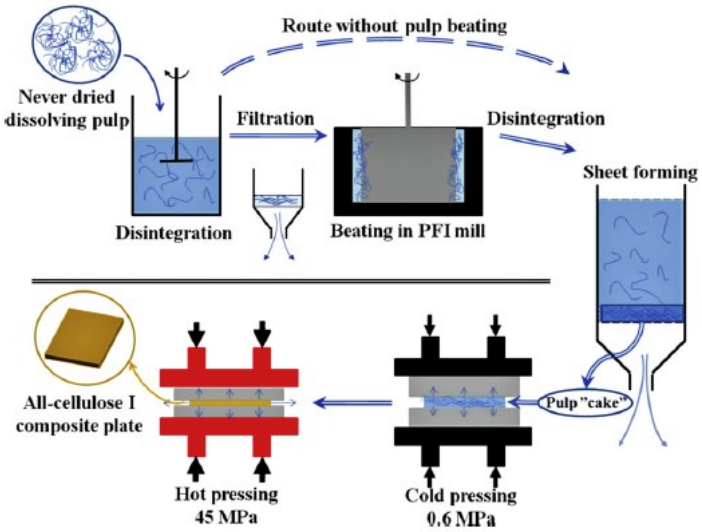

Figure 2.20. *Schematic presentation of the process of making ACC from beated pulp (Nilsson et al., 2010).*

Very similar method was used by Arévalo & Peijs (2015) to create all-cellulose fiber boards. Despite technically not being composites, their results and findings are of great relevance. Cut flax fibers (70 % cellulose, 16 % hemicellulose and 2 % lignin) were used as raw material. The fibers were mechanically refined in a beater forming extensively fibrillated fiber pulp. Plates were manufactured after dewatering combination of cold press (10 bar, ambient), and three-step hot press. Initial hot pressing of 40 bar at 140 °C was applied for 25 minutes, after which pressure was increased to 80 bar for another 25 minutes maintaining temperature. Lastly, temperature was let to cool down to ambient temperature while maintaining 80 bar pressure. An example of prepared all-cellulose plate is shown in Figure 2.21.

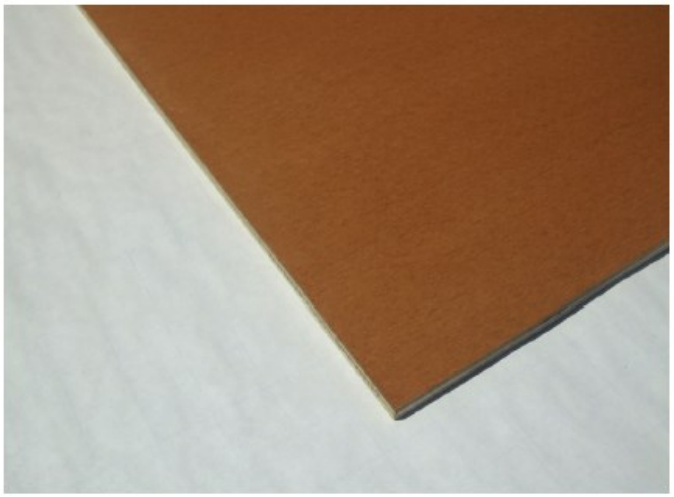

Figure 2.21. *An all-cellulose plate prepared from beated flax fibers with a combination of cold and hot pressing (Arévalo & Peijs, 2015).*

Only flexural modulus and strength were targeted in their research. For refinement time of 6 hours, flexural modulus of 7.5 ± 0.2 GPa and strength 85 ± 4 MPa were obtained. The team attributed strength of these produces plates to the extensive fibrillation of flax fibers suggesting that fibrils of an individual fiber occupy voids in surrounding network structure and that they also become entangled with other fibrils of other fibers. Effect of heat treatment on resulting structure and its properties was excluded from this study.

Binder free all-cellulose composites were fabricated by Zhou et al. (2011) from a mixture of cotton stalk fibers and enzymatic hydrolysis lignin (EHL). 10 % of EHL was combined with fibers and formed into sheets by a forming box and then into a solid plate by hot-pressing each specimen (60 s/mm; 5,0 MPa) at a chosen temperature: either at 170, 190 or at 210 °C. A number of finished plates were cut into specimen that were tested for internal bond strength (IBS). Results of these tests are presented in Figure 2.18.

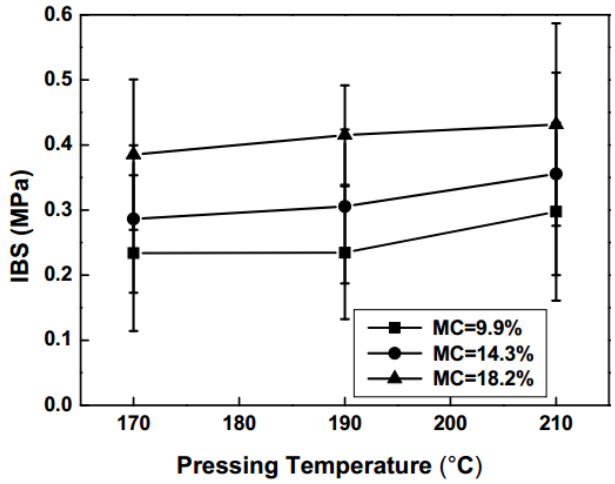

Figure 2.22. *Tests for internal bond strength (IBS) for three different binderless fiber board grades with different moisture content (MC) as a function of pressing temperature (Zhou et al., 2011).*

The reported results indicate greater internal bond strength at higher fiber moisture content. The team attributed this to the lowered softening temperature (glass transition temperature T_g) of lignin. Also, IBS is clearly more sensitive to changing temperature in the 170-190 °C temperature range at moisture content 18,2 % than at lower ones. I was also claimed that pressing temperature combined with higher moisture content would lead to plasticization of the fibers and result in higher density boards. (Zhou, ym., 2011) Lignin at cellulosic surfaces have previously been shown to soften and partake in lignin-lignin molecular entanglement with possible formation of covalent bond formation (Okuda et al., 2006).

2.4 Swelling and partial dissolution of cellulose

It is essential to know mechanisms of swelling and dissolution phenomena since most of the reviewed studies on all-cellulose composites have included processing aids in the form of water and solvents. Water will be at primary focus in the discussion of cellulose swelling and its characterization. Dissolving will be briefly discussed to explain the difference between the two phenomena.

Swelling of cellulose

The swelling phenomenon is the first stage of polymer dissolving process (Wertz et al., 2010) and its a combination of diffusion of solvent into the solute and solute into solvent. However, due to the size difference between solvent molecule and the solute, the diffusion into soluble material is dominant (Sperling, 2006). For cellulose, there are many swelling reagents, but some of them, like water, can penetrate only the amorphous regions of cellulose. This type of swelling is called intercrystalline swelling. More potent chemical reagents can penetrate cellulose crystal structure causing intracrystalline swelling. (Wertz et al., 2010) It is therefore logical that samples with high cellulose crystallinity will yield lower swelling results than those with lower crystallinity. Native cellulose fibers that are (crystal type I) swelled in water can yield an increase in cross-sectional area of 20 – 35 % while regenerated fibers (type II) show increase in range of 55 to 70 % (Wertz et al., 2010).

Cellulose water accessibility is evaluated by studying cellulose water sorption isotherms. Extensive studies have confirmed that cellulose can adsorb water in two ways. Water molecules are chemically adsorbed to accessible hydroxyl groups in amorphous regions and cellulose crystal surfaces. Secondly, water is physically sorbed through capillary condensation in the pores of the cellulose structure. These pores are further enlarged by the sorption and swelling process. (Wertz et al., 2010) This intercrystalline swelling can be evaluated using e.g. water retention value (WRV) or quartz crystal microbalance with dissipation (QCM-D) (Aulin, et al., 2009; Niskanen, 2008).

Cellulose-water interactions are essential for cellulose processing but also for the all-cellulose composite preparation. And as mentioned, the cellulose-water interactions are dependent on cellulose supramolecular structure, but also on chemical composition of cellulosic material (Wertz et al., 2010; Niskanen, 2008). Therefore, swelling behaviour of two cellulose structures will reviewed: Nanofibrillated cellulose film of neat cellulose, and a wood fiber containing lignin and hemicellulose. These are expected to serve as model surfaces for this thesis and give insight into water-cellulose interactions in composite preparation and explain how swelling will influence adhesion between cellulosic surfaces.

Ahola et al. (2008) studied model surfaces of cellulose by QCM-D using films of low charge (LC) and high charge (HC) density nanofibrillated cellulose. LC-NFC film was reported to be representative model for native cellulose surface. These films were formed by spin-coating cellulose dispersions onto smooth silica wafers. When water was introduced onto film surfaces, an increase in frequency was observed, indicating lightening of the film. This lightening phenomenon was attributed to desorption of loosely bound fibrils, since no loss of film coverage of the wafer was observed with subsequent AFM imaging (Ahola et al., 2008). These desorbed fibrils are the result of hydrogen bond breakage between cellulose and formation of new hydrogen bonds between introduced water molecules and cellulose (Wertz et al., 2010). This fibril desorption is facilitated by thermal energy that lowers the energy gap of breaking cellulose-cellulose hydrogen bonds (Nilsson, et al., 2010). Cellulose fibril desorption was also observed in an earlier study by Neuman et al. (1993) when studying MCC films produced by acid hydrolysis using trifluoroacetic acid (TFA). The team concluded from surface force and adhesion measurements that when immersed in water, desorbed cellulose fibrils extend outward from the film surface (Figure 2.23).

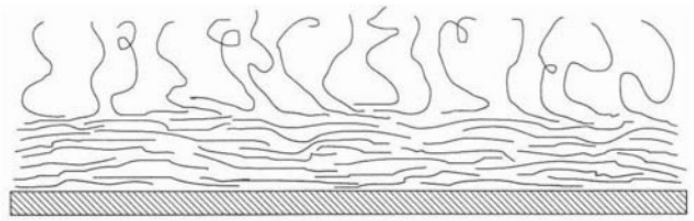

Figure 2.23. *Proposed structure of swollen cellulose surface. (Neuman et al., 1993)*

Ahola et al (2008) also measured surface interactions in the form of pull-off forces between the nanofibrillated cellulose films and cellulose spheres at pH 8. The surface forces between separating surfaces suggested that tiny cellulose fibril ‘tails’ of both unlike bodies become entangled when the surfaces are pressed together. The effect of this entanglement was reported to be increased by swelling of the surfaces. The desorbed fibrils are therefore likely to entangle or bond with neighbouring fibrous cellulose structures (Niskanen, 2008). This phenomenon is later referred to and discussed in section 2.5.

The swelling degree of wood fibers is significantly different than that of neat cellulose surface. The chemical composition of wood fibers depends on hemicellulose and lignin present in the structure. Hemicelluloses facilitate fiber swelling while lignin inhibits it. (Niskanen, 2008)

Partial dissolution of cellulose

After a solvent diffuses into both crystalline and amorphous structure of the polymer producing a swollen gel, the polymer can be dissolved into a true solution (Wertz et al., 2010). Unlike in swelling, in cellulose dissolution the original supramolecular structure is destroyed (Zhang et al., 2011). In the case of cellulose, and as discussed before, dissolved native type I cellulose will after precipitation in water form regenerated cellulose II and have completely different crystalline structure, but also distinctive mechanical and physical properties (Moon et al. 2011; Flink et al. 2001). The extent of dissolution can be restricted by controlling the time cellulose is immersed in the solvent. Dissolution then occurs only at the surfaces of solute morphological geometries i.e. fibers and films, leaving portion of the cellulose structure in its original form. In composite applications, this means that these the true solutions from dissolved surfaces can mix and meld together forming exceptionally strong interface after precipitation. This type of dissolution is referred to as partial dissolution or surface selective dissolution. (Soykeabkaew, 2007)

All-cellulose composites have been prepared from fibers using partial dissolution (Soykeabkaew, 2007; Lu et al., 2003; Soykeabkaew et al., 2008). In these experiments, cellulose bundles of parallel fibers were immersed in a solvent for controlled ammount of time, then washed and finally let to dry. In these coagulated bundles the regenerated surface cellulose serves as a uniform matrix while the untreated fiber core structures reamain as the fiber reinforcement of the composite structure. The interface is secure with strong interactions between the phases. (Soykeabkaew et al., 2008). It is also suggested that the regenerated cellulosic matrix can co-crystallizes on the undissolved cellulose type I surfaces (Duchemin et al., 2016). This process and the schematic of ACC structure are featured in Figure 2.24.

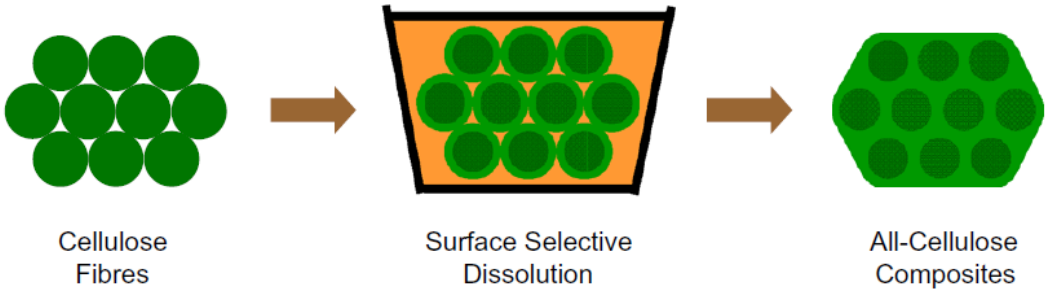

Figure 2.24. *Schematic of partial (surface selective) dissolution of aligned cellulose fibers with controlled immersion time. (Soykeabkaew et al., 2008)*

Another example of partial dissolution, discussed earlier in section 2.3, is presented in Figure 2.21. Fibers of filter paper were partially dissolved during sheet immersion in a solvent (Nishino & Arimoto, 2007).

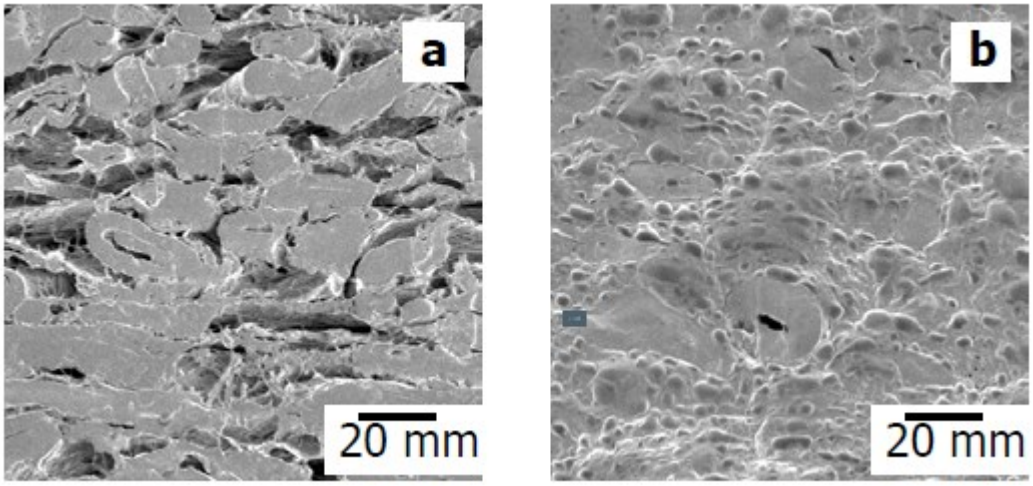

Figure 2.25. *SEM micrograph of cross-section of (a) filter paper and (a) all-cellulose composite after 12-hour immersion and compression. (Nishino & Arimoto, 2007)*

The swelling and subsequent dissolution causes the dissolved cellulose fiber surfaces to fill voids with a continuous matrix that binds fibers together firmly (Soykeabkaew, 2007). Similar effect is expected to happen between two or multiple film-like structures if they are partially dissolved on the surface and subsequently pressed together.

Finally, it is important to differentiate the two types of solvents: non-derivatizing and derivatizing solvents. Non-derivatizing solvents dissolve cellulose only by intermolecular interactions while derivatizing solvents systems dissolve cellulose in combination with the formation of an unstable ester, ether or acetal derivative. Both of these solvent types are either aqueous or non-aqueous. For instance, typically used non-derivatizing organic solvent, N-methyl-morpholine-N-oxide (NMMO) is non-aqueous. (Wertz et al., 2010)

2.5 Mechanisms of adhesion between cellulosic surfaces

The adhesion between cellulosic surfaces is a complex and not completely understood phenomenon (Delgado Fornué et al., 2011; Eriksson, 2006). It is, however, of great importance for current and future use of cellulose in composite applications (Gardner et al., 2008). For long it has been thought hydrogen bonds to be the sole contributor to inter fiber strength in paper products (Delgado Fornué et al., 2011). Recently, several theories have been proposed to describe adhesion phenomenon, but has become clear

that no single theory can provide individually satisfactory explanation (Delgado Fornué et al., 2011). It has been therefore suggested that the present theories and mechanisms overlap, simultaneously affecting adhesion and each other (Gardner et al., 2008). Main theories to describe adhesion between cellulosic surfaces are mechanical interlocking, adsorption or wetting, intermolecular diffusion and chemical interactions (Delgado Fornué et al., 2011; Eriksson, 2006; Gardner et al., 2008).

In mechanical interlocking the adhering material or the adhesive becomes entangled within irregularities and pores of a surface (Gardner et al., 2008). In swollen state, this effect is facilitated by intermolecular diffusion between the bound surfaces or between two surfaces, which is based on the thermodynamics of mixing (Hubbe, 2006). In essence fibrils of cellulose with increased mobility (induced by temperature and moisture content) can penetrate the opposing surface and become entangled through random steps of molecular motion in suspension, forming a mixed region that is referred to as interphase (Hubbe, 2006; Zhao & Kwon, 2011; Kanerva, 2014). The intermolecular diffusion process is accelerated when temperature is above the glass transition temperature of the polymer making chains, and subsequently fibrils more mobile (Zhao & Kwon, 2011; Nilsson et al., 2010). During drying and when water is removed e.g. during heat treatment in a hot press, capillary forces force fibrils and surfaces close to molecular contact (Delgado Fornué et al., 2011; Hubbe, 2006; Niskanen, 2008) Dehydration during drying is necessary to establish cellulose interfiber and interparticle bonds that are mostly close range chemical interactions that don't have strong influence in the presence of water. (Zhao & Kwon, 2011) Proposed visualizations of diffusion phenomenon are presented in Figure 2.26.

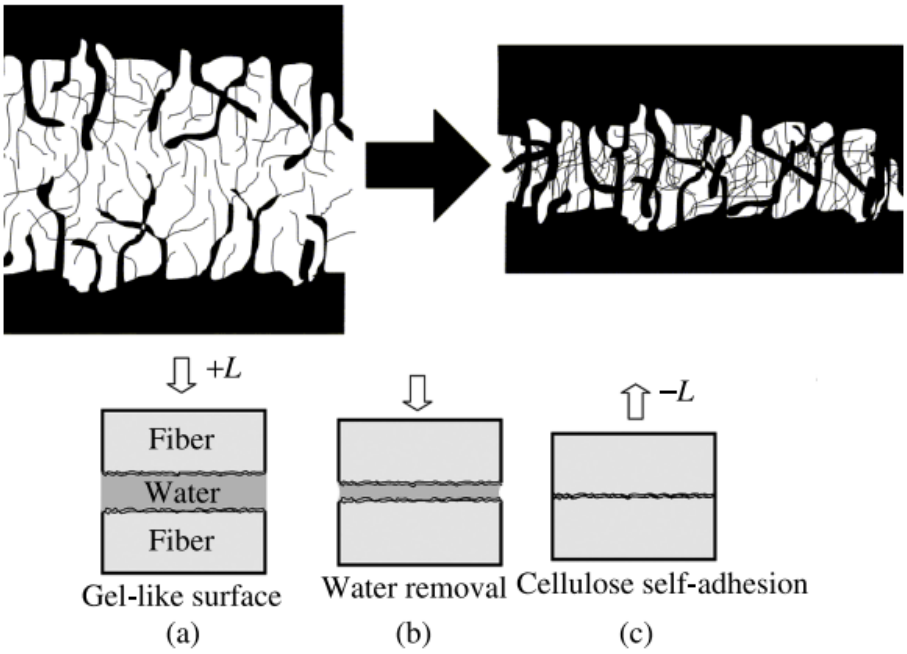

Figure 2.26. *Two conceptual illustrations featuring intermolecular diffusion. (Above): Diffusional mixing of macromolecular segments in swollen state (Hubbe, 2006). (Below): cellulose self-adhesion (Zhao & Kwon, 2011).*

Moving on to chemical interactions, which include acid-base interactions, electrostatic forces, van der Waals forces, and hydrogen bonding (Delgado Fornué et al., 2011). Out of these interaction types, only hydrogen bonding and van der Waals forces have a measurable bonding energy i.e. an individual bond provides a precise strength increment (Niskanen, 2008). These also have a measurable effective range and minimum distance for bond formation. Therefore, molecular contact is required for these interactions. (Delgado Fornué et al., 2011; Niskanen, 2008). Bonding energy of a hydrogen bond reportedly varies between 8 and 32 kJ/mol and the required formation distance ranges from 0,15 to 0,35 nm. Van der Waals forces are much weaker than hydrogen bonds with bonding energy at 2-8 kJ/mol but with a greater range extending from 0,30 to 0,5 nm. (Niskanen, 2008; Delgado Fornué et al., 2011) Although hydrogen bonds are much stronger, they are limited to available and accessible hydroxyl groups whereas van der Waals forces take effect in all directions (Niskanen, 2008).

Adsorption and wetting theories are related to localized intermolecular forces such as acid-base interactions, weaker dipole-dipole forces and van der Waals forces. The extent of the wetting phenomenon depends on differences in surface free energies of adhering surfaces (usually solid & liquid) and of their interface. Sufficient wetting of adhering liquid or polymer melt is a prequisite for good adhesion. (Gardner et al., 2008; Zhao & Kwon, 2011)

2.5.1 Characterization of cellulose self-adhesion

Adhesion between two polymers is most commonly evaluated by the interface resistance to applied mechanical force in either normal or lateral direction. Mechanical stress is difficult to apply directly to the interface. Therefore, force is imposed from a distance in certain mechanism so that a crack starts to propagate along the interface when certain amount of force is applied. (Zhao & Kwon, 2011) Three different types of adhesion tests are presented in Figure 2.27. For the purposes of this thesis, peel adhesion testing (c) was selected to characterize our laminate all-cellulose composites.

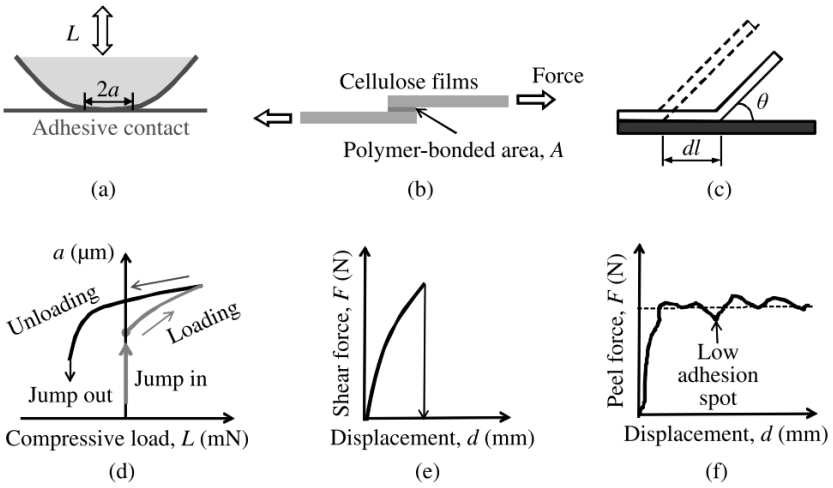

Figure 2.27. *(Above): Three typical adhesion tests: (a) JKR-contact adhesion testing, (b) single-lap shear testing and (c) peel adhesion testing. (Below): Expected test force curves: (d) JKR-type plot of contact radius a vs load L, (e) shear force vs displacement curve and (f) peel force vs displacement (or peel distance) curve. (Zhao & Kwon, 2011)*

The peel test is classified as a destructive test; it provides relatively low force for separation of two surfaces. The method also provides useful intricate data about the interface due to the sensitivity of the system. Spots of lower adhesion (Figure 2.27, (f)) may be indicators for poor surface quality. (Zhao & Kwon, 2011) The output of the peel test strongly depends on the peel angle that is usually 90º or 180º. The 180º-peel test, also referred to as T-peel test, is well suited for separation of flexible thin laminate layers (Durgun & Bayram, 2005). The test yields a test curve often like one featured in Figure 2.27 (f) or in Figure 2.18. The plotted peel strength is either expressed in form of applied peel force (N) or as bond strength with load per width of a sample (e.g. N/cm).

3 EXPERIMENTAL

In this section the design, goals and the procedures of the experimental work are discussed and described.

3.1 Goals and design

The experimental work of this thesis was conducted towards two goals. First goal of the experimental work was to develop methods to produce simple strip like specimen for adhesion testing and study correlations between acquired adhesion and superstructure and also with known chemistry of a material. The second goal was to innovate novel all-cellulose composite structures from chosen materials.

To study the interfacial adhesion of a given material combination, a T-peel type adhesion test method was selected to be used in this work. Average initial peak bond strength values (N/cm) as well as bond strength (N) – displacement (mm) curves are reported. Many other aspects and procedures were inspired by and developed from previous studies discussed in section 2.3.

Due to the myriad of potential material-adhesive-material combinations, the work was chosen to begin with laminate specimen of only one type of material but with different adhesives. These types of tests are referred to as self-adhesions tests. These tests were primarily used to study the influence of the adhesive method and the structure type of a sample, such as influence of porosity or air permeance on acquired interfacial adhesion. Differences between self-adhesion results of two similar materials with different chemistries and adhesives would hint at specific surface and sub-surface interactions. Experience from self-adhesion tests would also later facilitate understanding and better preparation for challenges with samples with combination two unlike materials and fabrication of all-cellulose composite specimen.

Characterization of adhesion was done based on mechanical testing and known chemical properties of each composite materials and processing conditions. For example, it was of great interest which wood cell constituents were present in each composite constituent. SEM imaging was chosen to support observations and claims based on obtained adhesion results. Basic properties and glass transition temperature were also determined for nanocellulose film materials.

3.2 Materials & methods

The materials chosen for this thesis included two grades of enzymatically pre-treated nanofibrillated cellulose films (nanocellulose films), blotter paperboard, UPM New Future LASER copy paper, thin veneer sheets (Hollolan Viilu ja Vaneri), brown wrapping paper and foamed cellulose sheets produced at VTT. The two grades of nanocellulose films prepared at VTT were prepared from bleached pulp (white NFC) and from partially bleached pulp containing 10% lignin (brown NFC). Properties of the materials are listed in table 3.1. Millipore water, liquid glue (Erikeeper) and a diluted white HefCel-nanofibrillated cellulose suspension were used as processing aids.

Table 3.1. *Table of materials used in peel tests and ACC composite fabrication. Basic properties grammage and density were measured. In addition, air permeance and Bendtsen surface roughness were determined and listed to represent the porosity of test material.*

Material	Density (g/cm^3)	Grammage (g/m^2)	Air permeance (um/Pa×s)	Bendtsen (ml/min)
Copy paper	0,77	80	8,31	250
Cellulose foam (White / CTMP)	0,012	720	-	-
Nanocellulose film (White)	1,27	104	-	320
Nanocellulose film (Brown; 10% Lignin)	1,27	94	-	250
Blotter paper (Ref)	0,48	250	32,8	4100
Veneer	0,58	304	-	-
CTMP paper	0,45	92	11,6	1400

Air permeance could not be determined for cellulose fiber foam due to its thickness of supplied and compressed pieces. Veneer specimen could not be measured due to extreme surface roughness, and nanocellulose films were nigh permeable for the L&W air permeance tester.

In later stages of the self-adhesion study, to further study the effect of porosity on measured adhesion, special blank sheets were refined from reference blotter paper sheets by calendaring (No. of passes; nip pressure (N)) and hot-pressing (4 min; 110 °C). The refined planks were then used to prepare specimen similarly to the reference material as described in the "Self-adhesion" paragraph in the next section. The air permeance properties of these specimen are also discussed later in section 4.2.

Additional material characterization was done to the white and brown HefCel-nanocellulose film grade specimen in form of dynamic mechanical analysis (DMA). In

addition to DMA testing, a DSC analysis was also performed for the film specimen with Mettler Toledo Differential Scanning Calorimeter (model DSC2). Results of these tests are reviewed in section 4.1.

Four different testing and preparation methods needed to be developed for this work: one for self-adhesion tests, one for combination adhesion test, one for ACC beams and one for ACC panels.

3.2.1 Peel test: specimen preparation

Specimen for the peel test method could be divided into three groups: self-adhesion, combinations using cellulose fiber foam and combinations using thin veneer. Preparation procedures for each group type are described below.

Self-adhesion

Self-adhesion tests were designed with practicality in mind and with the inspiration from the work of Shivyari et al. (2016). It was decided to incorporate strip type samples for the flexible materials. Manual screw press with heated elements was used and pressing temperature of 110 °C was selected in accordance to most typical drying temperatures and due to the thin nature of the dual strip samples. Pressing time of 4 minutes chosen and it was tested to be sufficient with preliminary paper strip samples. Size of the sample strips (20 mm × 257,4 mm) was derived from the standard A4 sized copy paper sheet. Other material blanks were trimmed down to this size before the strips were cut. All sample strips were folded in half so that the same sides of the unlike two-sided samples were faced against eachother. For example, for a material with one side more rough than the other, the rough surfaces were used. For materials with two sided surface roughness, the more rough side was used for joining. Samples were weighed at different stages of the procedure starting from the conditioning.

Before processing aid application, a precut piece of aluminum foil of exactly 45 mm in length was placed on the other side of the fold. The remaining edges of the foil were folded over the edges over the sample. The sample was then brought to application, where a simple transparency was used to limit the application of the desired adhesive or processing aid to the designated areas (20 mm × 83 mm) on opposite ends of the strip. In the case of millipore water and white 5% HefCel suspension, application was performed with a spray pen utilizing 2 bar pressure for water and 3 bar pressure for HefCel suspension. The amount of HefCel or glue applied was adjusted to be proportional to the basis weight of the sample material within the 2-7 % range.

The sample was then closed carefully along the initial fold and the strip halves were secured gently together with the help of paper cloth for fibrous specimen and additionally with silicon pads for film-type specimen. The paper cloth was also used to

remove excess water or hefcel protruding from the sides of the strips. Then the folded strips were then placed between thin sheets of aluminum used as pressure equalizers in the press. The folded aluminum foil between the folded sample strip would limit the opposite surfaces from sticking outside the aluminum sheets. Then the whole sample assembly was weighed and brought to the hot-press. Maximum force was applied with the hand operated press for 4 minutes. The whole sample assembly was then weighed after which the assembly was disassembled and the strip was placed in a drying oven for 15 minutes. Dried sample was then weighed and placed in an exicator for 24 hours. A total of 15 sample strips were prepared this way for one combination or test series.

Among the assumptions within this method included that with water joined specimens sufficient water induced swelling would occur between the application and pressing. Also, temperature conditions were expected to be closest to selected temperature

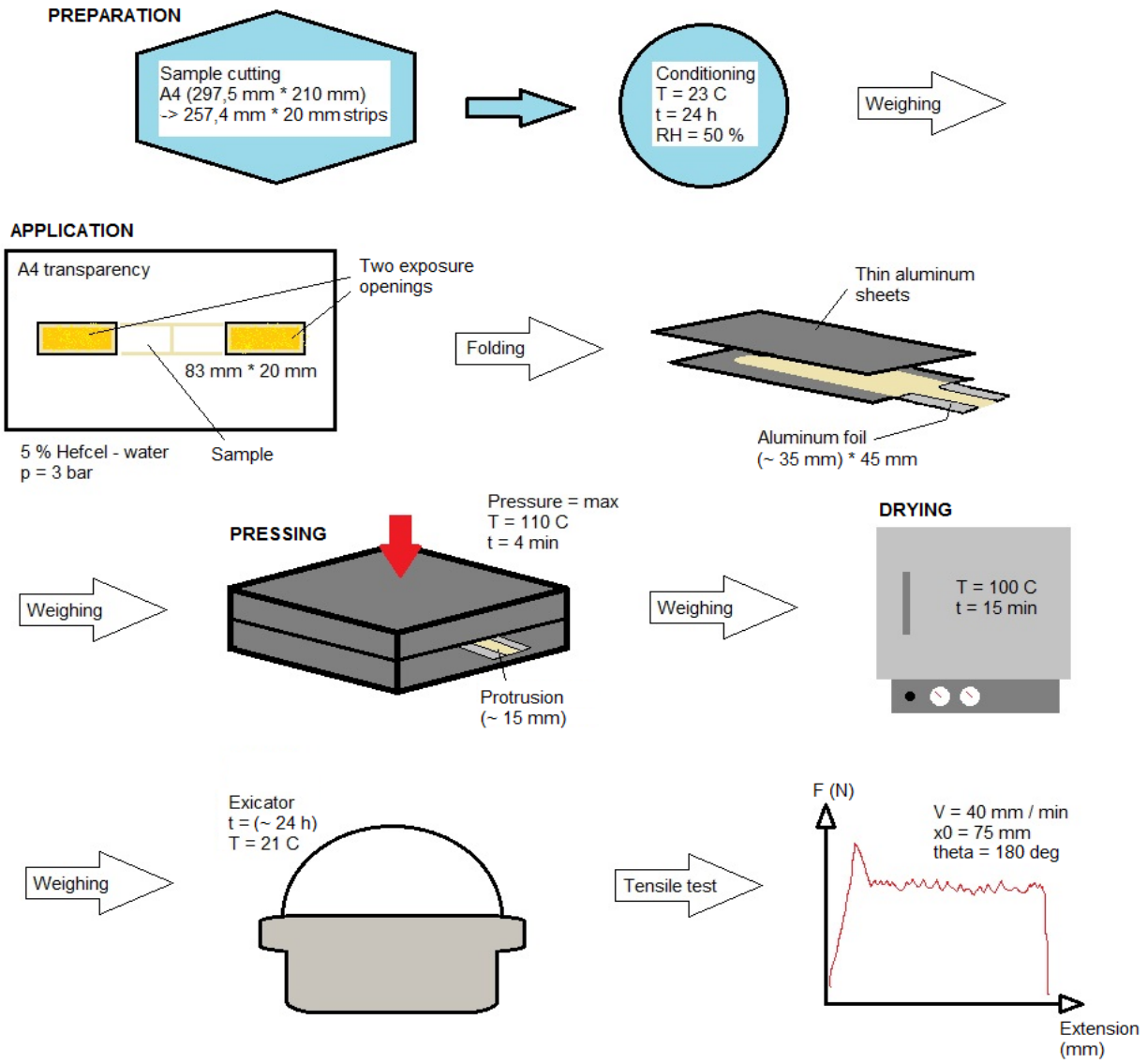

Figure 3.1. *Illustration of the self-adhesion procedure steps for strip-like samples.*

With nanocellulose film samples and foamed cellulose sheets, special preparations were needed after facing problems in initial trials. Nanocellulose films of both white and brown grades tended to flatten when subjected to full locking force of the press. The surface area of a strip was increased but its surface showed substantial “fracturing”. It was expected that the pressure between the aluminum pressure equalizers was too rough for the films. Simple reduction of pressing force resulted in poor adhesion with small amount of adhered area between strip halves which was visually observable. To counteract this, strips of 1,50 mm thick silicon were cut and added between the aluminum sheets when nanocellulose films were pressed. It was discovered that bringing heating elements to contact with the sample assembly provided the best surface finish and no fracture surface. Also, the effective contact area, where strip halves were visually seen adhered together, was increased. These silicon pads were also used later with joining nanocellulose film strips with foamed cellulose specimen.

Combinations: Foam-film

Two different types of foam-film combination specimen were designed and produced: white nanocellulose film joined with foamed cellulose using either water or hefcel-solution.

The supplied cellulose foam pieces were roughly (l) 300 × (w) 220 × (t) 70 mm in size, which made them difficult to cut and handle. Furthermore, the surface of every piece was not even, which can be seen in Figure 3.3. To make the foam pieces more workable and dense, the supplied specimen underwent a three-phase treatment. The pieces were first moisturized with a water spray from both sides with water equal to 50 % of the weight of the whole specimen. The moist piece was then put inside an air tight bag and sealed for four hours to allow the water to penetrate the whole piece. Then the specimen was placed between two metallic plates (size greatly exceeding the foams) with 20 × 20 mm aluminum profile bars as spacers on both short ends of the foam. A long weight of 15 kg supported by the top metal sheet and the aluminum bars was placed on top of the whole assembly. The constrained specimen was then placed in an oven (70 °C) for 24 hours.

Figure 3.2. *Left:* *Un-pressed, supplied cellulose foam piece. Right: oven-pressed 20 mm thick foam pieces made from two un-pressed pieces.*

The processed foam pieces were then trimmed and cut with specialized KAINDL Insucut saw blade into roughly (l) 106 × (w) 55 mm sized pads. The length and width was designed to house the 83 × 20 mm test area within the pad area. This size was also chosen while the housing jig for the tensile test machine was being designed. Finished pads were then conditioned along with nanocellulose film strips of (l) 297 × (w) 20 mm overnight before adhesive application and joining.

Adhesive application was done with in a manner similar to self-adhesion series: 2 bar pressure was used with water and 3 bar pressure with hefcel solution. However, amount of adhesive was not adjusted to the basis weight of the foam. Markings were added to the foam to indicate the area onto which the strip half of the specimen was to be folded on.

Compared to self-adhesion procedure, hot-pressing phase was done with the help of two additional tools: two (20 × 20 mm) aluminum spacers to limit the depth of the pressing motion and a long 0,6 mm thick metal sheet to help insert and remove the specimen from the press. A single strip of silicon and one sheet of thin aluminum, ones used in self-adhesion preparation, were placed on top of the nanocellulose film strip to ensure better contact with the film and the foam.

Combinations: Veneer-film

Like before with foam-film combinations, two cases of veneer-film combinations were produced: brown nanocellulose film joined with thin sheets of veneer using either water or 5% brown HefCel-solution.

Supplied veneer sheets were first cut into roughly (l) 106 × (w) 45 mm sized cards and placed in a zip-lock bag to avoid moisture intake. This was done to avoid unwanted wrinkling of thin veneer sheets as a smooth even surface was crucial for fabrication process. For this reason, cut veneer cards were not conditioned before composite

specimen assembly. The brown nanocellulose film strips, on the other hand, were conditioned prior to application and pressing.

Application procedure with water was done in similar fashion as before, however, brown hefcel solution was used instead of previous white grade. Also, during hot-pressing, the thermal elements were heated to 170 °C. This temperature was selected based on the understanding that lignin would experience glass transition in moist conditions and higher temperature. Lignin was expected to soften and flow more readily into molecular contact with other fibrils and with the surface of veneer. Silicon sheets on both sides of laminates between aluminum sheets were used to further facilitate feasible contact conditions during hot-pressing.

Preliminary tests suggested that slightly more pressure was required to ensure good contact with the film and wooden veneer surface. Light contact would lead to early delamination of the film-veneer laminate.

3.2.2 Three-point bending: specimen preparation

A sandwich composite configuration was chosen for desired low weight and good stiffness-to-weight ratio (Campbell, 2010; DIAB group, 2012). Typical sandwich structure consists of a thick foam core and thin face layers. These types of composites were prepared by Frisk (2016) from bio-based PU foam or NFC foam and kraft paper facings by vacuum infusion with epoxy resin, resulting in stiff panel structures. In our case however, the foamed cellulose fiber sheets were deemed too soft to be used as a core material alone. The wool-like foam sheets were easy to compress even after initial compressing procedures to 20 mm thick configurations. To continue with available foams and without strengthening particle impregnation, the sandwich composite structure was designed to include core dividing cell walls that would support the faces of the sandwich. Foam in turn would be enclosed into these cells and provide support during bending and twisting motions. Nanocellulose films were chosen as cell wall and face material. After initial trial specimen were fabricated, it became clear that faces and walls should be thicker and therefore, double layer films (joined with water) were used. Face and cell wall films would be joined with foam core pieces with 5% HefCel solution. The whole sandwich composite configuration is represented in Figure 3.4.

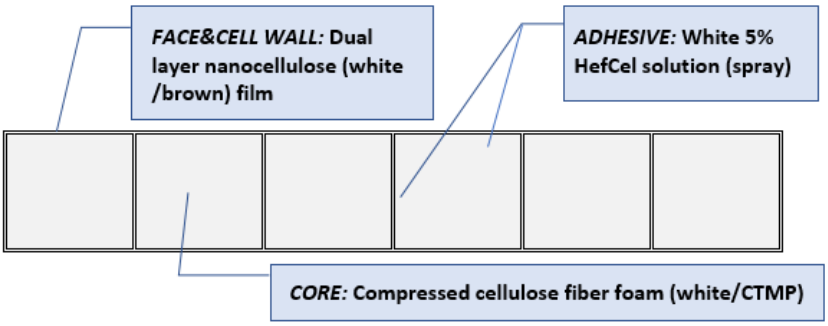

Figure 3.3. *Schematic illustration featuring the side profile of the designed sandwich.*

Two types of sample geometries were prepared for three-point bending tests: beams that represent the side profile of designed sandwich (Figure 3.4) and narrow panels with continuous cell walls along its length.

Common for the beam and panel fabrication was the compression of supplied foam pieces, either white or CTMP grade, to the target thickness of 20 mm with the method described earlier. From there, the large foam sheet was cut into (w) 20 x (h) 20 mm beams (7 for composite beam batch, and 3 for a single panel specimen) with length approximately 120 mm. Length of these foam beams would determine the number of bend test composite beam specimen that could be acquired. Length of the composite panels would be trimmed down to 105 mm at the end of the fabrication process even if the produced foam beams were slightly longer than intended.

After cutting and trimming of the foam beams, film strips corresponding to the foam used: Brown nanocellulose for CTMP foam and white nanocellulose for white foam. The cut strips were 20 mm in width and twice the length of the cut foam beams. The strips were then folded in half and brought to the assembly.

First step of the assembly procedure was to join the folded film strips together. For this, Millipore water was used as before in the self-adhesion tests. Roughly the same amount of water was sprayed onto both sides of the fold with 2 bar air pressure. Like in self-adhesion tests, strip halves were folded together, removing excess water with a paper cloth, but also pressing the laminate under silicon pads with a carbonate slide. These finished double layer strips were then placed in a zip lock bag for later use.

Second step included switching to 5% HefCel spray solution and increasing the pressure to 3 bar. The assembly would then continue by applying hefcel onto foam beam and double layer film surfaces and joining them together with the help of silicon pads.

Figure 3.4. *Pictures taken at different stages of an ACC assembly. Top left: trimming of foam pieces. Top right: Surface of a foam piece after HefCel application. Bottom left: Surface of two-fold film strip after HefCel application. Bottom right: Joining of two foam pieces together with where only the other piece has a film on its side.*

From here on, the fabrication methods would differ considerably, whether composite beams of panels were being prepared.

All-Cellulose Composite beams

The stacking procedure would be continued until seven foam beams were joined together as described above. The resulting "wet cake" (due to its high moisture content) would then be brought to the hot-press heated to 120 °C. The pressing assembly consisted of the heating elements, square profile (20 × 20 mm) aluminum beams and of adjustable clamps on both back and front side of the press. The cake was placed between the aluminum beams and then the elements were brought into contact, closing the system. Then the clamps were adjusted to the target width of 105 mm. Pressure was then increased to hold the cake and assembly in place for 12 minutes. After the heating under constrained conditions, the still wet cake would be taken to an oven (100 °C) and the specimen would again be constrained to the desired width with the help of aluminum beams. The cake would then be left to dry for 120 minutes. During this time, the press would be heated to 170 °C.

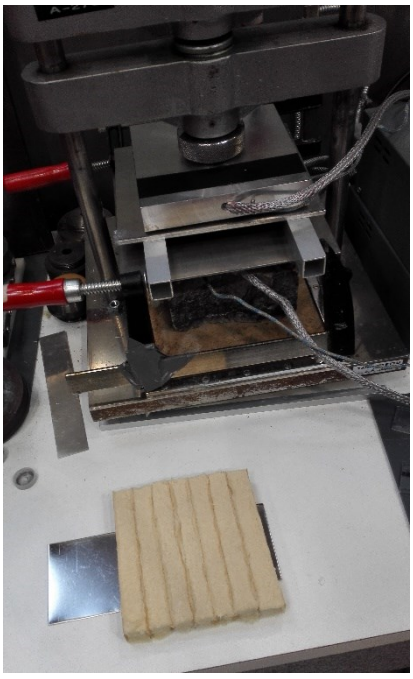

Figure 3.5. *Picture of the manual press device & the additional clamps and aluminum beams used in the ACC preparation. A brown ACC (CTMP + brown nanocellulose film) wet cake before 12-minute hot pressing at 120 °C.*

After drying, the cake was dry enough to be cut into individual beam specimen. The piece was first trimmed to bring out an even edge before cutting. A total of four composite beam blanks would be obtained this way. These pieces were then placed in a zip-lock bag to wait for individual final assembly.

Final assembly procedure of each composite beam began with creation of the face layers: Corresponding (w) 20 × (l) 240 nanocellulose film strips were first cut, folded and joined using water spray. The face layers were then glued onto both sides a composite beam blank using 5% white HefCel spray and securing them well using the silicon pads. The complete all-cellulose composite beam was then placed between silicon strips and aluminum sheets, and then the whole specimen assembly taken to the hot-press (170 °C). Specimen assembly was carefully placed inside the press while upper heating element were brought into contact with the upper aluminum sheet of the assembly. The contact was held for 2 minutes and then the whole assembly was removed and disassembled.

The pressed composite beam was taken into the oven and dried under constraints for 45 minutes. The resulting final thickness and width of the all-cellulose composite beam would be within the range of 18,50 ─ 19,50 mm. Length was measured to range from 105,00 mm to 109,00 mm. These dimensions are also indicated in the schematic illustration of an ACC beam in figure 3.6.

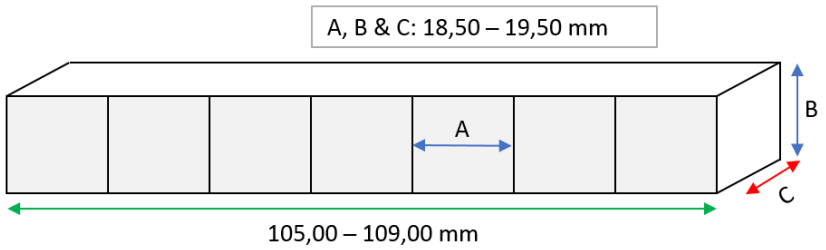

Figure 3.6. *Schematic illustration of an all-cellulose composite beam.*

Four additional white ACC and brown ACC beams were prepared for the flexure creep tests.

All-Cellulose Composite panels

Composite panel blank required three foam beams to be attached together. The similarly wet piece as in beam fabrication was taken to 120 °C hot-press. In this case the clamps were adjusted to 50 mm width. The piece was kept under the constraints for 10 minutes before removal. The unfinished panel piece was then dried under constrained in the oven for 75 minutes. The dried piece would then wait for the final assembly procedure. The face layer film pieces for panel composites were considerably large and wide which made them challenging to join together with water spray and hand pressing technique. The successful dual layer film face pieces were placed inside a zip-lock bag before joining them onto the panel piece with HefCel spray. Adding the face layers was the most crucial phase of the fabrication: it was important to make sure that there was full contact with the foam, cell wall films and with the face. Like before, after this procedure, the specimen was pressed under minimal pressure at 170 °C for 2 minutes. At this point, face layer would indicate how well the joining step was made: Poor contact would result

in small cracks and blistering in the face layer. This was due to the fact that the panel piece foam is significantly more confined by nanocellulose films. The only way for moisture and vapor to exit is through the ends of the enclosed panel.

As described, due to the enclosed nature of a panel piece, the drying of a single composite panel was done over 150 minutes while kept under elaborate constraints to prevent bending of the specimen.

The resulting finished all-cellulose composite panel measured between 15,00 to 17,50 mm in thickness, 48,00 to 50,00 mm in width and 103,00 to 108,00 mm (Figure 3.7.).

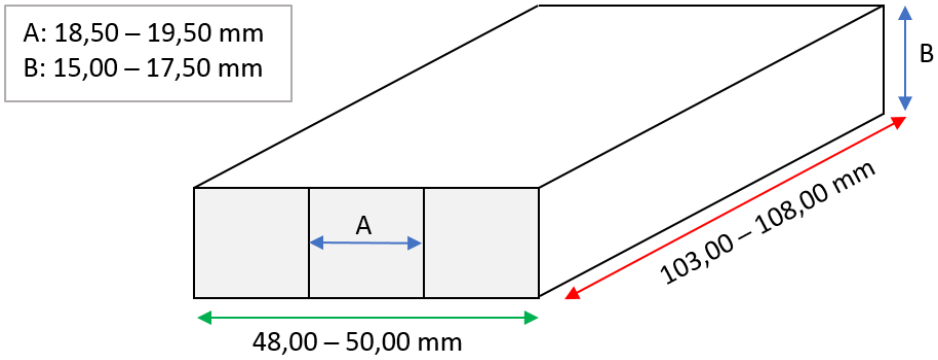

Figure 3.7. *Schematic illustration of an all-cellulose composite panel.*

A set of four panels was prepared for an individual test.

Reference specimen

Because many of the results, specimen and working constraints within the bending test methods did not fit most of the standard method descriptions and requirements, a set of reference specimen were prepared. The reference specimen was to both gauge the performance of the ACC specimen and provide understanding how structural geometry will influence the stiffness of a beam or a panel. Dual-layer corrugated board for hazardous goods (DS Smith) was selected for this purpose. Non-diluted PVA glue (Erikeeper, 43 %-dry weight) was used as an adhesive.

A set of four beams and four panels was created from the corrugated board. The goal was to achieve similar dimensions as with the ACC counterparts. Two pieces of the 7,00 mm thick chosen corrugated board were adhered together with thicker layers of the corrugated medium would be faced against each other using the PVA glue. The resulting CB structure would be 13,80 ─ 14,60 mm in thickness. The thinner corrugated layers with thicker top liners would form the face of these panel and beams. Corrugated board specimen length and width were copied from the final dimensions of ACC specimen.

3.3 Peel test

Peel tests were performed with an Ametek Lloyd LS5 tensile tester under standard conditions 50 RH and 20 °C. 100 N load cell and 40 mm/min head moving rate was used across all sample groups. Test raw data was logged including elapsed test time (s), displacement (mm) and load (N). Peel strength was calculated with the following equation:

$$G = \frac{F}{b}(1 - \cos\theta), \quad (1)$$

where G is bond strength, F is the load, θ is the peel angle and b is the width of the area of adhesion. For a T-peel test the angle is 180°. (Zhao & Kwon, 2011) This equation results in $G = F$ with current specimen geometry (b = 20mm).

All finished peel test specimen, as described in section 3.2.1, were placed inside of an exicator for overnight before testing.

Self-adhesion

In self-adhesion peel tests, the specimen was carefully opened up where the initial fold was made during the specimen fabrication in order to place the free strip ends between the clamps of the testing machine. The zero-gauge length was set at 65 mm. Each individual test was continued until the laminate was completely peeled or if the specimen failed by fracturing, tearing or snapping into two.

Self-adhesion test data was used to plot bond strength (N/cm) against displacement of the peel using formula 1.

Combinations

Two of the materials used in the combination adhesion tests were rigid: the veneer and the cellulose fiber foam. In order to test composite laminates consisting of these materials, a different type of adhesion testing machine or a special jig was needed. The option latter was chosen and an enclosure-like jig was designed to be tooled and folded out of Plexiglas. It was designed to include a wide enough opening in the middle to allow peeling of the laminate to occur in the direction of the moving head at a 180 ° separation angle. The jig was also meant to fit into the clamps of the tensile tester. The fabricated jig is featured in Figure 3.8.

Specimen were inserted into the enclosure before fastening the jig into the clamps. The 20 mm thick foam-film laminate specimen proved difficult to insert without bending of the film. To counteract this, a simple small piece of tape was needed for

the more brittle film specimen to be glued onto the surface of nanocellulose films as a backing aid before placing the whole specimen assembly into the jig. Veneer-film combinations didn't need similar preparations before testing. However, these thin laminates needed to be secured close to the opening in the jig with a piece of foam.

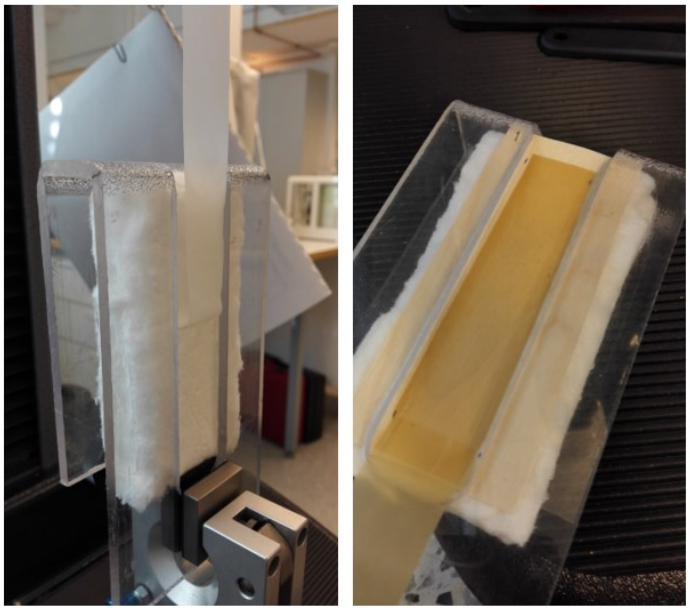

Figure 3.8. *Jig for combination samples with rigid components. Left: Cellulose foam pad and nanocellulose film strip are presented. Right: Veneer sheet and brown nanocellulose film strip specimen secured in place by an unused foam piece.*

Gauge length was zeroed at 25 mm above the jig and the free strip end of the laminate was placed between the upper clamps before testing. Like before, the test was terminated in the case of sample failure or if the laminate was completely peeled.

3.4 Three-point bending tests

Three-point bending tests were conducted under standard conditions of 50% RH and 20 °C with a modified Instron 4502 universal testing machine with a 1 kN load cell. Loading speed was adjusted to face layer strain rate of 3 %/min based on the geometry of a specimen type according to the SFS-EN ISO 178 standard. Elapsed test time (s), load (N), flexure load (load complement), flexure displacement (mm) and flexure strain (mm/mm) were logged for all four specimens for later analysis. Span length was set at 64mm.

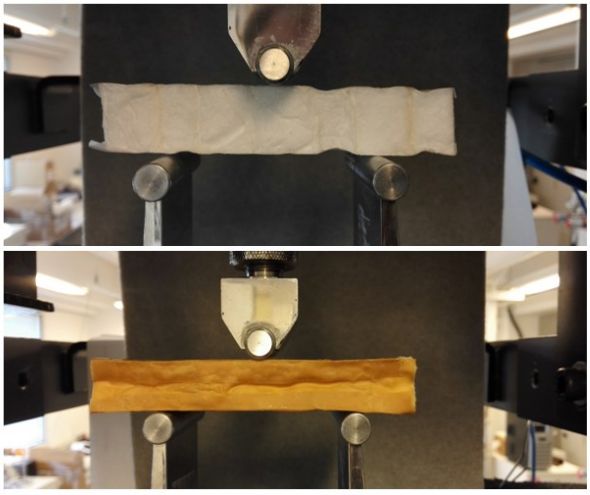

Figure 3.9. *Above: white all-cellulose beam (WACCB). Below: brown all-cellulose panel (BACCP)*

One sets of brown and white ACC beam specimen were dried in an oven (100) for one hour before testing. Other specimens were conditioned for 24 hours (50 RH, 20 °C) before testing.

3.5 Flexure creep

Two series of flexure creep test were performed on white ACC and brown ACC beams. Likewise, in the three-point bending series, the tests were performed on the Instron universal testing machine and specimen were conditioned for 24 hours in the same conditions.

The test itself was designed to last for 60 minutes with constant load of 5,00 N. The target load was reached moving the head at 20 mm / min. Support span was kept at the same length as with regular three point bending tests.

3.6 SEM Characterization

Adhesion characterization was performed on peeled self-adhesion specimen and based on micrographs obtained with ZEISS Merlin-42-63 Field Emission Scanning Electron Microscope with GEMINI electron optics. Studied SEM specimen of roughly 10 × 10 mm dimensions were harvested from exemplary strips. The thicker side of peeled laminate was chosen to be studied. Studied specimen were harvested from tested strips so that non-adhered, off-peeled and intact areas could be examined. The non-adhered areas without any adhesive in the free strip ends were used as a reference. Extracted specimen were adhered onto metal tabs on a carrier with conductive carbon tape.

4 RESULTS AND FINDINGS

Test data is represented and discussed by comparing bond strength curves of the series. Adhesion is characterized based on the understanding of the materials in the compared series.

4.1 DSC & DMA analysis

A DMA data curve is represented for both brown and white nanocellulose films in Figure 4.1.

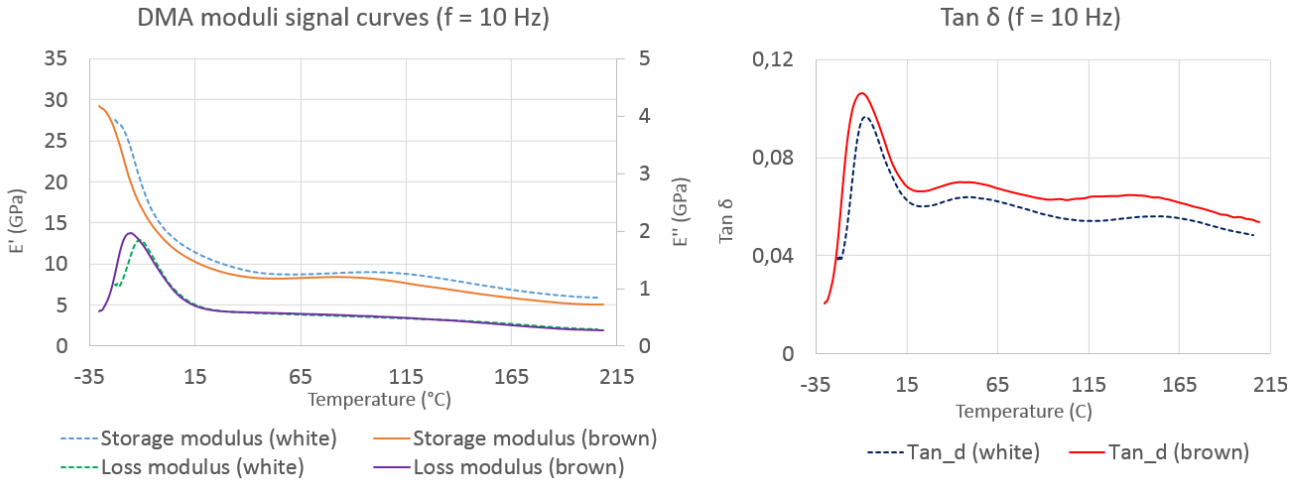

Figure 4.1. *DMA analysis performed for both white and brown nanocellulose film grades.*

The data shows that brown film might perform better in mechanical damping component than white film. Glass transition for both materials occurs is observed in the -20 °C region. The two heating runs during DSC analysis yielded an average glass transition temperature of 5,2 °C for white and 6,9 °C for brown nanocellulose film. This difference may be caused by the sorbitol (glass transition at -25 °C) used in the film formation process. Also, it's important to note that the acquired glass transition is representative of the whole film structure, not of cellulose or lignin.

4.2 Peel test

Using the Equation 1, the measured load of peel test data was adjusted into bond strength and plotted against the measured displacement of the moving head of the test machine. Only the considerable specimen data curves for the analysis are represented here.

Self-adhesion tests

First data comparison was done between the copy paper specimen types. The comparisons would help understand the reinforcing influence of adhesive HefCel particles within a given laminate structure.

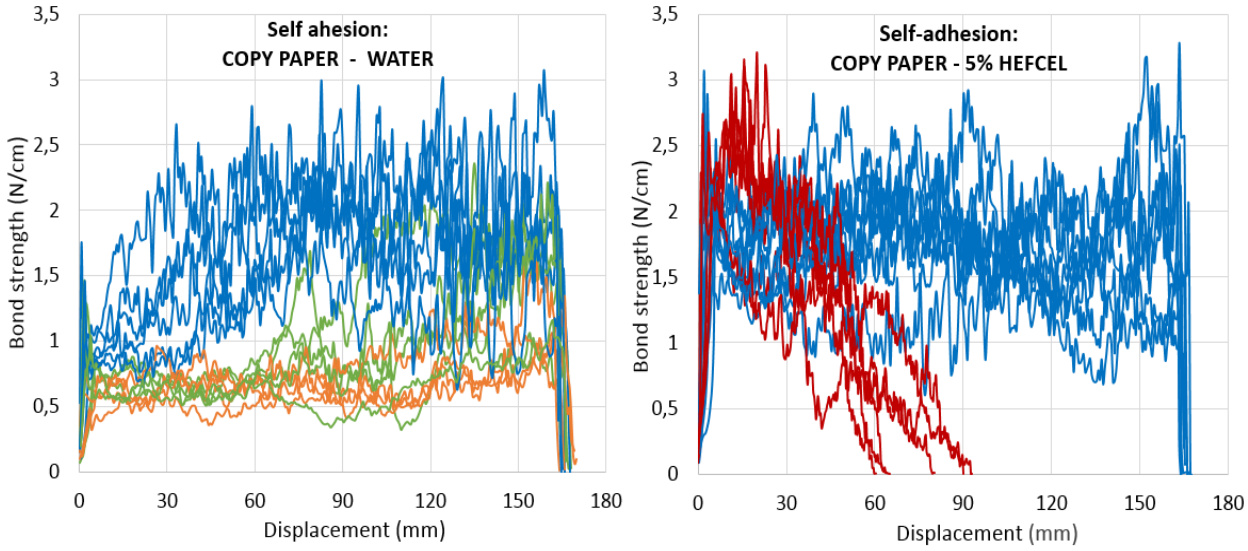

Figure 4.2. *Self-adhesion T-peel data for copy paper samples joined with (Left) Milli-Q water displays three different modes of failure: a mode with relatively low cohesive failure (orange curves), a mode with increasing amount of cohesive failure (green curves) and a mode with complete cohesive failure of the sample (blue curves), (Right) 5% HefCel solution displays two different modes of failure: complete cohesive failure of the sample (blue curves) and premature failure of the composite network structure (red curves).*

In the work of Shivyari et al. (2016), copy paper strip samples swollen in water and dried under a weight in laboratory conditions showed no self-adhesion. Here, in contrast, copy paper samples show relatively great bonding capabilities when high temperature and pressure is used. The high-end performance samples (blue curves) have bond strength of similar magnitude than copy paper samples joined with Hefcel solution in this study and dilute solutions of NFC in earlier study (Figure 2.14.). The acquired bond strength in water treated copy paper samples is likely to be affected positively and negatively by unknown grades and quantities of paper additives. Water bound samples might

also have been more sensitive to the temperature variations in the heating elements and since there are no adhesive to remedy for the undesired irregularities.

An improvement in adhesion can be observed when comparing the sample series in their entirety. The increase is not merely a factor of increased bond strength. The failure mechanism across the sample population is an important indicator: water treated samples exhibited poorly bonded samples and local variation in bond strength while all the hefcel treated samples were perfectly joined together. The shift to the failure of the sample structure during peeling demonstrates further improvement of adhesion and internal bond strength. As stated by Zhao & Kwon (2011) in their work with polymer film-paper laminates, the maximum bond strength of a laminate is limited by the cohesive strength of its constituents. In this instance, not only has this limit been reached with water treated samples, it has been exceeded by hefcel treated samples that have had their cohesive strength improved by added nanocellulose particles.

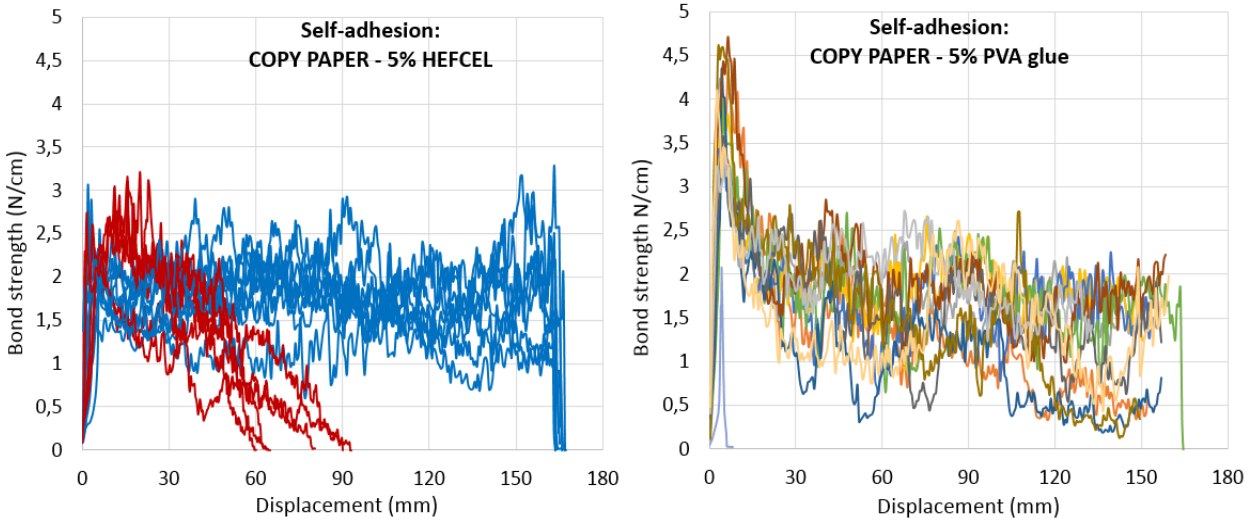

Figure 4.3. *Self-adhesion T-peel data for copy paper sample strips joined with (left): 5% HefCel suspension and (right): 5% PVA liquid glue. The missing ends of the curves (right) are considered to have been caused due to data loss during data export process.*

Similarly to the HefCel-bound copy paper samples, water bound nanocellulose film specimens achieved excellent bonding, resulting in failure of one of the laminate layers before extensive delamination would occur (Figure 4.4.).

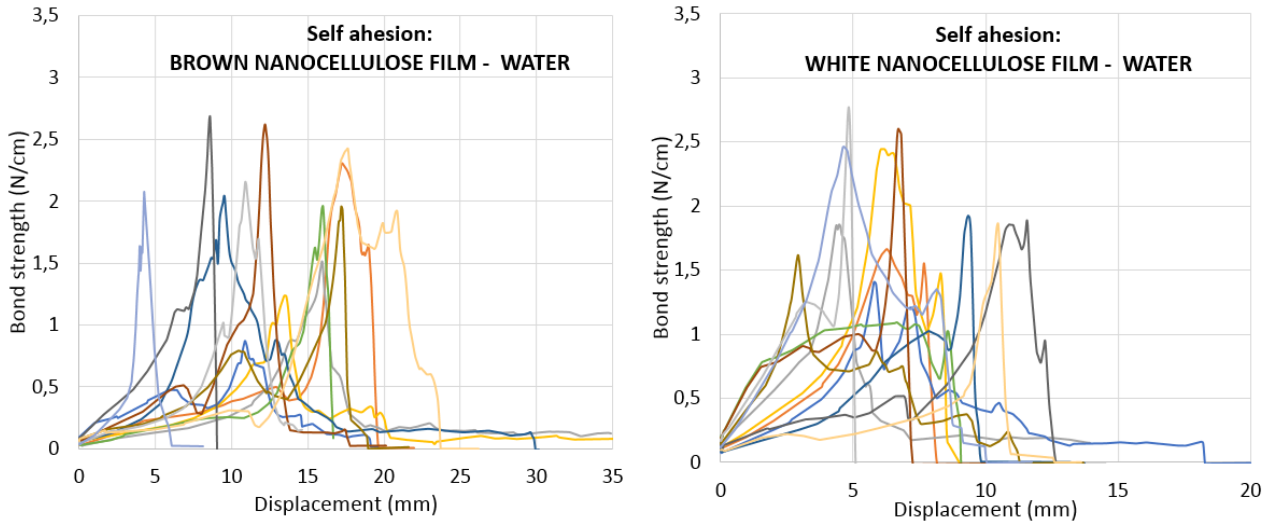

Figure 4.4. *Self-adhesion T-peel data for (left): Brown nanocellulose film samples and (right) white nanocellulose film samples joined with water.*

The nanocellulose films joined with water swelling displayed visually incredible adhesion: the film halves were seemingly so closely bound that the joined laminate area was observably more transparent than single layer film strip. In addition to the peel tests, separation of the laminate layers was attempted with conventional sharp tools and small blades. The initial cuts could not be made to propagate along the assumed interface.

It was also contrary to the expectations that brown nanocellulose film specimens didn't display higher bond strength, yet both series displayed similar level of adhesion. Lignin present in brown films was expected to strengthen the interface bonds via covalent bond interactions between similar surfaces. The lack of covalent bonds might be due to the relatively low temperature used in the joining process. Alternatively, pressing time may not have been long enough for the kinetics of covalent bond formation.

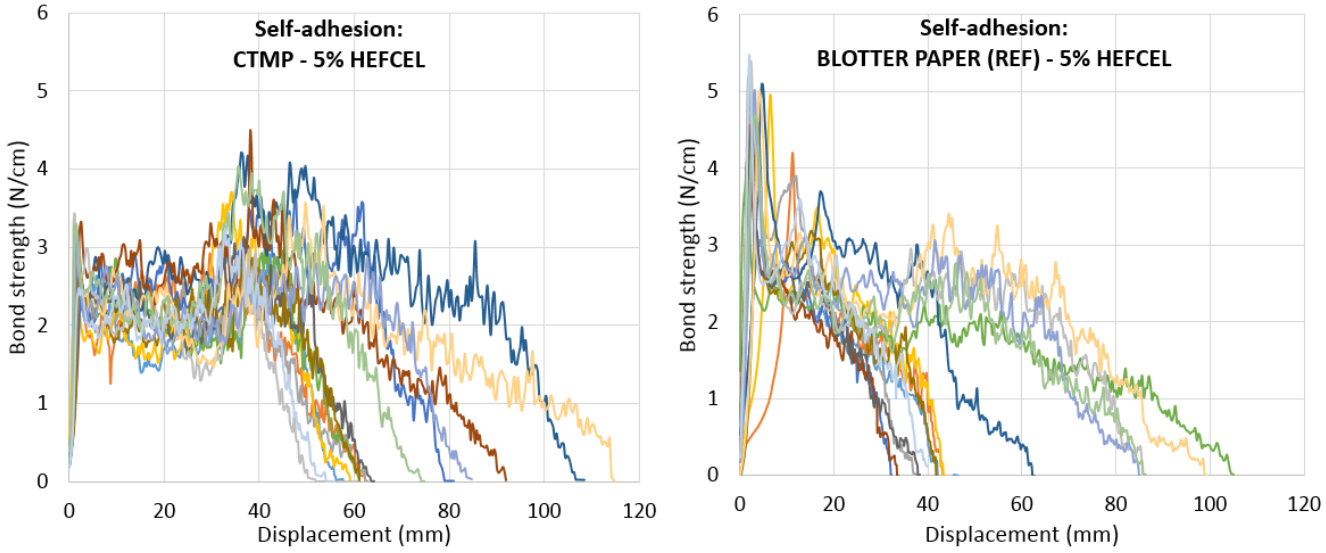

Figure 4.5. *Self-adhesion T-peel data for (left): CTMP board samples and (right) Blotter paper samples joined with 5% hefcel.*

Self-adhesion results for CTMP board and blotter paper display similar failure behaviour across each sample population. Although blotter paper samples displayed much higher initial peak bond strength than CTMP samples.

Self-adhesion test data for HefCel-joined samples was used to study influence of macrostructure on peel strength. To this end, a discrete representative bond strength value was needed for a given type of specimen. Typically, a plateau of even peel force can be seen in the peel curve, which is used as a peel average and ultimately to represent specimen's adhesion (Zhao & Kwon, 2011). However, many of the tested specimen didn't exhibit this type of even peeling: one of the diverging strip halves would fail from within resulting in an ever-thinner piece until fracture, which can be seen as downward trending curves in Figures 4.2., 4.3., and 4.5. This can also be considered as an indicator of good bonding between layers since a laminate layer will fail where the local bonding is weakest, which is expected to be random. Due to the random nature of this type of peeling, an initial peak of bond strength of a given peel curve is recommended within literature as a representative value for adhesion (Zhao & Kwon, 2011).

Averages of initial bond strength peak values are presented in Table 4.1 for specimen joined with 5% HefCel solution.

Table 4.1. *Average initial peak bond strengths of each material tested for self-adhesion. The average HefCel coating for a sample per sample grammage is also reported.*

Material	Peak bond strength (N/cm)	Hefcel coating grammage / Sample grammage (%)
Copy paper	2,23	2,1 %
Nanocellulose film (White)	1,25	1,6 %
Blotter paper	4,69	3,1 %
CTMP board	2,78	4,2 %

The ratio of applied HefCel to the grammage of sample material was difficult to regulate. However, specific hand motion to adjust the time exposure, and ultimately the resulting weight of the adhesive of the strips was practiced and learned. A system applying a specific dose of adhesive into the spray is recommended in future adaptation of this method. Despite this, the grammage ratio of HefCel and substrate had little to no effect within such small quantities.

Results on influence of macrostructure of the material on self-adhesion are featured in Figure 4.6.

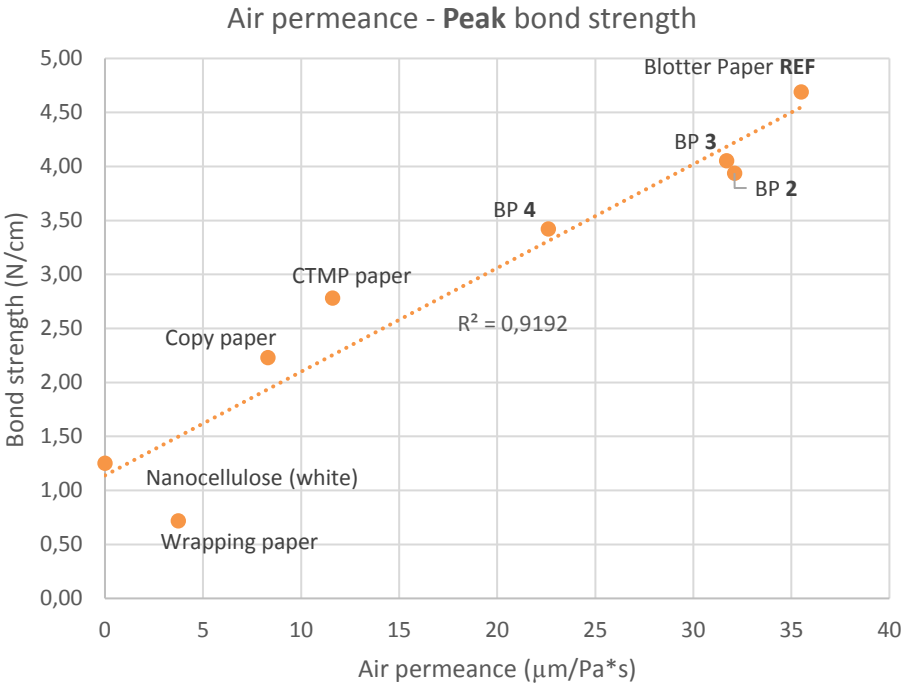

Figure 4.6. *Peak bond strength of self-adhesion samples joined with white 5% HefCel plotted against measured air permeance of a given material.*

Adhesion in terms of measured bond strength shows extremely strong correlation to material air permeance. This may be attributed to the ability of HefCel particles to penetrate the porous material deeper than a dense one. As discussed earlier, the HefCel particles strengthen the material and in the case of porous structure, this effect will be extended deep into the laminate layers. The HefCel particles in the suspension are expected to coalesce (hydrogen bonds & mechanical interlocking) onto multiple fibers whilst retaining some level of cohesion within the impregnating suspension. Drying will then result in a network that binds fibers of a porous material to one another.

This can further be reasoned with comparison of the peel curves of porous blotter paper reference and dense batch4 blotter paper (BP 4) series in Figure 4.6. These blotter paper grades are later referred to as porous and dense blotter paper.

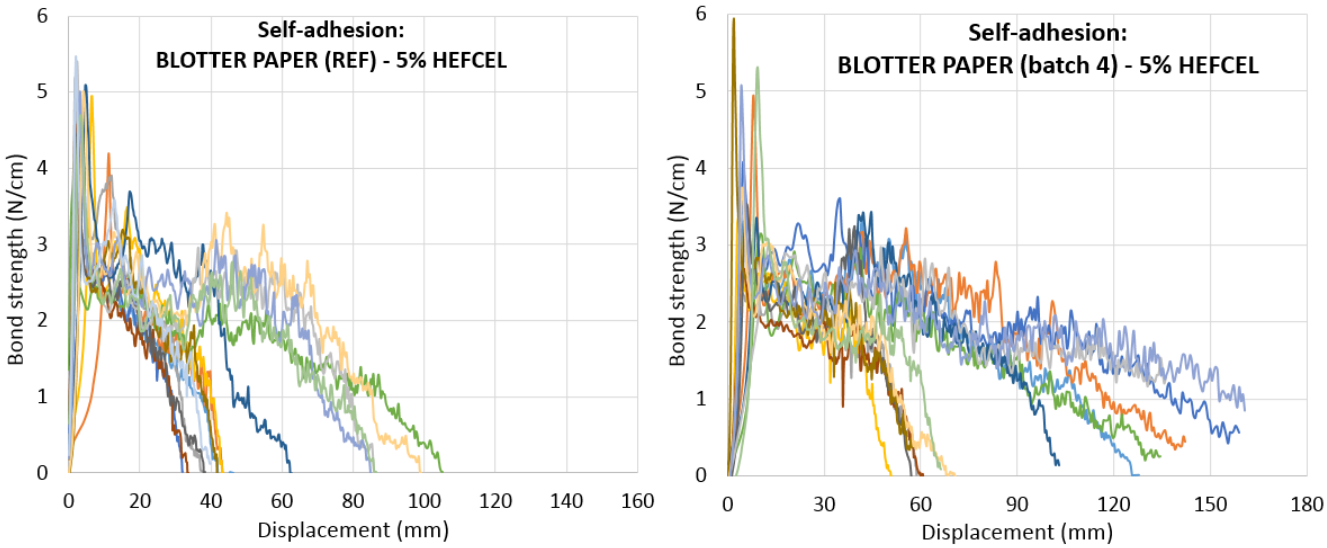

Figure 4.7. *Peel curves of (left): reference porous blotter paper and (right): dense blotter paper series. Data loss is observed in the curves on the right.*

Even with lower average of initial bond strength of the dense blotter paper, the dense blotter paper grade does show one extremely high peak of adhesion. However, comparing the two series reveals how some the dense strip specimen peel the full length of the test (166 mm) and many reach greater displacement readings than any of the porous counterparts. This suggests and reinforces our understanding that a laminate with greater internal bond strength and good adhesion will more likely fail cohesively rather than delaminate. The reinforcement effect is not as extensive in the dense structure as it is in a porous one.

In addition to air permeance, self-adhesion was also evaluated using measured surface roughness. These results are featured in Figure 4.8.

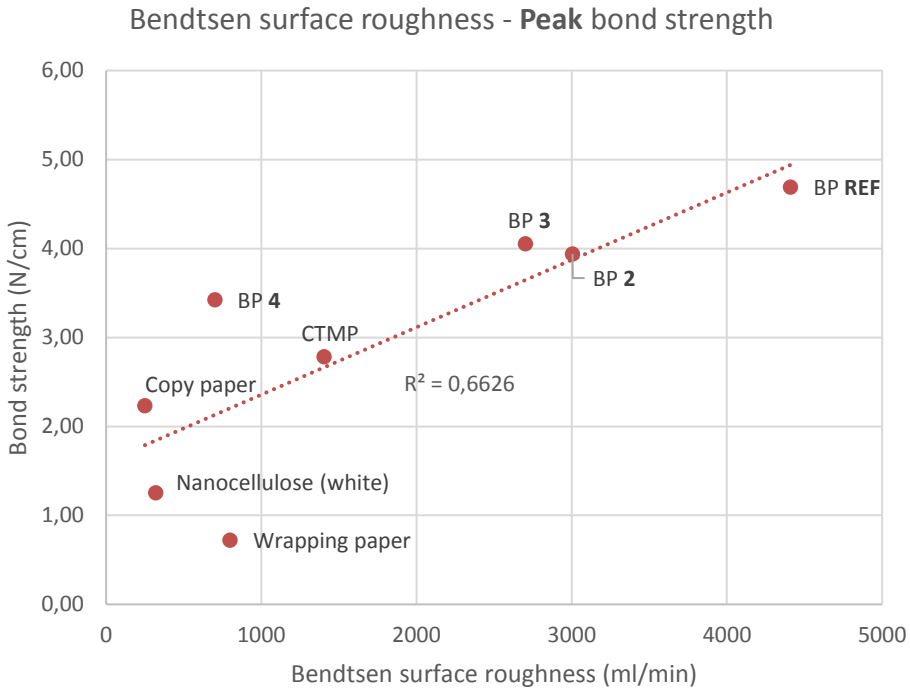

Figure 4.8. *Peak bond strength of self-adhesion samples joined with 5% HefCel plotted against measured Bendtsen surface roughness of a given material.*

The correlation is not as significant as observed with air permeance study. However, this clear trend further reinforces the connection with porosity and self-adhesion explained earlier.

Combinations

Due to the custom nature of the method used for rigid combination materials, the bond strength Equation (1) is not applicable. Therefore, results are presented as load (N) versus displacement (mm). The load reading of these tests is still considered to represent closely the adhesion between combination constituents.

Data comparisons for white cellulose fiber foam and white nanocellulose film specimen are featured in Figure 4.9.

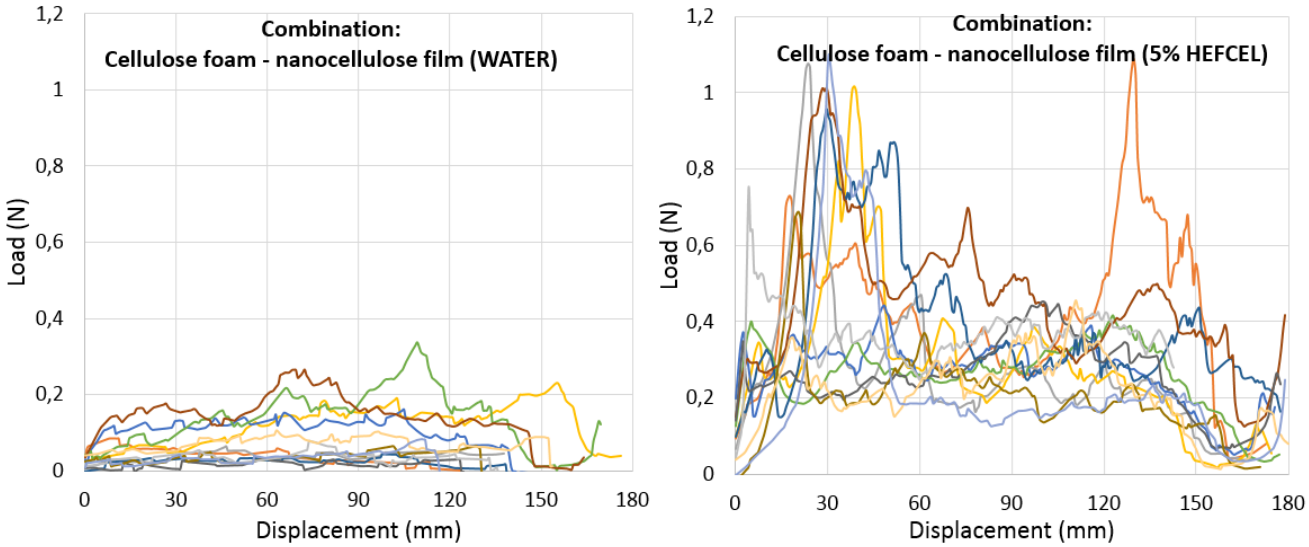

Figure 4.9. *Modified peel test for combined samples of foamed cellulose and white NFC films joined with (left) water and (right) 5% hefcel. The plot scatter on the left reveals that the poor adhesion affected the total distance of peel before complete delamination.*

Minimal adhesion is observed between white cellulose fiber foam and white nanocellulose film when water is used as a processing aid. The water joined specimen also exhibited unfortunate early delamination prior to testing: The film strip of the specimen would detach from where the peeling would normally begin.

HefCel bound foam and film specimen show significant improvement in adhesion over water bound counterparts. This is largely due to the reinforcing effect of the HefCel particles that penetrate the foam material. The reinforcing effect is likely due to hydrogen bonding and mechanical interlocking of long fibrils of the nanofibrillated HefCel particles. There was also a stark visual difference between the amount of peeled off foam on the two different types of strips (Water / HefCel).

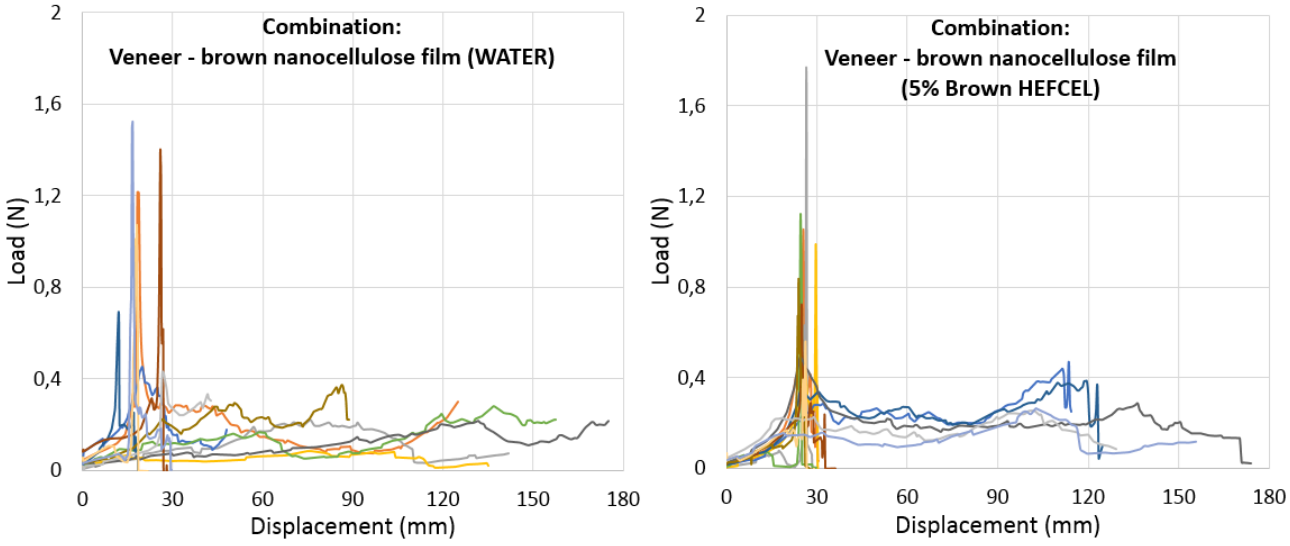

Figure 4.10. *Modified peel test for combined samples of veneer and brown nanocellulose films joined with (left) water and (right) brown 5% HefCel suspension.*

Two observations can be made based on the data and one from the specimen fabrication. There is a slight level difference in the peel force for the water joined film strips and the hefcel joined strips. Secondly, only four specimens in both series delaminated completely.

Interestingly, the initial peaks of breaking in both these series are not of the same level (N = N/cm, equation 1) as before when a film fails during peel loading as seen in Figure 4.4. This most likely an indication of the difference between the methods, because like before, and as is observed in this instance, the load cannot reach a point where delamination would occur because of the failing of the film.

Comparison of the two series also indicates that this type of laminate can't be strengthened further by HefCel-like adhesive if feasible adhesion is achieved with adhesion induced by optimized moisture, heat and pressure.

In Table 4.2 overall performance between all self-adhesion and combination peel tests is reviewed.

Table 4.2. *Table featuring all peel tests conducted in this work. Tests are divided by their type: self-adhesion (S-A) and combination (Comb.). Average initial peak bond strength (in N/cm or in N) was chosen to represent a test series and used to rank self-adhesion tests. Also, amount of peel during a test and failure mode are evaluated.*

TEST TYPE	MATERIAL (Adhesive / processing aid)	Average initial peak bond strength		Estimated peel (Full / Partial / None) & failure description
S-A	Wrapping paper (5% HefCel)	0,72	N/cm	*Full* - Fiber tearing
S-A	Copy paper (Water)	1,15	N/cm	*Full* - Fiber tearing
S-A	White nanocellulose film (5% HefCel)	1,25	N/cm	*None* - Force buildup & break
S-A	Brown nanocellulose film (5% PVA glue)	1,54	N/cm	*None* - Force buildup & break
S-A	Brown nanocellulose film (Water)	1,93	N/cm	*None* - Force buildup & break
S-A	White nanocellulose film (Water)	2,00	N/cm	*None* - Force buildup & break
S-A	Copy paper (5% PVA glue)	2,08	N/cm	*Partial* - Fiber tearing
S-A	Copy paper (5% HefCel)	2,23	N/cm	*Partial* - Fiber tearing
S-A	CTMP (5% HefCel)	2,78	N/cm	*Partial* - Fiber tearing
S-A	Blotter paper DENSE[batch4] (5%HefCel)	3,42	N/cm	*Partial* - Fiber tearing
S-A	Blotter paper POROUS[ref] (5%HefCel)	4,69	N/cm	*Partial* - Fiber tearing
Comb.	Veneer + Brown nanocellulose film (*Brown* 5% HefCel)	0,63	N	*Partial* - Steady peel + Force buildup & film break
Comb.	Veneer + Brown nanocellulose film (Water)	0,88	N	*Partial* - Steady peel + Force buildup & film break
Comb.	White nanocellulose film + white foam (Water)	0,06	N	*Full* - Fiber tearing (small quantities of foam stick to film strip)
Comb.	White nanocellulose film + white foam (5% HefCel)	0,57	N	*Full* - Fiber tearing (large quantities of foam stick to film strip)

Comparing the water joined copy paper series with HefCel-joined white nanocellulose film strips shows how two different failure modes don't necessarily correlate with the obtained bond strength. A much fair comparison can be made between water-joined and

HefCel-joined copy paper strips: an improvement of 100% in bond strength is observed in this case. Also for fiber based materials, comparisons can be made by looking into the amount of strip peel observed within a series: Greater bond strength significantly limits the total displacement before specimen material fails.

4.3 Three-point bending test

The three-point bending results are divided into sections respective to the composite specimen type.

All-Cellulose Composite beams

Bending test data for WACCB and BACCB specimen are shown in Figure 4.11.

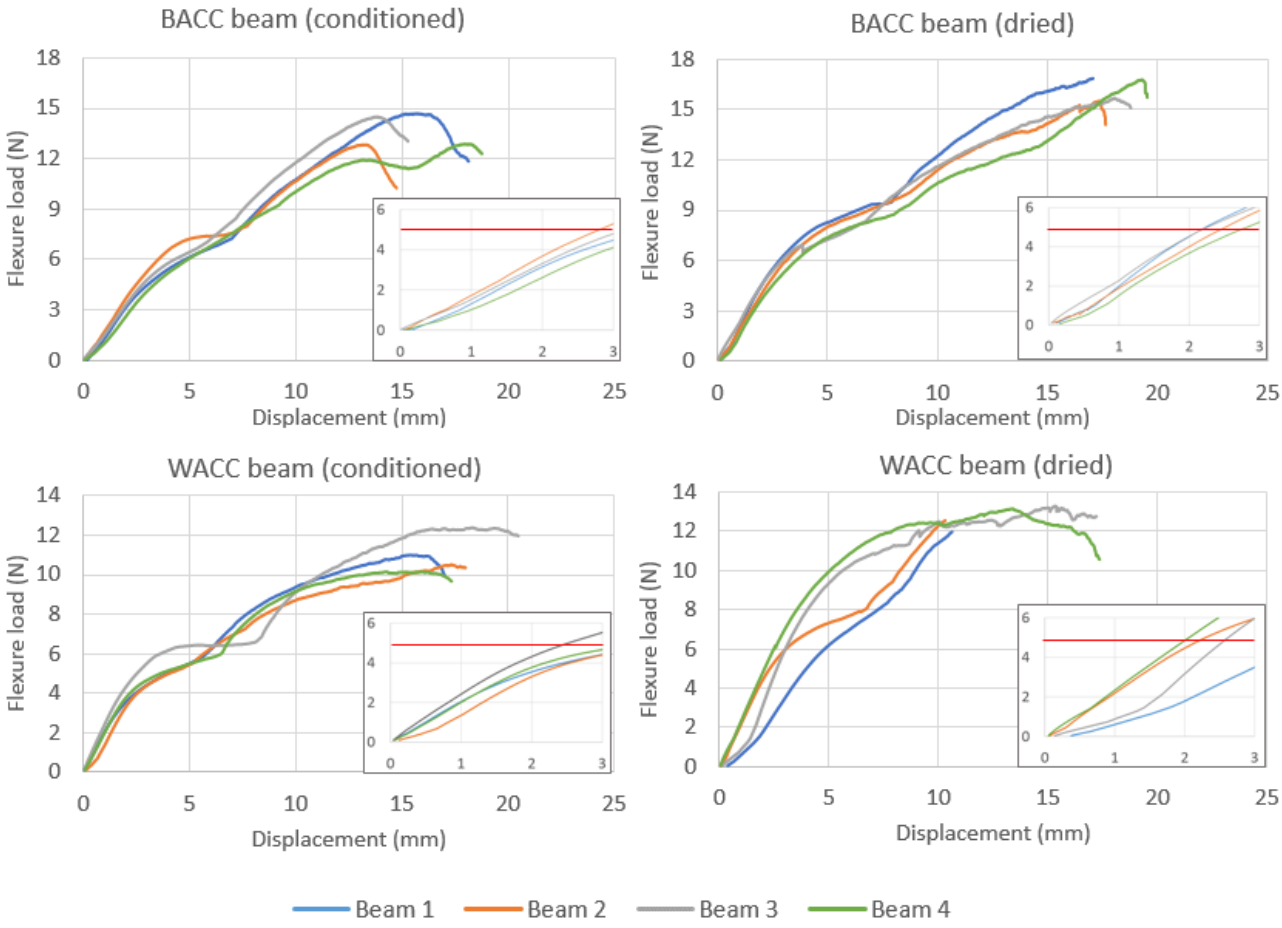

Figure 4.11. *All-cellulose composite beam specimen three-point bending data. Each chart features a more detailed view (0 – 3 mm; 0 – 6 N) on the initial linear region of the bending with 5,00 N mark highlighted with a red line. The shorter curves in the bottom right series (WACC beam, dried) were the result of unintentional termination of the test procedure due to the wrong limit values given to the controlling software.*

A typical feature of any beam specimen bending data is a dent in the loading curve around the 6 to 8 mm displacement range. This is speculated be caused by the uneven surface of a beam with wave like rims (result of drying) but also by the denting of the face layer and the underlying foam. The following offset after the dent is believed to be the result of the load transferring to the bottom half of the beam that is still relatively stiff and unbent.

Next it is clear that BACC beam specimen display greater maximum load values than WACC beams: Comparing the conditioned cases, the average maximum load of the WACC beam series is 79,1 % of the average maximum load of the BACC series. Also, there is much more dispersion within the WACC beams and they lack clear behavioral pattern to which there seems to be no explanation.

It is also evident that conditioned specimens are less stiff and achieve much lower levels of load until yielding than their dried counterparts.

All-Cellulose Composite panels

Bending test data for WACCP and BACCP specimen are shown in Figure 4.12.

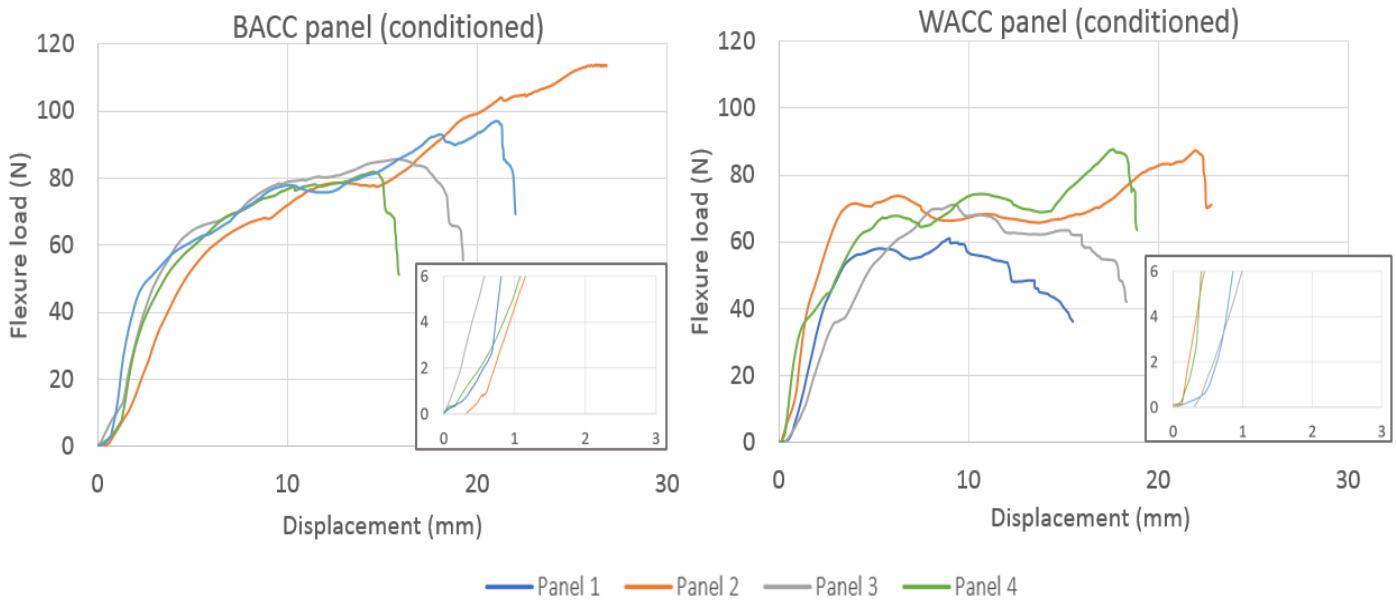

Figure 4.12. *All-cellulose composite panel specimen three-point bending data. Each chart features a more detailed view (0 – 3 mm; 0 – 6 N) on the initial linear region of the bending.*

Typical failure mode for most of the specimen was cracking of the bottom face of the beam. These cracks could propagate from fabrications defects that were mostly caused

by the hot-pressing of the face layers in the final assembly phase. Panel 2 of the BACCP didn't display any cracking and was successfully bent to the maximum yield controlled by the test setup. The piece is shown in Figure 4.13.

The initial region of the bending is similar between the two series, displaying equally rigid behaviour. However, after the 4 – 5 mm displacement range, the WACC panels begin to level off between loads of 58 N and 70 N while the BACC panels show steady increase in flexure load until failure caused by described fracturing.

Figure 4.13. *BACCP specimen after three-point bending shows no damage to the bottom face layer of the panel. The hole in the up-left corner is a fabrication defect caused by metal pliers.*

Based on the observations made with BACCP 2-specimen, a thicker face layer is strongly recommended in future designs.

As was observed with the ACC beam specimens, the WACC series displayed significantly lower average maximum load than the brown counterparts: this ratio is approximately 81,2 %.

Reference specimen

Reference specimen bending test results are reported in Figure 4.14.

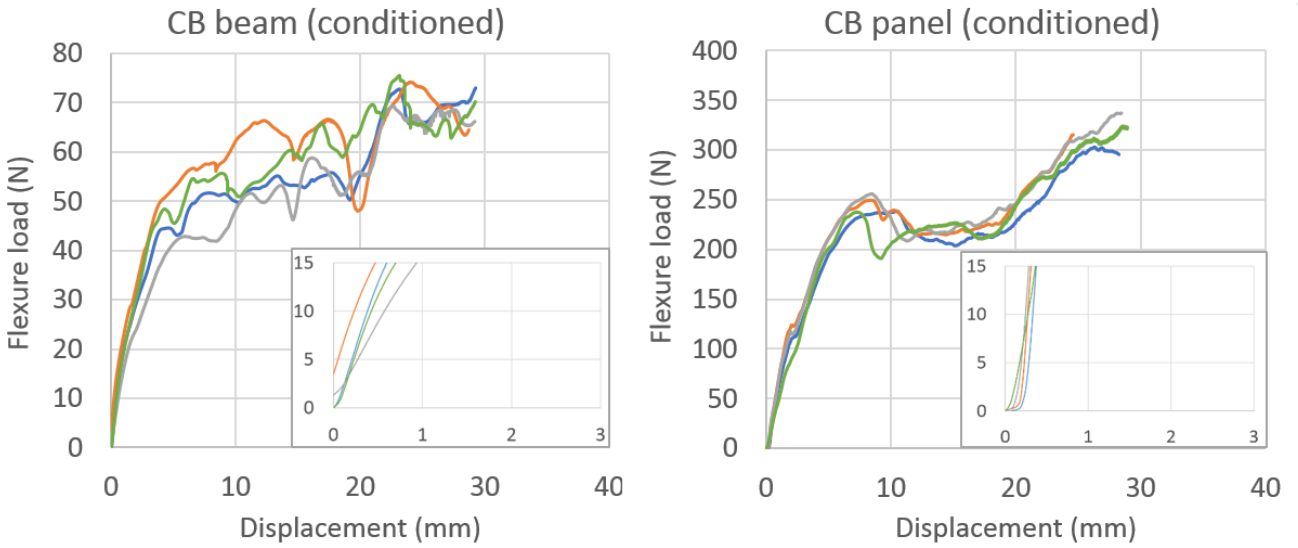

Figure 4.14. *(Left): corrugated board beam and (right): corrugated board panel three-point bending data. Each chart features a more detailed view (0 – 3 mm; 0 – 15 N) on the initial phase of the bending. All of the tests were terminated at controlled 60% flexure yield (28 mm displacement).*

The rippling pattern in the CB beam specimen bending curves is an indication of the compression induced crushing of a layer of corrugated medium and the following loading and resistance of a second layer. With a total of four layers of corrugated material, the effect is to be expected to be multiplied. Bending curves of the CB panels are much more in line with one another with very similar shape. These panel bending curves also feature similarity with ACC beam bending data: there is a clear dent occurring at 7,00 mm displacement. This is believed to be caused by the crushing of the upper half of the beam after which the lower half begins to resist further bending.

When compared to the all-cellulose composite beams and panels, it is obvious that these corrugated board counterparts surpass them in bending strength and stiffness. This comparison is further discussed in detail in section 5.2.1.

4.4 Flexure creep

Test data for studied ACC beam flexure creep is represented in Figure 4.15.

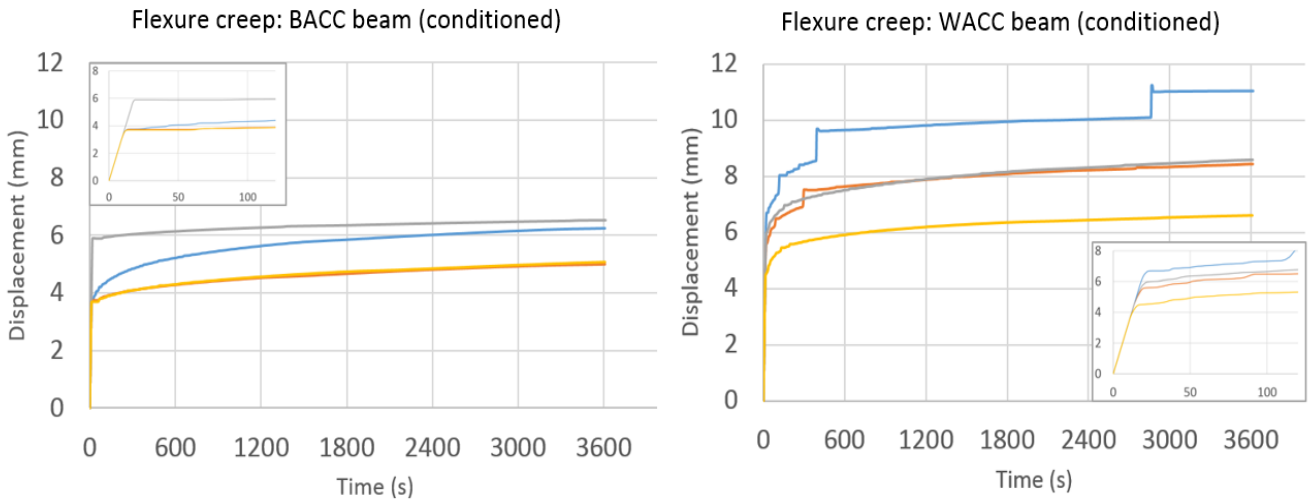

Figure 4.15. *(Left): corrugated board beam and (right): corrugated board panel three-point bending flexure creep data. Both charts feature a more detailed view on the initial phase of the creep test (0 – 120 s; 0 – 8 mm). Force was increased from 0 to 5,00 N with head speed of 20 mm / min.*

The initial displacement during loading in the 0 – 20 second range is significantly higher for WACC beams than for BACC beams. These observations are in line with the previous indications of three-point beam bending data.

Also, the notches in the curves of WACC creep data may suggest that 5,00 N is well above the linear range of a WACC beam bending (Figure 4.11).

In the flexural creep tests, brown nanocellulose films experienced an average total creep of 2,23 mm while white films 4,41 mm. Overall WACC beams are more susceptible to bending in low and moderate constant loads than BACC beams.

4.5 SEM micrographs

The micrograph images were taken at two magnifications: 100× and 1000×. The added scale reference bars within the images are 10 µm for 1000× and 100 µm for 100× magnifications.

To facilitate discussion and comparisons between specimen, an illustration is made (Figure 4.16) on typical sample harvest points of what areas of interests could be observed in a given specimen.

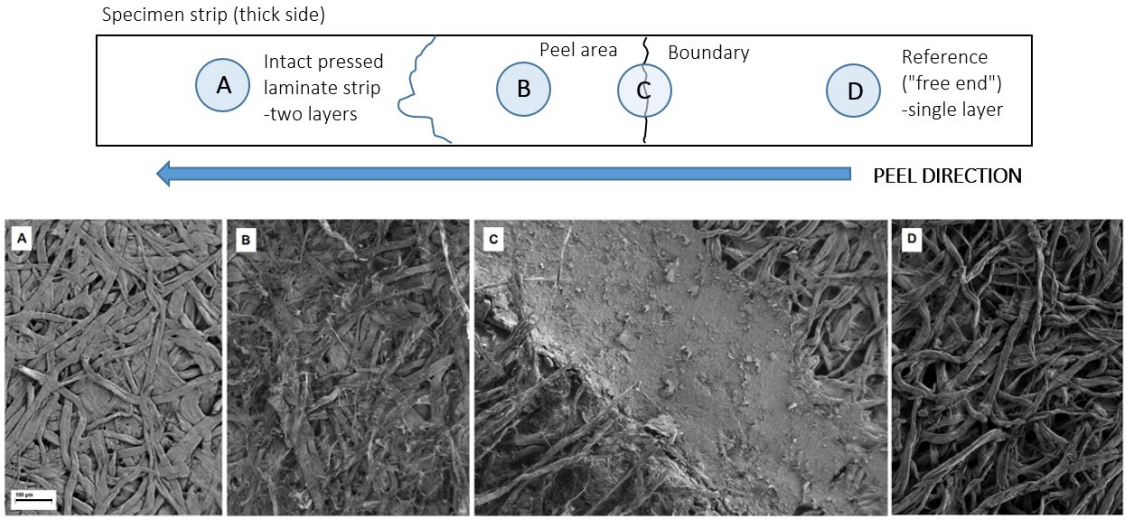

Figure 4.16. *(Top): Schematic of the thick side of peel test sample strip featuring areas of interest.* ***A*** *– intact laminate where two layers are still adhered,* ***B*** *– Peel area of delamination,* ***C*** *– Boundary between peel area and reference area, and* ***D*** *– Reference area with no adhesion or adhesive. Direction of advancing peel is also shown (Bottom): FE-SEM micrographs for respective areas of interest (****A****,* ***B****,* ***C*** *and* ***D****) taken from a porous (reference) blotter paper strip.*

In the subsequent micrograph figure series, the peel direction from top right to bottom left in each image is followed as shown in Figure 4.16. Areas of interest terms are explained in more detail below (the capital letter system is not used in future figures of multiple micrographs):

A *Intact laminate* – If the peeling of the strip terminated due to failure of one of the layers before the test was complete, an intact laminate can be examined (double layer). This area has been exposed to the adhesive, pressure and temperature of the self-adhesion specimen preparation process.

B *Peel area* – Area of mixed failure: interface or cohesive failure. It is important to note that these graphs feature the combined view of the intact, underlying laminate layer and remnants of the thin peeled off layer (mixed layers). This area has been exposed to the adhesive, pressure and temperature of the self-adhesion specimen preparation process.

C *Boundary* – The area where peeling initiates and where peeled of surface and intact surface can be seen. Some specimen display how the used adhesive has spread over the intended area of application. This area has been exposed partially to the adhesive, pressure and temperature of the self-adhesion specimen preparation process.

D *Reference* – Area where there is no adhesion and no adhesive or processing aids (Also referred to as free strip ends that are fastened into the clamps of a tensile tester.). In addition, this area has not been subjected to pressure in the hot-press process.

The effect of material microstructure on self-adhesion properties with 5% white HefCel solution was characterized by micrograph comparison series in Figure 4.17. In this comparison, blotter paper grades of both dense (compressed paper, Batch 4) and porous types (reference paper) were studied.

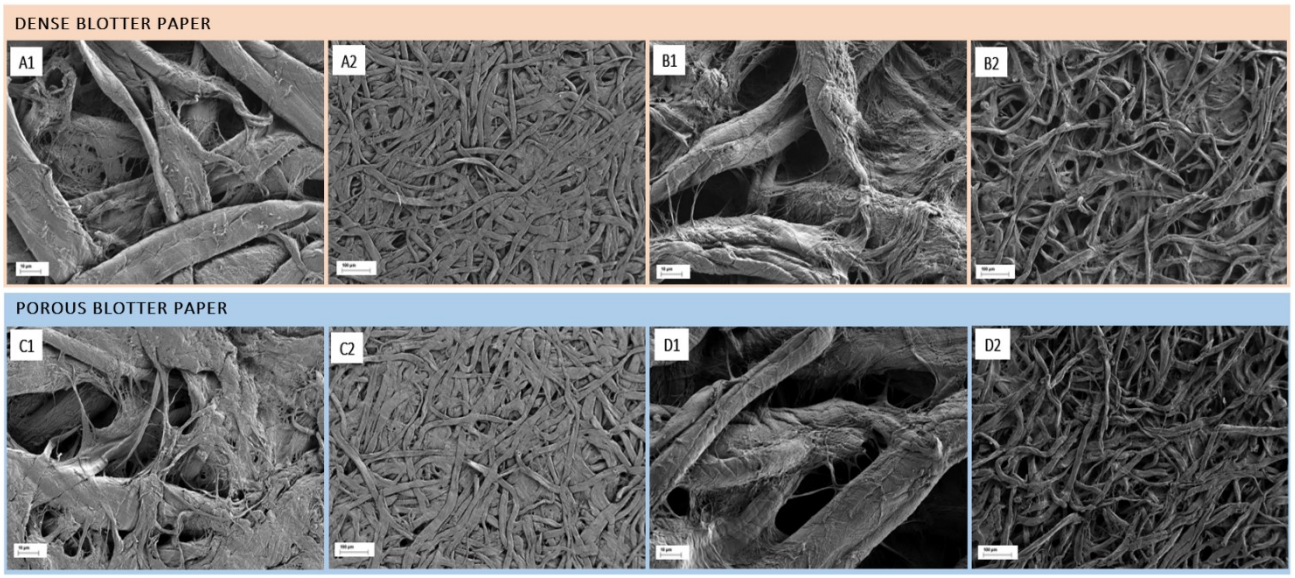

Figure 4.17. *FE-SEM micrographs of (Top) dense blotter paper and (Below) porous blotter paper. Between the graph pairs, picture 1 is taken at 1000x (scale bar - 10 µm) and picture 2 at 100x magnification (scale bar – 100 µm). A1 – A2 and C1 – C2: intact laminate; B1 – B2 and D1 – D2: reference area. Presence of dried HefCel solution can be seen in intact laminates.*

The difference in porosity between the two sample types is clear: the fibers seen in the reference area (B2 in Figure 4.17) are slightly compressed and more of the underlying network fibers can be seen when comparing B1 and D1. However, an unknown binder polymer is expected to have filled some of the pores in the dense blotter paper specimen. Fiber interactions of this polymer can be observed in images B1 and D1 with stronger interactions in B1.

Intact laminate areas reveal the inverted difference in surface “density”. In image C2, extensive grey areas are observed between the fibers where as in A2 spaces between fibers are clearer. This is more evident in 1000x magnifications in A1 and C1 where dense paper grade appears more porous than the porous grade. In C1 the spaces between the fibers are filled with HefCel that has penetrated through the both of the laminate layers and formed film and web like structures around the fibers. In A1, slight traces of HefCel can be seen between the underlying fibers of the paper network. These findings of HefCel penetrating a porous structure whilst improving internal bond strength of the material is supported by the self-adhesion data in Figure 4.8.

Next, the differences in copy paper self-adhesion experiments were studied. Copy paper was the only material type successfully joined with all types of adhesives and processing aids. Micrographs of these specimen series are presented in Figure 4.18.

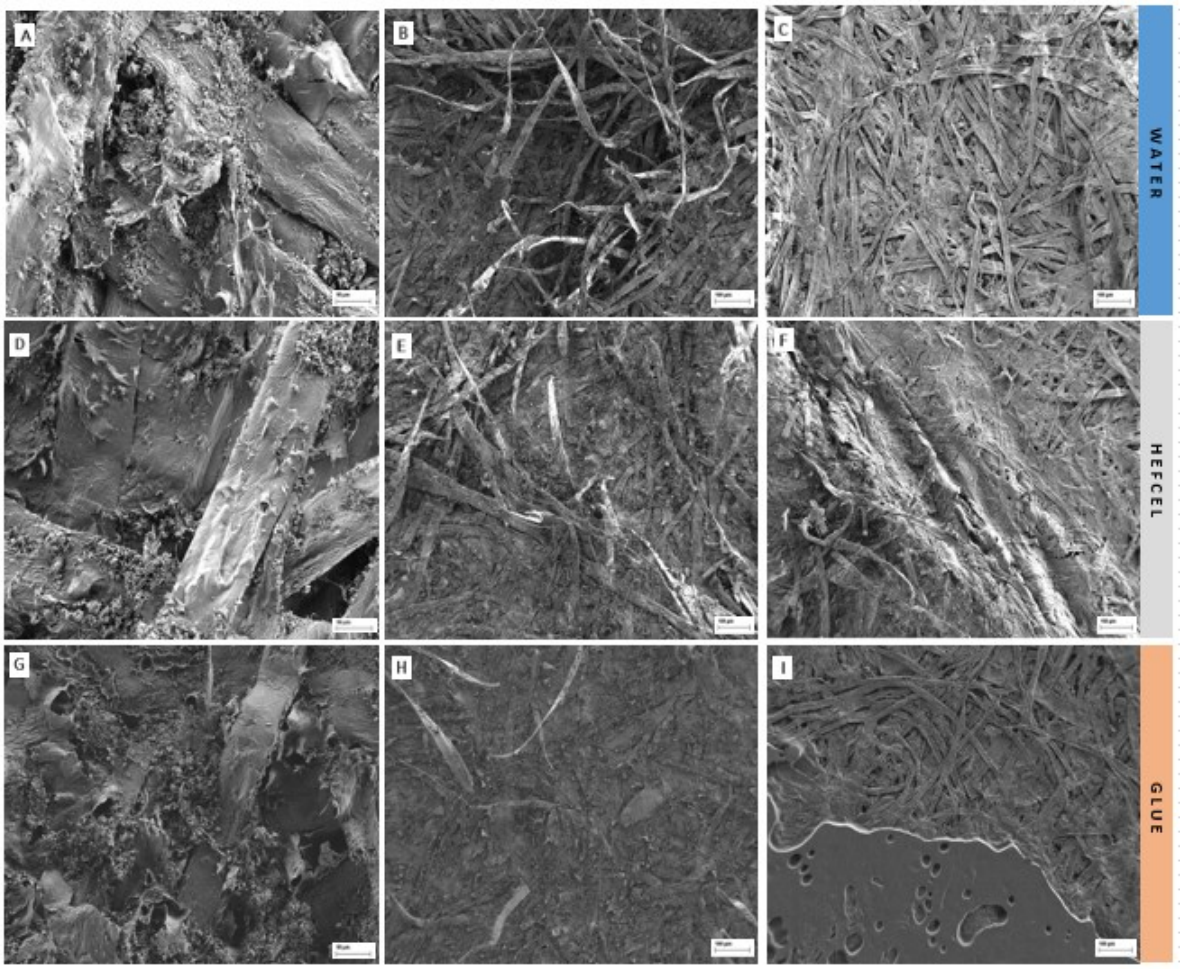

Figure 4.18. *FE-SEM micrographs of Copy paper joined with (A – C): water, (D – F): white 5% HefCel suspension and (G – I): 5% PVA liquid glue suspension. Images A, D and G are taken with 1000x magnification (scale bar - 10 µm) and others with 100x magnification (scale bar – 100 µm).*

The micrographs confirm that fibers in copy paper are closely associated with fillers and additive particles. The peel area of water joined specimen in image B in Figure 4.10 displays remarkable amount of loose fibers, which may be because of how the water joined fiber network fail during loading. Since there are no additional adhesive particles, the two joined layers of paper can be considered to be uniform in composition. It may be suspected, that when this type of laminate is subjected to peel, the relatively weak interfiber bonds break at random places close to the interface. This results in a peel area where there are fibers from both strip halves. But when an adhesive such as HefCel or PVA is used, it can't penetrate deep into the material and stays closer to the interface due to the relatively low porosity (air permeance) of the copy paper, binding fibers that are on the strip surfaces. For reference, copy paper was measured to have air permeance

of 8,31 µm/Pa×s while the most porous specimen type in the self-adhesion series has air permeance of 35,5 µm/Pa×s. For these reason, it is reasonable to expect a much smoother peel area with HefCel and PVA joined laminate specimen as seen in peel area images E and H in Figure 4.18. This assessment is further featured in Figure 4.19.

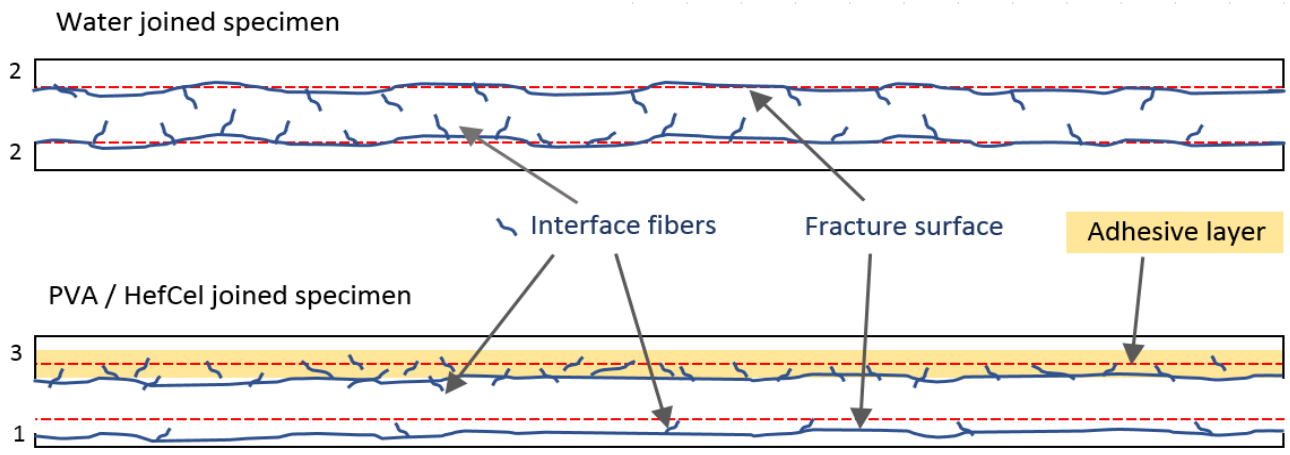

Figure 4.19. *Schematic presentation of the differences between peeled (Above) water joined and (Below) PVA / HefCel joined specimen strips. Both have an equal amount of fibers at the initial interface before lamination. However, once laminated, the interface fibers are strongly joined together by the adhesive, that has partially penetrated the copy paper. The red dashed line indicates where intact strip halves would form the interface during hot-pressing. Numbers at the left-hand side of the strips are an arbitrary representation of laminate thickness.*

Film formation by HefCel particles can be seen on the surfaces of copy paper fibers in image D and in the boundary area in image F. Similarly, films of PVA are visible in images G (peel area) and I (boundary area).

Lastly, the peel mechanisms are reviewed by studying micrographs taken from white and brown nanocellulose film surfaces. For reference purposes, both specimen types studied are strips that have been joined using water.

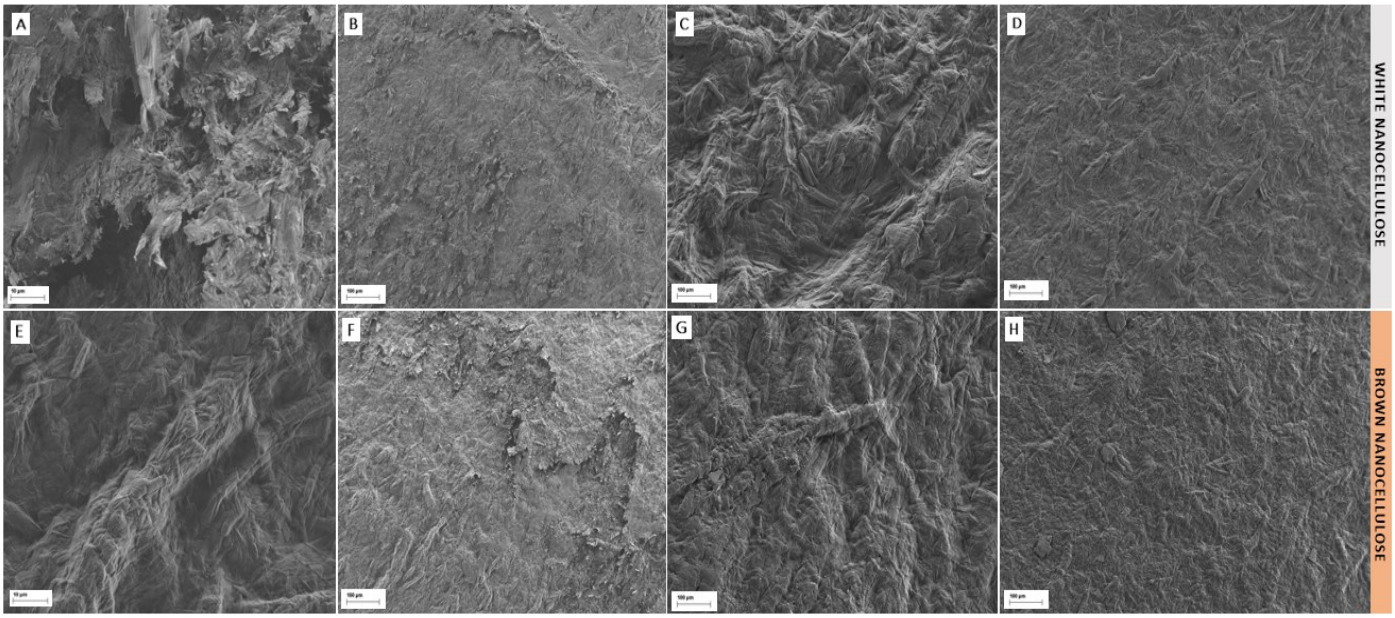

Figure 4.20. *FE-SEM micrographs of (A – D): white nanocellulose and (E – H): brown nanocellulose films joined with water. Images A, C, E and G are taken with 1000x magnification (scale bar - 10 µm) B, D, F and H with 100x magnification (scale bar – 100 µm).*

Both film types appear similar when observing their reference areas (C, D, G and H). However, with 1000x magnification, the surface roughness of brown nanocellulose film seems to be greater than that of the white film. However, this is also the case when comparing Bendtsen surface roughness data of the films: surface roughness of 350 ml/min is measured for white grade and 250 ml/min for brown. The differences in the images are then most likely due to differences in focusing of the scanning electron beam.

The boundary are images B and F reveal how the fracturing of the films has occurred in the peel test. The fracture surface visually supports the observation that the nanocellulose films strips are so tightly bound together that the single layer film will shear through from the point of adhesion across its thickness to the surface and snap off.

5 CONCLUSIONS

In this section, conclusions and summaries are made based on the work made along the thesis process.

5.1 Peel tests

In conclusion, a decently accurate method for depicting and comparing adhesion of similar flexible materials has been developed. The test advantages are the individual control of the applied adhesive and the adjustability (Hot-press temperature, pressing time and pressure) and simplicity. However, this method has been considerably constrained by available equipment, limiting the adaptation of features from industry standard methods or procedures. This has limited the result comparison with other similar studies, decreasing its value.

The peel tests, both self-adhesion and combination tests have revealed that sufficient adhesion between two lignocellulosic surfaces can be achieved with correct temperature and pressure while using only water as a processing aid. This property can be linked to the extensive hydrogen bond formation at the molecular level when a moist cellulosic material is being dried and while kept under pressure. Moisture content lowers the glass transition temperature of the material constituents, such as hemicellulose and lignin, making them more mobile in terms of molecular level motion. Aided by sufficient pressure into the material superstructure, more molecular contact is achieved and subsequently, more hydrogen bonding. The increase in hydrogen bonding before and after joining of two nanocellulose films of other fiber boards should prove an interesting study. Furthermore, future work should also utilize similar method as developed here to study self-adhesion properties of a set of materials or combinations over a broad temperature range and with varying pressing time. The kinetics of swelling, drying and hydrogen bond formation were grievously overlooked in this study.

The possible formation of covalent bonds in lignin containing surfaces could not be verified in this thesis. The work and insight of Zhou et al. (2011) suggests that lignin is to be chemically activated to promote adhesion between fibers containing lignin during a hot pressing procedure. This type of modified lignin has already reached commercialization phase as reactive lignin that aims to replace phenol based adhesives as wood adhesives (Wikberg, 2017). Therefore, confirmation of temperature induced covalent bonding of non-modified and modified lignin grades should also be investigated further.

The peel tests also indicate a connection between material porosity, measured as air permeance, and self-adhesion that is induced by dilute water suspension of nano-

fibrillated cellulose (HefCel) made from bleached enzyme pre-treated pulp. Porosity of a composite material makes it possible for the highly fibrillated cellulose suspension particles to penetrate inward into adherents in a composite strengthen the "joint" beyond the interface. The strengthening effect is likely due to hydrogen bonding and mechanical interlocking of long fibrils of the nanofibrillated particles. This way in fibrous composite materials fused with HefCel-like suspension, the interfaces becomes more obscure and resembling a continuous gradient-like interface. Study of these suggested gradients should be a focus in future studies.

Also, the discovery of good adhesive properties between nanocellulose film and cellulose fiber foam lead to their selection to be used in the innovative all-cellulose composite sandwich structures. In similar fashion, it is suggested that the applications possibilities and tests are continued further with nanocellulose film and thin veneer combinations.

5.2 All-cellulose composites

Novel all-cellulose sandwich composites were designed, fabricated and mechanically tested by three-point bending. Two types of specimen geometries were prepared featuring the same sandwich structure: ACC beams and panels. Beams were prepared to test the structure for bending along the reinforcing cell walls made of nanocellulose films. Panels were tested for bending against these supporting walls and provide understanding on the load bearing abilities of these composites.

The tested ACC pieces were lightweight and sustained moderate force before yielding. Brown ACC specimen, made of partially delignified nanocellulose films and CTMP-fiber foam provided superior to the ones made of white (bleached) nanocellulose films and of white, delignified fiber foam. Two series of beam specimen were also tested in their dry state which confirmed the adverse effects of moisture on the mechanical properties of this type of composites.

The relative performance between the tested ACC specimen types is best done via an evaluation method such as used by Frisk (2016). A modified version of this type of performance ranking is featured as an index ratio of average density to the average maximum load reached in the bending test. The smaller the index, the better the material is from a design stand point. An additional index of maximum force divided by average weight of a specimen type. These properties and indexes for Brown all-cellulose composite beams (BACCB) and panels (BACCP) as well for White all-cellulose composite beams (WACCB) and panels (WACCP) are presented in Table 5.1.

Table 5.1. *Table of different all-cellulose composite types and their described index properties.*

ACC type	Avg. density (g/cm^3)	Avg. weight (g)	Avg. maximum load (N)	Index (Density / $Force_{max}$)	Index ($Force_{max}$ / Weight)
BACCB	0,107	3,96	13,91	0,00772	3,51
WACCB	0,100	3,98	11,00	0,00913	2,76
BACCP	0,122	9,60	94,38	0,00129	9,83
WACCP	0,117	9,96	76,59	0,00153	7,69

The data presented in the table shows how future ACC design should prefer the components used in brown composite beams and panels. The adaptation of brown, partially delignified HefCel suspension instead of the utilized white counterpart would prove interesting to test with similar methods.

It is worth noting that the panel specimens were significantly wider (~50 mm) than beam specimen (~20 mm), but these index values still illustrate the importance of bending direction on continuous cell wall sandwich. The beams featuring side profiles of this type of sandwich are extremely sensitive to bending. This was further pointed out by the flexure creep tests performed to the ACC beams.

Along the property measurements that were desired to be made within this work included compression testing of the prepared specimen and acoustic testing. Challenges were faced with preparation of a perfectly small round specimen for the impedance tube. It is also suggested that thicker face nanocellulose layers are to be used in following adaptations and iterations of similar ACCs as prepared here.

5.2.1 Comparisons with reference specimen

Design wise most well performing ACC composite BACCP was compared with the highly rigid and strong beams and panels made from dual-layer corrugated packaging board designed for hazardous goods. This comparison of the properties and chosen indexes is presented in Table 5.2.

Table 5.2. *Table for comparison of BACCP specimen with reference specimen.*

	Avg. density (g/cm^3)	Avg. weight (g)	Avg. maximum load (N)	Index (Density / $Force_{max}$)	Index ($Force_{max}$ / Weight)
BACCP	0,122	9,6	94,38	0,00129	9,83
CBB	0,188	5,82	72,75	0,00259	12,5
CBP	0,191	13,28	318,73	0,0006	24,0

It is important to note that the density-force index of the fabricated all-cellulose composite panel is only double that of the corrugated board panel. This comparison should also give an idea of where this current ACC sandwich development lies in respect to highly engineered high performance multi-layer product.

Interestingly the thickness of the face layer of a CB beam or panel (512,4 µm) is nearly three and a half times the face thickness in a BACC beam or panel (Two-layer film: 148,3 µm). For this reason, the face thickness should be increased in the future. An increase in face thickness will increase the average density, but greatly increase the maximum flexure force. As was reported in the results and observations, cracking of the face layer was the most common failure mode of the panels. Increased face thickness would also counteract panel sensitivity to crack formation.

Furthermore, based on these comparisons, more elaborate ACC configurations are suggested: Preparation of multilayer composite structure or corrugating nanocellulose film for a core material should prove great but interesting challenges.

5.2.2 Recommended use

Current builds and iterations of ACC sandwich structures could be used in few applications: sound and heat insulators in cars and in non-supportive structures. Insulation capabilities are increased with treatment with fire retardants and protection from excess moisture. Refined ACC panels could also be used in furnishing as decorative sound absorbers and fashionable panels.

Due to their light weight, ACCs can also find use as casing materials for electronics and in packaging. High performance ACCs might find applications in automotive or in aerospace industries to replace other light weight composite components in less demanding tasks.

An important value within the ACC is their biodegradability as noted in the introductory. The demand for more environmentally sustainable parts for current non-biodegradeable components will also provide interesting and unexpected application prospects for these types of ACCs.

REFERENCES

Adler, D. C., & Buehler, M. J. (2013). Mesoscale mechanics of wood cell walls under axial strain. *Soft Matter*, (9): 7138-7144.

Adusumali, R.-b., Moritz, R., Weber, H., Roeder, T., Sixta, H., & Gindl, W. (2006). Mechanical Properties of Regenerated Cellulose Fibres for Composites. *Macromol. symp.*, 244, 119-125.

Agarwal, U. P., Reiner, R. R., & Ralph, S. A. (2011). CELLULOSE CRYSTALLINITY OF WOODS, WOOD PULPS, AND AGRICULTURAL FIBERS BY FT-RAMAN SPECTROSCOPY. *International symposium on wood, fiber and pulping chemistry* (pp. 69-74). Tianjin: China Light Industry Press.

Ahlstrom. (2014). Retrieved 12 11, 2013, from http://www.ahlstrom.com/fi/ahlstrom/Sanasto/

Ahola, S., Salmi, J., Johansson, L.-S., Laine, J., & Österberg, M. (2008). Model Films from Native Cellulose Nanofibrils. Preparation, Swelling, and Surface Interactions. *Biomacromolecules*, (9): 1273–1282.

Altaner, C. M., & Jarvis, M. C. (2008). Modelling polymer interactions of the 'molecular Velcro' type in wood under mechanical stress. *Journal of Theoretical Biology*, (253): 434-445.

Arévalo, R., & Peijs, T. (2015). Binderless all-cellulose fibreboard from microfibrillated lignocellulosic. *Composites: Part A*.

Aulin, C., Ahola, S., Josesson, P., Nishino, T., Hirose, Y., Österberg, M., & Wågberg, L. (2009). *Nanoscale Cellulose Films with Different Crystallinities and Mesostructures - Their Surface Properties and Interaction with Water.* Langmuir.

Aulin, C., Salazar-Alvarez, G., & Lindström, T. (2012). High strength, flexible and transparent nonofibrillated cellulose-nanoclay biohybrid films with tunable oxygen and water vapor permeability. *Nanoscale*, (4): 6622-6628.

Bernt, I., Roggenstein, W., Woodings, C., & Harms, H. (2012). *Patent No. US20120209234 A1*.

Besombes, S., & Mazeau, K. (2005). The cellulose/lignin assembly assessed by molecular modeling. Part 2: seeking for evidence of organization of lignin molecules at the interface with cellulose. *Plant Physiology and Biochemistry*, (43): 277-286.

Bhatnagar, A., & Sain, M. (2005). Processing of Cellulose Nanofiber reinforced Composites. *Journal of Reinforced Plastics and Composites*, (24): 1259-1268.

Brebu, M., & Vasile, C. (n.d.). Thermal Degradation of Lignin - A Review. *Cellulose Chemistry and Technology*.

Brecht, W., Knittweis, H.-J., & Schmidt, W. (1971). *Neuere Unterschungen uber das Dehnungsverhalten verschiedener Papiere.*

Campbell, F. C. (2010). *Structural Composite Materials.* ASM International.

Carillo, F., Colom, X., Sunol, J. J., & Saurina, J. (2004). Structural FTIR analysis and thermal characterisation of lyocell and viscose-type fibres. *European Polymer Journal*, (40): 2229-2234.

Castroa, J., & Ostoja-Starzewski, M. (2003). *Elasto-plasticity of paper.* Elsevier Ltd.

Caulfield, D. (1990). EFFECT OF MOISTURE AND TEMPERATURE ON THE MECHANICAL PROPERTIES OF PAPER. *Proceedings of National Science Foundation workshop*, 50-62.

Chanzy, H., Dubé, M., & Marchessault, R. H. (1979). Crystallization of cellulose with N-methylmorpholine N-oxide: A new method of texturing cellulose. *Journal of Polymer Science: Polymer Letters Edition*, (17): 219-226.

Chaplin, M. (2013, 5 23). *Water Structure and Science*. Retrieved 6 5, 2013, from http://www.lsbu.ac.uk/water/hycel.html

Chirayil, C. J., Mathew, L., & Thomas, S. (2014). Review of recent research in nanocellulose preparation from different lignocellulosic fibers. *Reviews on advanced materials science*, (37): 20-28.

Delgado Fornué, E., Allan, G. G., Contreras Quiñones, H. J., Toriz González, G., & Turrado Saucedo, J. (2011). Fundamental aspects of adhesion between cellulosic surfaces in contact - a review. *O papel*, (72): 85-90.

DIAB group. (2012). *DIAB Guide to core and sandwich.* Laholm.

Duchemin, B., Le Corre, D., Leray, N., Dufresne, A., & Staiger, M. P. (2016). All-cellulose composites based on microfibrillated cellulose and filter paper via a NaOH-urea solvent system. *Cellulose*, (1): 593-609.

Durgun, H., & Bayram, G. (2005). Improvement of adhesion between poly(ethylene terephtalate) and polyethylene. *Journal of Adhesion Science and Technology*, (19): 407-425.

Eriksson, M. (2006). *The Influence of Molecular Adhesion on Paper Strength.* Stockholm: KTH, Royal Institute of Technology.

Farabee, M. (2010, 5 18). *CHEMISTRY II: WATER AND ORGANIC MOLECULES*. Retrieved 6 10, 2013, from http://www.emc.maricopa.edu/faculty/farabee/biobk/biobookchem2.html

Flink, H.-P., Weigel, P., Purz, H. J., & Ganster, J. (2001). Structure formation of regenerated cellulose materials from NMMO-solutions. *Progress in Polymer Science*, 1473–1524.

Frisk, N. (2016). *Manufacturing of Lightweight Sandwich Composites with Bio-Based PU Foam Core and Cellulose Fiber Network Skin.* Lulea: Luleå University of Technology.

Gardner, D. J., Oporto, G. S., Mills, R., & Azizi Samir, M. A. (2008). Adhesion and Surface Issues in Cellulose and Nanocellulose. *Journal of Adhesion Science and Technology*, (22): 545-567.

Glatfelter. (2005). Technical Bulletin. *Moisture and Relative Humidity*, pp. 1-12.

Granström, M. (2009). *Cellulose Derivatives: Synthesis,Properties and Applications.* Helsinki.

Hafren, J., Fujino, T., & Itoh, T. (1999). Changes in Cell Wall Architecture of Differentiating Tracheids of Pinus thunbergii during Lignification. *Plan Cell Physiology*, (5): 532-541.

Halonen, H. (2012). *Structural changes during cellulose composite processing*. Stockholm, Sweden.

Harmsen, P. F., Huijgen, W. J., Bermúdez López, L. M., & Bakker, R. R. (2010). *Literature Review of Physical and Pretreatment Processes for Lignocellulosic Biomass.* ResearchGate.

Haygreen , J. G., & Bowyer, J. L. (1982). In *Forest products and wood science.* Ames: The Iowa State University Press.

Heino, J.;& Vuento, M. (2007). *Biokemian ja solubiologian perusteet.* WSOY.

Henriksson, M., Berglund, L., Lindström, T., Isaksson, P., & Nishino, T. (2008). Cellulose Nanopaper of High Toughness. Ruotsi.

Hubbe, M. A. (2006). Bonding between cellulosic fibers in the absence and presence of dry-strength agents - a review. *Bioresources*, (2): 281-318.

Huber, T., Pang, S., & Staiger, M. P. (2012). All-cellulose composite laminates. *Composites*, (43): 1738-1745.

Jin, K., Qin, Z., & Buehler, M. J. (2015). Molecular deformation mechanisms of the wood cell wall materials. *Journal of the mechanical behaviour of biomedical materials*, (42): 198-206.

Jin, Z., Katsumata, K. S., Lam, T. B., & Iiyama, K. (2006). Covalent Linkages between Cellulose and Lignin in Cell Walls of Coniferous and Nonconiferous Woods. *Biopolymers*, (83): 103-110.

Kanerva, M. (2014). *Strength of rough interfaces - A micro-scale approach to steel-epoxy and composite systems.* Helsinki: Aalto University.

Kang, T., & Paulapuro, H. (2006). *Effect of External Fibrillation.* Pulp & Paper Canada.

Klemm, D., Schumann, D., Kramer, F., Heßler, N., Hornung, M., Schmauder, H.-P., & March, S. (2006). Nanocelluloses as Innovative Polymers in Research and Application. In D. Klemm, *Polysaccharides II* (pp. 49-97).

Kubat, J., Martin-Lof, S., & Soremark, C. (1969). *Svensk Papperstidn*.

Kumar, V., Bollström, R., Yang, A., Chen, Q., Chen, G., Salminen, P., . . . Toivakka, M. (2014). Comparison of nano- and microfibrillated cellulose films. *Cellulose*, (21): 3443-3456.

Lavoine, N., Desloges, I., Dufresne, A., & Bras, J. (2012). Microfibrillated cellulose – Its barrier properties and applications in cellulosic materials: A review. *Carbohydrate Polymers*, (90): 735-764.

Laws, D. D., Bitter, H.-M. L., & Jerschow, A. (2002). Solid-State NMR Spectroscopic Methods in Chemistry. *Angewandte Chemie International Edition*, (41): 3096-3129.

Lee, H. V., Hamid, S. B., & Zain, S. K. (2014). Conversion of Lignocellulosic Biomass to Nanocellulose:. *The Scientific World Journal*.

Leney, L. (1980). *A Technique for Measuring Fibril Angle Using Polarized Light.*

Liu, J.-C., Moon, R. J., Rudie, A., & Youngblood, J. P. (2014). *Mechanical performance of cellulose nanofibril film-wood flake laminate.* Vienna.

Lu, X., Zhang, M. Q., Rong, M. Z., Shi, G., & Yang, G. C. (2003). Self-reinforced melt processable composites of sisal. *Composites Science and Technology*, (63): 177-186.

Mark, R. E. (1968). In *Cell Wall Mechanics of Tracheids* (p. 152). New Haven: Yale University Press.

Maximova, N., Österberg, M., Koljonen, K., & Stenius, P. (2001). Lignin adsorption on cellulose fibre surfaces: Effect on surface chemistry,surface morphology and paper strength. *Cellulose*, (8): 113-125.

Metso. (2013). *Chemical pulp production*. Retrieved 13 6, 2013, from http://www.metso.com/corporation/info_eng.nsf/WebWID/WTB-060629-2256F-5A4FA?OpenDocument

Michels, C., & Kosan, B. (2005). Contribution of the dissolution state of cellulose and cellulose derivatives. *Lenzinger Berichte*, (84): 62-70.

Moon, R. J., Martini, A., Nairn, J., Simonsen, J., & Youngblood, J. (2011). Cellulose nanomaterials reveiw: structure, properties and nanocomposites. *Nanoscience and Nanotechnology Commons*.

Mott, L., Groom, L., & Shaler, S. (2002). Mechanical properties of individual southern pine fibers part II comparison of earlywood and latewood fibers with respect to tree height and juvenility. *Wood and Fiber Science*, (34): 221-237.

Neuman, R. D., Berg, J. M., & Claesson, P. M. (1993). Direct measurement of surface forces in papermaking and paper coating systems. *Nordic Pulp and Paper Research*, (11): 96-104.

Nilsson, H., Galland, S., Larsson, P. T., Gamstedt, E. K., Nishino, T., Berglund, L. A., & Iversen, T. (2010). A non-solvent approach for high-stiffness all-cellulose biocomposites based on pure wood cellulose. *Composites Science and Technology*, (70): 1704-1712.

Nilsson, H., Galland, S., Larsson, P. T., Gamstedt, E. K., Nishino, T., Berglund, L. A., & Iversen, T. (2010). A non-solvent approach for high-stiffness all-cellulose biocomposites based on pure wood cellulose. *Composite Science and Technology*, (70): 1704-1712.

Nishino, T., & Arimoto, N. (2007). All-Cellulose Composite Prepared by Selective Dissolving of Fiber Surface. *Biomacromolecules*, (8): 2712-2716.

Niskanen, K. (2008). *Papermaking Science and Technology: Paper Physics.* Paperi ja Puu Oy.

Okuda, N., Hori, K., & Sato, M. (2006). Chemical changes of kenaf core binderless boards during hot pressing. *Journal of wood science*.

Olsson, A.-M., Bjurhager, I., Gerber, L., Sundberg, B., & Salmen, L. (2011). Ultra-structural organisation of cell wall polymers in normal and tension wood of aspen revealed by polarisation FTIR microspectroscopy. *Planta*, (233): 1277-1286.

Paavilainen, S., McWhirter, J. L., Rog, T., Järvinen, J., Vattulainen, I., & Ketoja, J. A. (2012). Mechanical properties of cellulose nanofibrils determined through atomistic molecular dynamic simulation. *Nordic Pulp and Paper Research Journal*, (27): 282-286.

Paunonen, S. (2013, 4 3). *Strenght and Barrier Enhancements of Cellophane and Cellulose Derivative Films: A Review*.

Peijs, T. (2003). Composites for recyclability. *Materials Today*, 30-35.

Pérez, S., & Mackie, W. (2001). *Structure and morphology of cellulose*. Retrieved 6 5, 2013, from http://www.cermav.cnrs.fr/glyco3d/lessons/cellulose/index.html

Roig, F., Dantras, E., Dandurand, J., & Lacabanne, C. (2011). Influence of hydrogen bonds on glass transition and dielectric relaxations of cellulose. *Journal of Physics*.

Rosenau, T., Potthast, A., Sixta, H., & Kosma, P. (2001). The chemistry of side reactions and byproduct formation in the system NMMO/cellulose (Lyocell process). *Progress in polymer science*, (26): 1763-1837.

Rusli, R., & Eichhorn, S. J. (2008). Determination of the stiffness of cellulose nanowhiskers and the fiber-matrix interface in a nanocomposite using Raman spectroscopy. *Applied Physics Letters*, (93): 033111: 3.

Sˇturcova, A., His, I., Apperley, D. C., Sugiyama, J., & Jarvis, M. C. (2004). Structural Details of Crystalline Cellulose from Higher Plants. *Biomacromolecules*, (5): 1333-1339.

Salmen, L. (1982). *Temperature and Water Induced Softening Behaviour of Wood Fiber Based Materials.* Stockholm: The Royal Institute of Technology.

Satas, S. (1989). *Handbook of Pressure Sensitive Adhesive Technology.* Van Nostrand Reinhold: New York.

Sehaqui, H., Allais, M., Zhou, Q., & Berglund, L. A. (2011). Wood cellulose biocomposites with fibrous structures at micro- and nanoscale. *Composites Science and Technology*, (71): 382-387.

Shivyari, N. Y., Tajvidi, M., Bousfield, D. W., & Gardner, D. J. (2016). *Production and characterization of laminates of paper and cellulose nanofibrils.* Orono: American Chemical Society.

Siqun, W., Seung-Hwan, L., & Qingzheng, C. (2010). Mechanical properties of cellulosic materials at micro- and nanoscale levels. In A. Lejeune, & T. Deprez, *Cellulose: Structure and properties* (pp. 459-500). Nova Science Publishers, Inc.

Siro, I., & Plackett, D. (2010). Microfibrillated cellulose and new nanocomposite materials: a reveiw. *Cellulose*, (17): 459-494.

Soykeabkaew, N. (2007). *All-Cellulose Composites.* London: Queen Mary, University of London.

Soykeabkaew, N., Arimoto, N., Nishino, T., & Peijs, T. (2008). All-cellulose composites by surface selective dissolution of aligned. *Composites Science and Technology*.

Spence, K. L., Venditti, R. A., Rojas, O. J., Habibi, Y., & Pawlak, J. J. (2010). The effect of chemical composition on microfibrillar cellulose films from wood pulps: water interactions and physical properties for packaging applications. *Cellulose*, (17) 835-848.

Sperling, L. H. (2006). *Introduction to physical polymer science.* Hoboken: John Wiley & Sons, Inc.

Srndovic, J. S. (2011). *Interactions between Wood Polymers in Wood Cell Walls and Cellulose/Hemicellulose Biocomposites.* Göteborg: Chalmers University of Technology.

Suzuki, S., Shintani, H., Park, S.-Y., Saito, K., Laemsak, N., Okuma, M., & Iiyama, K. (1998). Preparation of Binderless Boards from Steam Exploded Pulps of Oil Palm (Elaeis guneensis Jaxq.) Fronds and Structural Characteristics of Lignin and Wall Polysaccharides in Steam Exploded Pulps to be Disc. *Holzforschung*, (52): 417-426.

Szczes´niak, L., Rachocki, A., & Tritt-Goc, J. (2007, 11 27). Glass transition temperature and thermal decomposition of cellulose powder. Retrieved 1 12, 2014, from http://link.springer.com/article/10.1007%2Fs10570-007-9192-2

Temap. (n.d.). Retrieved 12 7, 2013, from http://www.temap.com/prp/glossary.html

Terashima, N., Kojima, M., Kitano, K., & Westermark, U. (2009). Nanostructural assembly of cellulose, hemicellulose, and lignin in the middle layer of secondary wall of ginkgo tracheid. *Journal of Wood Science*, (6): 409-416.

ThermoWood. (2003). *ThermoWood Handbook.* Helsinki: Finnish Thermowood Association.

Torres, F. G., Troncoso, O. P., Torres, C., & Grande, C. J. (2013). Cellulose Based Blends, Composites and Nanocomposites. In S. Thomas, P. M. Visakh, & A. P. Mathew, *Advances in Natural Polymers - Composites and Nanocomposites* (pp. 21-25). Springer.

University of California. (2010). *UC Davis ChemWiki*. Retrieved 6 10, 2013, from http://chemwiki.ucdavis.edu/Organic_Chemistry/Organic_Chemistry_With_a_Biological_Emphasis/Chapter__3%3A_Conformations_and_Stereochemistry/Section_3.2%3A_Conformations_of_cyclic_organic_molecules

Wang, Y.-S., Koo, W.-M., & Kim, H.-D. (2003). Preparation and Properties of New Regenerated Cellulose Fibers. *Textile Research Journal*, 998-1004. doi:10.1177/004051750307301110

Weigel, G. (2005). *Collection Mémoires et thèses électroniques*. Retrieved 8 10, 2013, from http://theses.ulaval.ca/archimede/fichiers/22655/ch01.html

Wertz, J.-L., Bédué, O., & Mercier, J. (2010). In *Cellulose science and technology* (pp. 101 - 169). Taylor & Francis Group.

Wertz, J.-L., Bédué, O., & Mercier, J. (2010). Cellulose science and technology. Taylor & Francis Group.

Wikberg, H. (2017). Reactive lignin replaces phenol. (K. Krabbe, Interviewer) Retrieved from http://www.paperijapuu.fi/reactive-lignin-replaces-phenol/

Winkworth-Smith, C. G. (2014). *Cellulose composite structures – by design.* Loughborough: The University of Nottingham.

Visakh, P. M., Mathew, A. P., & Thomas, S. (2012). Natural Polymers: Their Blends, Composites and Nanocomposites: State of Art, New Challenges and Opportunities. In *Advances in Natural Polymers* (pp. 1-21). Springer Berlin Heidelberg.

Yang, H., Yan, R., Chen, H., Ho Lee, D., & Zheng, C. (2007). Characteristics of hemicellulose, cellulose and lignin pyrolysis. *Fuel*, (86): 1780-1788.

Zhang, N., Li, S., Xiong, L., Hong, Y., & Chen, Y. (2015). Cellulose-hemicellulose interaction in wood cell-wall. *Modelling and Simulation in Materials Science and Engineering*, (23): 1-15.

Zhang, X., Yang, W., & Blasiak, W. (2011). Modeling Study of Woody Biomass: Interactions of Cellulose, Hemicellulose, and Lignin. *energy&fuels*, (25): 4786-4795.

Zhao, B., & Kwon, H. J. (2011). Adhesion of Polymers in Paper Products from the Macroscopic to Molecular Level — An Overview. *Journal of Adhesion Science and Technology*, (25): 557-579.

Zhao, X., Liu, D., & Zhang, L. (2012). Biomass recalcitrance. Part II: Fundamentals of different pre-treatments to increase the enzymatic digestibility of lignocellulose. *Biofuels Bioproducts and Biorefining*, (6): 561-579.

Zhou, X., Tan, L., Zhang, W., Lv, C., Zheng, F., Zhang, R., . . . Liu, X. (2011). Lignin as binder for biocomposites. *Bioresources.com*, (6): 253-264.

Åkerholm, M. (2003). Ultrastructural Aspects of Pulp Fibers as Studied by Dynamic FT-IR Spectroscopy. Tukholma.

APENDIX A: DMA DATA FOR WHITE AND BROWN NANOCELL ULOSE FILMS

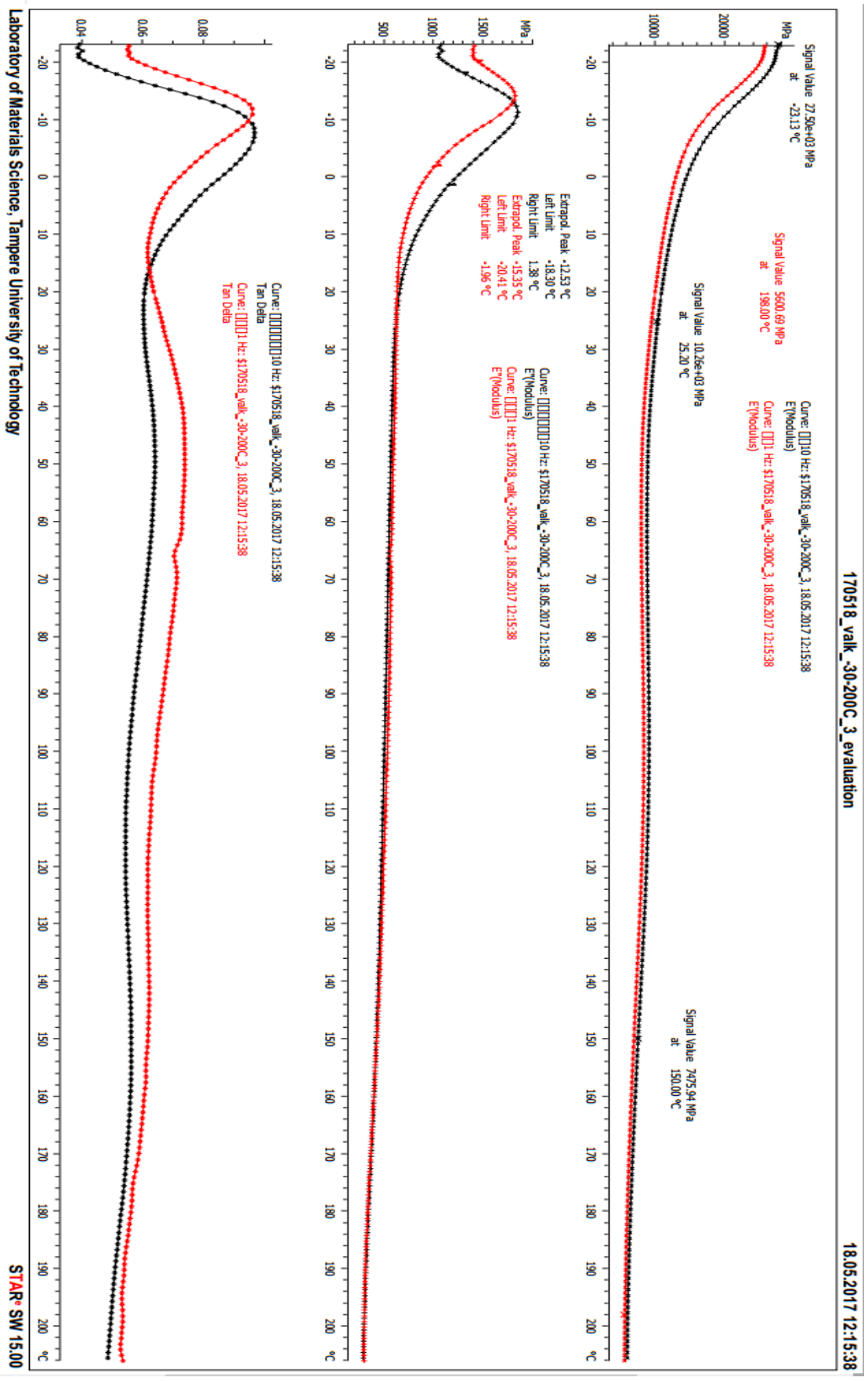

Figure A.1. *DMA sweep (-30 – 200 ˚C) for white nanofibrillated cellulose film specimen*

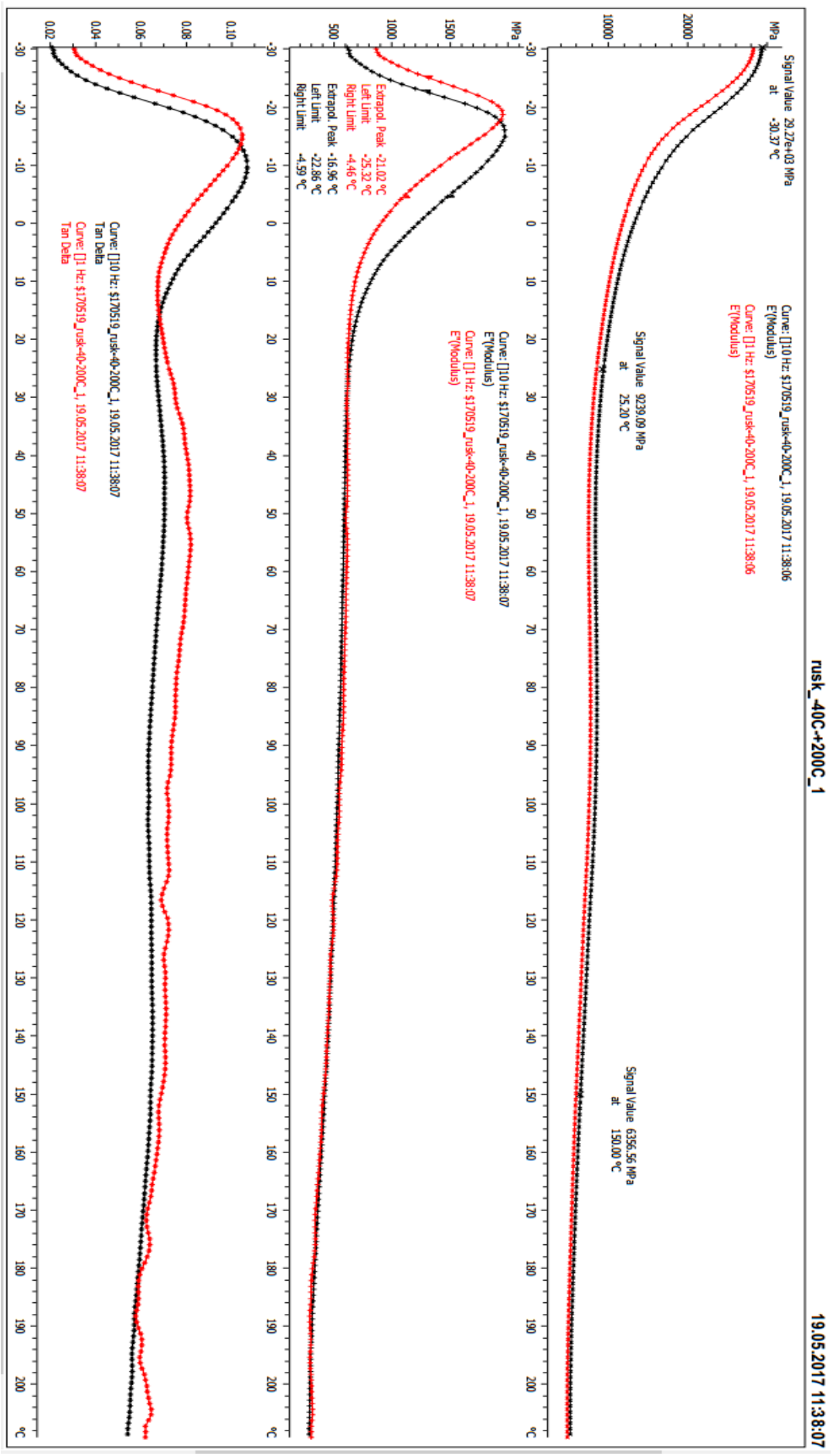

Figure A.2. *DMA sweep (-40 – 200 ˚C) for brown nanofibrillated cellulose film specimen*

APENDIX B: DSC DATA FOR WHITE AND BROWN NANOCELLULOSE FILMS

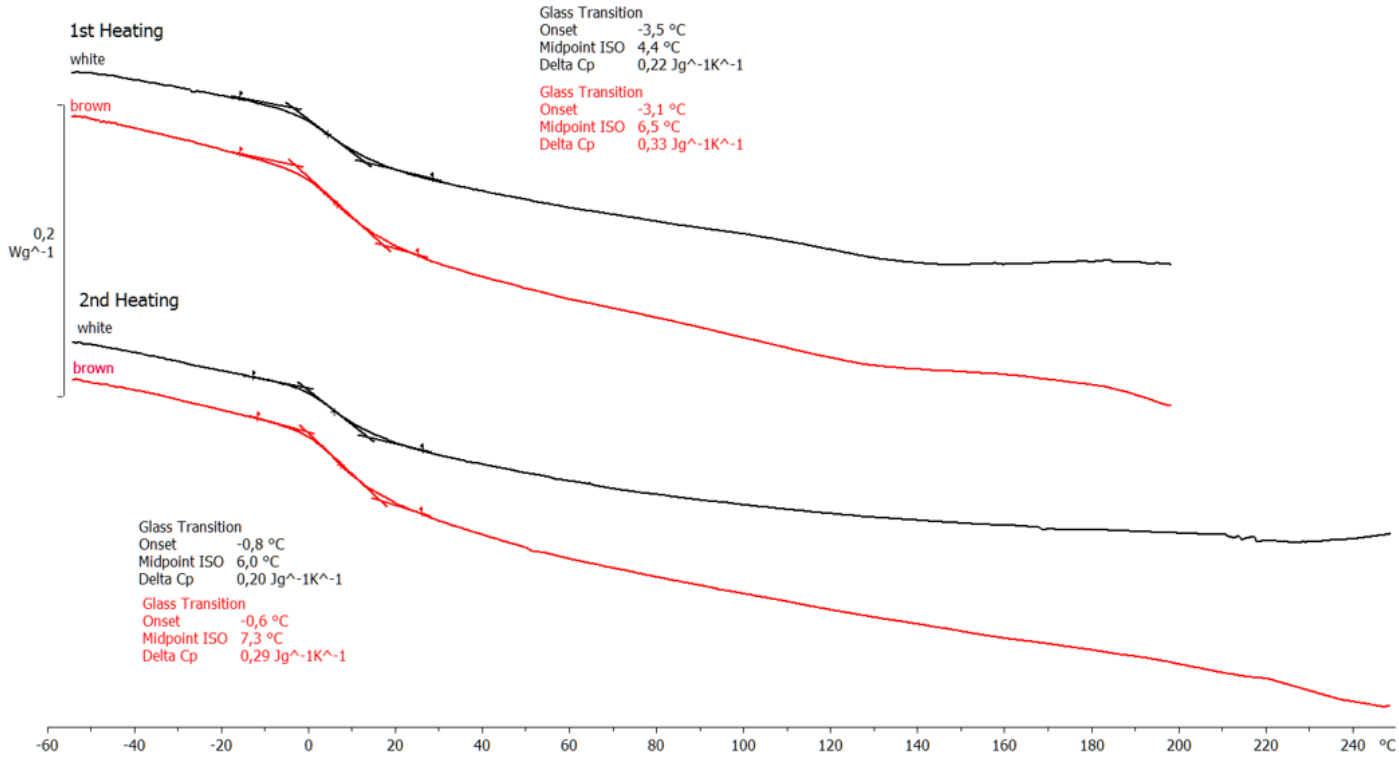

Figure B.1. *DSC sweeps for both white and brown nanofibrillated cellulose film specimens.*

Glass Transition Temperatures

	1st heating		2nd heating	
Sample	**Tg1 (°C)**	**ΔCP1 (J g^{-1} K^{-1})**	**Tg2 (°C)**	**ΔCP2 (J g^{-1} K^{-1})**
white	4,4	0,22	6,0	0,20
brown	6,5	0,33	7,3	0,29

Figure B.2. *DSC report data for white and brown nanofibrillated cellulose film specimens for 1st and 2nd heating.*